



University of Kerbala
College of Education for Pure Science
Department of Chemistry

Synthesis, Characterization of SnO₂ Nanoparticles and their application in the Removal of Mefenamic Acid from Aqueous Solutions

A Thesis

Submitted to the Council of College of Education for Pure Science, University of
Kerbala/ In Partial Fulfilment of the Requirements for the Degree of Master in
Chemistry Sciences

Written by

Hiba Ali Hamzah

Supervised by

Asst .Prof .Dr.

Aula Mahdi Abd Ali

1445 A.H

Asst. Prof. Dr.

Fouad Fadhil Al-Qaim

2023 A.D

بِسْمِ اللَّهِ الرَّحْمَنِ الرَّحِيمِ

((وَجَعَلْنَا مِنْ الْمَاءِ كُلَّ شَيْءٍ حَيٍّ))

صَدَقَ اللَّهُ الْعَلِيِّ الْعَظِيمِ

سورة الأنبياء

الآية ٣٠

Supervisor Certification

We attest that this thesis (**Synthesis, Characterization of SnO₂ Nanoparticles and their application in the Removal of Mefenamic Acid from Aqueous Solutions**) was created under our direction by(**Hiba Ali Hamzah**) at the University of Kerbala / Iraq' College of Education for Pure Sciences' Chemistry Department, in partial requirements for the master's degree in Chemistry.

Signature:

Supervisor

Assist. Prof. Dr. **Aula Mahdi Abd Ali**

Signature:

Supervisor

Assist. Prof. Dr. **Fouad Fadhil Al-Qaim**

Address: Department of chemistry
College of Education for Pure Sciences
University of Kerbala
Date: 31/7/2023

Address: College of Science for Girls
University of Babylon/Iraq
Date: 31/7/2023

Signature:

Name: Prof. Dr. Hamida Idan Salman

University of Kerbala

Date: 31/7/2023

Committee Certification

We are the examination committee, certify that we have read the thesis entitled **(Synthesis, Characterization of SnO₂ Nanoparticles and their application in the Removal of Mefenamic Acid from Aqueous Solutions)** and examined the student **(Hiba Ali Hamzah)** in its content and that in our opinion it is adequate as a thesis for the degree of Master of Science in Chemistry


Chairman Signature: 

Name: Prof. Dr. Hamida Idan Salman

Address: University of Kerbala

Date: 31/7/2023

Member


Signature: 

Name: Oraas Adnan

Address: University of AI-Qadislyah

Date: / / 2023

Member

Signature: 

Name: Assist. Prof. Hasan Faisal Namaa

Address: University of Kerbala

Date: / / 2023

Supervisor and Member 


Assist. Prof. Dr. Aula Mahdi Abd Ali

Address: Department of chemistry

College of Education for Pure Sciences

University of Kerbala

Date: / / 2023

Supervisor and Member 

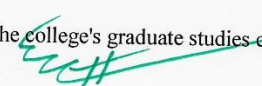
Assist. Prof. Dr. Fouad Fadhil Al-Qaim

Address: College of Science for Girls

University of Babylon/Iraq

Date: / / 2023

Approved by the college's graduate studies committee

Signature: 

Name: Prof. Dr. Hamida Idan Salman (Dean of the college)

Date: / / 2023

31/7/2023

Audit Certificate

I confirm having read the thesis titled (**Synthesis , Characterization of SnO₂ Nanoparticles and their application in the Removal of Mefenamic Acid from Aqueous Solutions**) , by (**Hiba Ali Hamzah**), and have rectified every grammar error I discovered. It can thus be discussed by the examination committee.

Signature: 

Name: Prof. Dr. Muayyad Omran Chiad

Address:

University of Kerbala

Date: / ⁵7 / 2023

Certification by scientific

I attest that this thesis (**Synthesis, Characterization of SnO₂ Nanoparticles and their application in the Removal of Mefenamic Acid from Aqueous Solutions**), by (**Hiba Ali Hamzah**), was evaluate it scientifically and present it for consideration.

Signature:



Name: Asst .Prof.Dr.Majida Hameed Obiad Khazaak

Address : University of Kufa

Date: 31 / 7 / 2023

Signature:



Name: Asst .Prof.Dr.Ahmed Saadoon Abbas

Address : University of Babylon

Date: 1 / 2023 31 / 7 / 2023

Dedication

To my sleeping princess, your daughter has grown up and it's time for the harvest.... my mother, may Allah have mercy on her.

*To my supervisors, Asst. Prof. Dr. Aula Mahdi Al Hindawi and
Asst. Prof. Dr. Fouad fadhil Al-Qaim*

To the one whom I am proud of his martyrdom and carried his name to those whom I have missed all my life and my eyes have never seen (my dear father). And to all the martyrs of the former's regime who were martyred unjustly and treacherously, and were deprived of seeing their children in defense of their wounded Iraq.

To my support, my strength, and my refuge after Allah, to those who preferred

me over themselves ,to my brothers, Dr. Hussein , Eng. Meghath, and My sister Assistant Lecturer Sara.

ACKNOWLEDGEMENTS

My first thanks go to Allah (glory be to Him) who enabled me to complete this work. And to those who are not disappointed by the hope who supported me in every adversity and gave me their strength and patience and chose the right path for me the pure Imams

I have the honour to thank my dear supervisor .Asst. Prof. Dr. Aula Mahdi Al Hindawi for her support and for me throughout the completion of this work. we ask Allah for her health and wellness and for us to remain a lamp for science and knowledge. I ask Allah to give her double what she wishes . It was an honor to be one of her students.

I also would like to extend my sincere thanks and appreciation to my professor Asst.Prof.Dr.Fouad Fadhil-Al-Qaim for his continuous support and encouragement and the distinguished and continuous efforts he showed to accomplish this work. Iask that Allah give him double what he wishes. It was an honor to be one of his students.

I also extend my sincere thanks and gratitude to the dean of the college and the presidency of the chemistry department for the help they have shown me. We ask Allah to grant them continued success and continuous giving.

In conclusion, my thanks and gratitude to my brothers who supported me and stood by my side and endured hardships with me.

Hiba

Abstract

SnO₂ nanoparticles have been prepared using the chemical precipitation method and the green method. Different parameters such as the concentration of the starting materials, reaction time, and pH of the solution were studied to control the growth process of tin oxide nanoparticles. The formation of Tin oxide nanocrystals was confirmed through Field emission Scanning Electron Microscopy (FE-SEM), Energy Dispersive X-ray Spectroscopy (EDX), Fourier transform infrared (FT-IR), X-Ray Diffraction (XRD), and Transmission Electron Microscopy (TEM). The UV-visible curve in the DRS spectrum was used to estimate the band gap energy and it turned out to be 3.7 eV and 4.2 eV for both bare SnO₂ and SnO₂:P.O NPs, respectively. Indicating, the effect of quantum confinement which is believed to appear as the particle's size gets smaller. The adsorption behavior of SnO₂ nanoparticles was demonstrated and it was found that SnO₂ particles can adsorb mefenamic acid (MFA) from aqueous solutions. The maximum removal efficiency for the removal of mefenamic acid using SnO₂:P.O nanoparticles is 97% after 30 minutes. Whilst, bare SnO₂ nanoparticles gave 92 % after 80 minutes.

Thermodynamic estimation (Gibbs free energy ΔG , enthalpy ΔH , and entropy ΔS) showed that the adsorption of the MFA on bare SnO₂ NPs was spontaneous and endothermic, while on the SnO₂:P.O NPs was spontaneous and exothermic. The rates of adsorption of MFA onto the samples were investigated using Pseudo-first order (PFOM) and Pseudo-second order (PSOM). Was found follows a pseudo-second-order model, (PSOM) for all bare SnO₂ NPs and SnO₂:P.O NPs. The adsorption of MFA on bare SnO₂ and SnO₂ :P.O NPs fitted with Freundlich model.

<i>Contents</i>		
Acknowledgements		
Abstract		
Contents		I - III
List of tables		IV-V
List of figure and schemes		V I- VII
List of abbreviations and symbols		VIII-IX
<i>No.</i>	<i>Chapter One: Introduction</i>	<i>Pages</i>
1.1	Nanotechnology	1
1.2	History of nanotechnology	1-2
1.3	Approaches for synthesizing nano materials	2-3
1.3.1	Top-Down approaches	3-4
1.3.2	Bottom-up approaches	4-5
1.3.2.1	Biological synthesis	5-6
1.3.2.1.1	Plant extraction method	6-7
1.4	Semiconductor	7-8
1.5	Nano sized semiconductors	8-10
1.6	Tin oxide SnO ₂ Nano particles	10-11
1.6.1	Applications of tin oxide	12-13
1.7	Portulaca oleracea and its chemical composition	13-14
1.7.1	Health benefits of P. oleracea.	14-15
1.8.	Water pollution with mefenamic acid	15-17
1.9	Adsorption	18
1.9.1	Adsorption Mechanism	19
1.10	Influences of different parameter on the adsorption Process	20
1.10.1.1	Natural of adsorbent nature of the Adsorbent	20
1.10.1.2	Contact time	20
1.10.1.3	Effect of pH	20
1.10.1.4	Temperature	21
1.11	Adsorption Isotherms	21
1.11.1	Langmuir isotherm	21-22
1.11.2	Frundlich isotherm	22
1.12	Adsorption kinetics	23-24
1.13	Thermodynamic study of adsorption	24-25
1.14	Literature Review (SnO ₂ NPs)	25-27
	Aims of Study	28

Chapter two: Experimental part		
2.1	Introduction	30
2.2	Chemicals Materials	30
2.3	Instruments	31
2.4	Samples preparation	32
2.4.1	Preparation of NaOH solution	32
2.4.2	Preparation of HCl	32
2.4.3	Preparation of <i>Portulaca oleracea</i> extract	32-33
2.5	Chemical Precipitation Method	33
2.5.1	Preparation of tin oxide nanoparticles	33-34
2.5.2	The effect of concentration on the formation process of SnO ₂ NPs	35
2.5.3	The effect of the reaction time on tin oxide nanoparticles growth	35
2.5.4	The effect of temperature on the SnO ₂ NPs	35
2.6	Green synthesis approach	36-37
2.6.1	Biosynthesis of tin oxide nanoparticles(SnO ₂ :P.O)	36-37
2.6.2	Optimum conditions for preparing SnO ₂ :P.O NPs	38
2.6.2.1	The effect of extract concentration	38
2.6.2.2	The influence of reaction time	38
2.6.2.3	The influence of PH	38
2.6.2.4	Effect of temperature	39
2.7	Characterization of SnO ₂ nanoparticles	39
2.8	Adsorption process for mefenamic acid (MFA)	39-40
2.8.1	Calibration curve for of M FA solutions	40-41
2.8.2	The influences of different parameters on the adsorption process	41-42
2.8.2.1	The influences of contact time on the adsorption process	41-42
2.8.2.2	The influences of adsorbent dose	42
2.8.2.3	Effect of pH	42
2.8.2.4	Effect of temperature	43
2.9	Adsorption Isotherms	43
2.10	Determination Point of zero charges pH _{PZC}	44
Chapter three: Results and discussions		
3	Introduction	46
3.1	Chemical precipitation method	46
3.1.1	Optical properties of bare SnO ₂ NPs	46
3.1.1.2	The Effect of precursor concentration on the formation process of SnO ₂ NPs	46-47
3.2.1.2	The Effect of reaction time on the absorption of tin oxide	47-48

	nanoparticles	
3.2.1.3	The Effect of pH on the SnO ₂ formation	48-49
3.2.1.4	The effect of temperature on the formation of SnO ₂ NPs	49-50
3.2.1.5	The optical band gap energy	50-51
3.2.2.1	FTIR analysis	52
3.2.2.2.	XRD analysis	53-54
3.2.2.3	Morphological and EDX Analysis	54-55
3.3	Biosynthesis approaches	55
3.3.1	Optimal conditions for preparing SnO ₂ :P.O nanoparticles	55
3.3.1.1	The influence of extract amount	55-56
3.3.1.2	Effect of reaction time on SnO ₂ :P.O nanoparticles growth	57
3.3.1.3	The effect of pH on the formation of SnO ₂ :P.O NPs	58
3.3.1.4	The effect of temperature on the SnO ₂ :P.ONPs formation	59
3.3.1.5	Band gap energy for SnO ₂ :P.O nanoparticles	60
3.2.2	Structural properties of SnO ₂ :P.ONPs	61-62
3.3.2.1	FT-IR analysis	62-63
3.3.2.2	XRD analysis	63-64
3.4	Adsorption behaviour of SnO ₂ nanoparticles	64
3.4.1	Study of factors effecting MFA removal from aqueous solutions using SnO ₂ NPs and SnO ₂ :P.ONPs as adsorbent t surfaces	64
3.4.1.1	Effect of the contact time on the adsorption process	64-66
3.4.1.2	The influence of SnO ₂ particles dose	66-67
3.4.1.3	Effect of initial concentration of Mefenamic acid	68-69
3.4.1.4	Effect of PH	69-70
3.4.1.5	The zero charges pH _{PZC}	71
3.4.1.6	Effect of temperature	72-73
3.4.1.7	Calculation of thermodynamic functions	74-77
3.4.1.8	Adsorption Isotherms	78-84
3.5	Adsorption Kinetics	85-86
3.6	Conclusions	88-89
3.7	Future works	89
	References	90-103

	<i>List Tables</i>	<i>Page</i>
1.1	Physical-chemical properties of SnO ₂	11
1.2	Properties of physisorption and chemisorption	21
2.1	Chemical materials and their formula	30
2.2	Instrumentation and manufacturers	31
2.3	Statistics data of calibration for different concentrations of MFA	41
3.1	The removal efficiency of MFA using two surfaces bare SnO ₂ and SnO ₂ :P.ONP _s at different contact times	65
3.2	Effect of adsorbent dose on the removal efficiency of MFA on bare SnO ₂ and SnO ₂ :P.O nanoparticles	67
3.3	The effect of initial MFA concentration on adsorption using bare SnO ₂ NPs as an adsorbent surface at 298 k	68
3.4	The effect of initial MFA concentration on adsorption using SnO ₂ :P.O NPs as an adsorbent surface	68
3.5	The effect of the pH function on the removal efficiency of MFA removal on the surfaces of bare SnO ₂ NPs and (SnO ₂ : P.O)NPs at temperature 298 K	70
3.6	Effect of temperature on adsorption of MFA on the SnO ₂ NPs at different temperatures.	72
3.7	Effect of temperature on adsorption of MFA on the SnO ₂ : P.O NPs at different temperatures.	73
3.8	Values of the equilibrium constant for MFA using bare SnO ₂ NPs at different temperatures	76
3.9	Thermodynamic adsorption parameters of the mefenamic acid over bare SnO ₂ NPs	76
3.10	Values of the equilibrium constant for MFA using SnO ₂ :P.O NP _s at different temperatures.	76
3.11	Thermodynamic adsorption parameters of the mefenamic acid SnO ₂ :P.ONPs at different temperature	77
3.12	Ce and qe values for the adsorption of MFA on bare SnO ₂ NPs at different temperatures	78
3.13	Ce and qe values for the adsorption of MFA on to SnO ₂ :P.ONPs samples at different	79
3.14	Data on MFA adsorption on a surface SnO ₂ NPs at different temperatures by applying Langmuir equation	81
3.15	Data on MFA adsorption on a surface SnO ₂ NPs at different temperatures by applying Freundlich equation	81
3.16	Langmuir and Freundlich parameters of adsorption isotherms MFA on bare SnO ₂ NPs at (298 – 328) K	82
3.17	Data on MFA adsorption on a surface (SnO ₂ :P.O) NPs at different temperatures by applying Langmuir equation	83
3.18	Data on MFA adsorption on a surface (SnO ₂ :P.O) NPs at different temperatures by applying Freundlich equation	83

3.19	Langmuir and Freundlich parameters of adsorption isotherms MFA on (SnO ₂ :P.O) NPs at (298 – 328) K	84
3.20	Kinetic parameters for pseudo-first-order and pseudo-second-order	85

	<i>List of figure and schemes</i>	<i>Page</i>
1.1	Illustration shows the synthesis of nanostructure using top-down and bottom-up methods.	3
1.2	Methods for biosynthesis of nanoparticles	6
1.3	Diagram showing differences among the three types of materials: insulator, semiconductor and conductor	8
1.4	Simplified optical transition of a semiconductor. (a) Direct band gap, and (b) indirect band gap	10
1.5	Crystal structure of SnO ₂ in the rutile phase	11
1.6	Potential applications of SnO ₂ NPs	13
1.7	Photo showing the chemical structure of P. oleracea	17
1.8	P.Oleracea plant	18
1.9	Chemical structure of MFA	20
1.10	Mechanism of the physical and chemical adsorption	22
2.1	Images showing the preparation steps of Portulaca oleracea extract	33
2.2	Schematic showing the formation process of SnO ₂ nanoparticle using chemical precipitation method.	34
2.3	Diagram showing the Biosynthesis formation of SnO ₂ nanoparticles	37
2.4	UV-Visible absorption spectrum of MAF	40
2.5	calibration curve of Mefenamic acid	41
3.1	UV-Vis absorption spectra of tin oxide nanoparticles as a function of the tin chloride concentration	47
3.2	The optical absorption spectrum of SnO ₂ nanoparticles at different reaction time, the concentration of the precursor was (0.01 M) .	48
3.3	The effect of pH on the absorption spectra of as-prepared SnO ₂ nanoparticles, the concentration of the precursors was 0.01 M and the reaction time was 3 hour	49
3.4	UV-Vis absorption spectra of as-prepared SnO ₂ nanoparticles as a function of temperature. The concentration of the precursor was 0.01 M and the reaction time was 3 hour.	50
3.5	UV-DRS spectrum of bare SnO ₂ particles (a) and the optical band gap energy estimated from Kubelka-Munk formula (b)	51
3.6	FTIR spectrum for SnO ₂ nanoparticles formed from chemical precipitation method	52
3.7	XRD pattern of synthesized SnO ₂ nanoparticles calcined at 600°C	54
3.8	FESEM image of SnO ₂ particles (a), TEM image of synthesized SnO ₂ nan crystals, and (c) EDS graph.	55
3.9	UV-Vis spectra of tin oxide nanoparticles formed in the presence of p.oleracea extract as a function of the extract concentrations after one hour of starring.	56
3.10	The optical absorption spectrum of SnO ₂ :P.O nanoparticles at different reaction time	57
3.11	The effect of pH on the absorption spectra of as-prepared SnO ₂ nanoparticles, the concentration of the precursors was 0.01 M and the reaction time was 1 hour	58
3.12	UV-Visible spectra of SnO ₂ :P.O nanoparticles at different temperatures at after 1hour of stirring.	59

3.13	UV-DRS spectrum of SnO ₂ :P.O NPs((a) and the band gap energy estimated from Kubelka-Munk formula((b	60
3.14	FE-SEM images for the biosynthesized (SnO ₂ :P.O) nanoparticles formed in the presence of Portulaca oleracea extract	61
3.15	TEM image of SnO ₂ nanoparticles (a) and EDX chart showing the elemental analysis (b)	62
3.16	FT-IR analysis of (SnO ₂ :P.O) nanoparticles annealed at 600 oC	63
3.17	XRD pattern of biosynthesized (SnO ₂ :P.O) nanoparticles calcined to 600°C	64
3.18	The influence of contact time on the removal efficiency of MAF used bare SnO ₂ NPs,SnO ₂ :P.ONPs surface ,(T=298K ,PH 6)	66
3.19	The influence of dose on the removal efficiency of MAF used SnO ₂ NPs,SnO ₂ :P.ONPs surface,(T=298K,PH 6)	67
3.20	The influence of initial MFA concentration on the removal efficiency of MAF used SnO ₂ NPs,SnO ₂ :P.ONPs surface ,(T=298K ,PH 6)	69
3.21	The influence of solution pH on the removal efficiency of MAF used SnO ₂ NPs,SnO ₂ :P.ONPs surface ,(T=298K , 0.6g)	70
3.22	Point Zero charge of bare SnO ₂ NPs and SnO ₂ :P.O NPs , (contact time 24 h, and mass adsorbents 0.6 g).	71
3.23	Effect of temperature on the adsorption of MAF on(bareSnO ₂ and SnO ₂ :P.O) NPs	73
3.24	Plot Lnkeq against the absolute temperature. of the adsorption MFA on to bare SnO ₂ NPs and SnO ₂ :P.O NPs.	77
3.25	The adsorption isotherm for MFA on the bare SnO ₂ and SnO ₂ :P.O NPs at different temperatures.	79
3.26	Freundlich and Langmuir isotherm for adsorption of MFA on surface bare SnO ₂ NPs	82
3.27	Langmuir and Freundlich isotherm for adsorption of MFA on surface SnO ₂ :P.O NPs	84
3.28	Adsorption kinetics of MFA on bare SnO ₂ NPs pseudo-first-order model and pseudo-second-order model	86
3.29	Adsorption kinetics of MFA on SnO ₂ :P.O NPs pseudo-first-order model and pseudo-second-order model	86
3.30	UV-Visible absorption spectrum of MAF before and after the adsorption	87

Table list of abbreviations

Abbreviations and symbols	The Meaning of symbol
E_g	Band gap energy
θ	Bragg angle.
SnO ₂ : P.O	Tin oxide nanoparticles in the presence of Portulaca oleracea
C_e	Concentration of MFA at equilibrium
CB	Conduction Band
eV	electron Volt
FE-SEM	Field Emission-Scanning Electron Microscopy
FTIR	Fourier Transfer Infra-Red Spectrometer
FWHM	Full width half –maximum
C_o	Initial Concentration
n	Integer called the order of reflection (n=1, 2, 3)
MFA	Mfenamic acid
NPs	Nanoparticles
D	The average crystallite size
K	The constant crystal lattice
β	The full width at half maximum in radians
%R	The percentage of MFA removal
λ	The wavelength of x-ray.
TEM	Transmission Electron Microscopy
P.O	Protulaca Oleracea
UV-Vis	Ultraviolet-visible spectrophotometer
VB	Valance Band
XRD	X-Ray Diffraction

SnO ₂	Tin oxide
K	Kelvin
kJ	Kilo joule
L	Litter
M	Molarity
mg	Milligram
min	Minute
mL	Millilitre
nm	Nanometre
R ²	Correlation coefficient
Rpm	Rounds per minute
T	Temperature
λ_{\max}	Wavelength at maximum absorption
G	Gram
E.X	Extract
PFOM	pseudo-first-order kinetic model
PSOM	pseudo-second -order kinetic model
EDX	Energy Dispersive X-ray Spectroscopy
DRS	Diffuse reflectance spectroscopy

CHAPTER
ONE
INTRODUCTION

1.1 Nanotechnology

Nanotechnology has been considered to be one of the most intriguing fields focusing on the creation and manipulation of objects at the nanoscale level. At this scale, atoms and molecules work differently compared to their bulk¹. One of the particular interest in nanoscience is that all the essential properties (melting point, hardness and conductivity) of nanosized materials are size dependent. For example the nano-sized conductive wire do not follow ohm's law, instead, the electrons flow through the nanowire cross section producing an electrical current. Furthermore, Copper (Cu) in its bulk form can be bent freely, but when its size decreased to less than 40 nm, it forms a highly rigid structure². Moreover, it is well known that bulk gold is inert chemically and cannot be used as a catalyst, however, as gold dimensions shrink to the nanoscale level, it becomes an excellent catalyst^{3,4}.

Nanotechnology could be used in many different electronics, communications, and computing applications, providing smaller, faster, and more portable systems. These systems can store large amounts of data⁵.

Nanotechnology is concerned with the creation of particles with one or more dimensions that fall within the range of 1 to 100 nm, which is called nanoparticles⁵. These particles have incredible physical and optical properties compared to their bulk counterpart due to their small sized. This tiny size increased the surface-to-volume ratio and then leading to increment in the number of surface atoms compared to those inside⁶. A consequence, many applications have been proposed in different fields from medicine to manufacturing to computing, and even to textiles and cosmetics⁷.

1.2 History of nanotechnology

The term nanotechnology was proposed many years ago. It is not possible to specify a specific date for the beginning of nanotechnology, however, it was found that the colloidal Au nanoparticles were used as raw materials in the manufacturing of glasses in the middle ages As well as, the color of the ancient roman cup, which

was made in the 14th century for King Lycurgus, was changed from red to green depending on the light source position. The color changing has been interpreted in terms of the presence of gold and silver nanoparticles (their size ranged from 50–100 nm) within the cup. These particles absorb and scatter light differently according to their size^{8,9}.

Nanotechnology concept was first introduced by the American physicist Richard Feynman (1959) in the “American Physical Society”. Feynman said in his talk that there are several rooms in the bottom, suggesting it is possible to manipulate matter at a tiny scale and provide a variety of surprising and interesting use¹⁰.

In 1990s Norio Taniguchi was first defined nanotechnology term in Tokyo. He defined "nanotechnology" as a process of separation and merging of materials by manipulating one atom or one molecule¹¹. The invention of electronic and probe microscopic techniques in 1980s helps the speeding up the researchers to developing the nano science¹². At present, the field of nanotechnology has emerged as an amazing area offering incredible applications.

1.3 Approaches for synthesizing nanomaterial

There are different physical and chemical methods for successfully synthesizing NPs as presented in (Figure 1.1). One can classify all these methods into two main approaches that can apply to any research in the field of nan scale science bottom-up approaches and top-down approaches. Each of which has specific characterization and application.

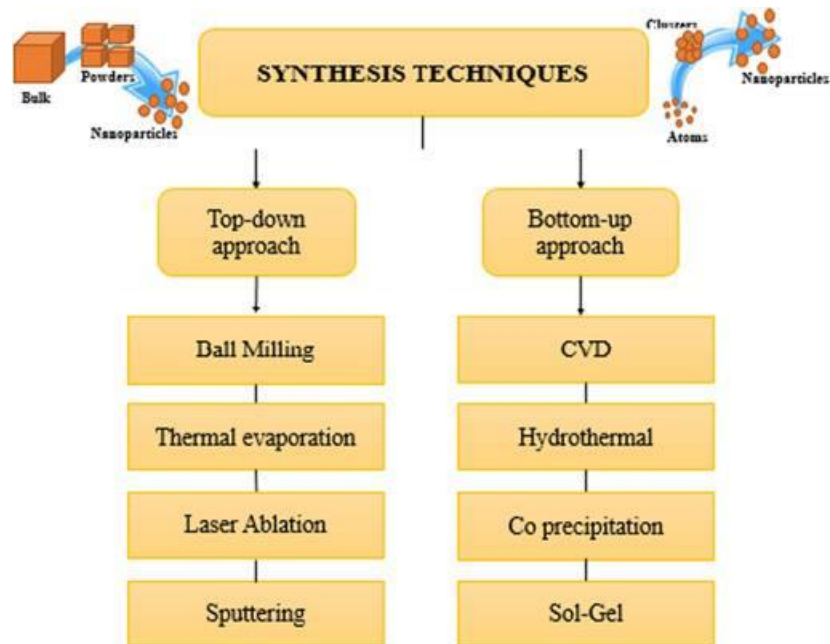


Figure 1.1 Illustration showing the synthesis of nanostructure using top-down and bottom-up methods. This illustration was taken from ref³.

1.3.1 Top-Down approaches

In this technique, bulk materials break down into smaller molecules in the nano sized level using different chemical or mechanical form of energy. Different methods have been used in top-down approaches, such as physical vapour deposition, mechanical milling, laser ablation, Lithography and etc.¹³.

Lithography technique is an example of top-down approaches which is widely used in the production of printed circuit boards and computer boards. However, it is costly due to the need for venture sources, such as electron beams with high energies³.

Mechanical milling or ball milling is a means used for synthesis nanoparticles which involved transferring kinetic energy from the grinding machine to the

substances undergoing reduction¹⁴. Particles produced by this technique have dimensions between a few tens and hundreds of nanometres, meaning it is not possible to reach very small sizes. Furthermore, the resulted particles could have some pollutants from the milling media and defect in their surface resulting from attrition¹⁵. Generally, top-down approaches have been widely used for the formation of nanostructures but they have some disadvantages such as surface imperfections which can cause serious restriction as the material surface structure plays a vital role in surface chemistry and physical properties of a material and the very small size can hardly be reached. Such tiny particles may be significant in many potential applications, like catalysis.

1.3.2 Bottom-up approaches

The basic idea behind this technique is the synthesis process of nanostructures starts with the self-assembly of atoms or molecules into clusters and afterwards the formation of particles at the nano scale range. Chemical vapour deposition (CVD), Sol-gel and biological synthesis are examples of bottom-up method¹⁶.

Sol-gel technique is the most common rout to prepare metal and metal oxide nanoparticles involves converting sol (liquid phase) to the gel (solid phase)^{17,18}. To form metal oxide nanoparticles, the resulted gel should be dried and calcinated at various temperatures. The sol-gel method has a number of benefits, including the ability to manufacture metastable materials at moderate temperatures with high purity and compositional homogeneities. The shape, porosity, and composition of nanostructures can also be controlled within this method to produce materials with high surface-to-area ratios.^{19,20}

Chemical precipitation method is another example for the bottom-up technique²¹. This process includes three steps: chemical reaction followed by nucleation and then the growth of crystals. One of the limitations of this technique is the difficulty in controlling the shape and size of particles due to the agglomeration process which could be happened during the formation process, leading to broad size particle distribution. Protecting agents (capping agents) has been proposed to solve this problem and enable the fabrication of controlled particles with narrow size distribution. It is expected that by introducing these protecting agents to the formation process, the addition of further atoms will be stopped from being attach to the surface of as-prepared particles.

In this method, the particles growth and agglomeration could effect by several parameters, for instance, the PH of solution, reaction time, temperature or/and the concentration of precursors. The resulting precipitate is a subject to several processes such as washing and drying.

Chemical vapor deposition is a means utilized for synthesis nanoparticles which involved the reaction of reactive components with catalyst or surface of template. This method is considered as an economical way to produce carbon nanotubes by passing any source of carbon (methane or acetylene) over catalyst such as Ni or Fe²². When the formal decomposed into carbon atoms, the carbon nanotubes are produced via the catalyst^{23,24}.

1.3.2.1 Biological synthesis

Biosynthesis techniques have drawn attention because of their incredible features such as simple, low-cost and eco-friendly. They relies on using biomolecules present in the plant, yeast and bacteria (see Figure 1.2) for the synthesis of nanomaterial. It is believed that these molecules can serve as reducing

agents and capping agents which hopefully controlled the growth process of nanomaterial ²⁵.

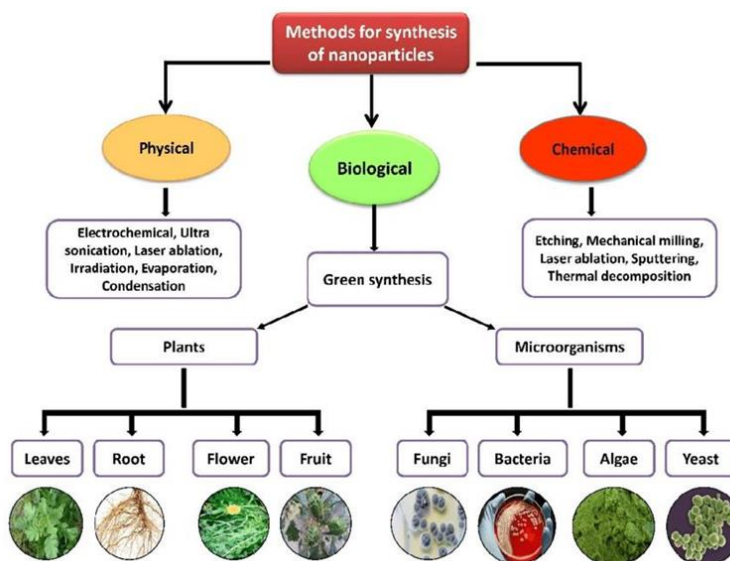


Figure 1.2 Methods for biosynthesis of nanoparticles. This diagram was taken from ref ²⁵

1.3.2.1.1 Plant extraction method

Plant extraction method, which is class on green synthesis method, have been recently used for the formation of metal and semiconductor nanomaterial. Various part of plants (e.g. leaves, seeds, roots and stems) can be used as capping agents, stabilizing agents and reducing agents ²⁶. Unlike microorganisms, plant extract has many potential benefits in the term of nanoparticles formation. For instance, the formation process of nanoparticles using plant extract takes several minutes to few hours, whereas, the bio-particles formed from microorganisms could take few days under ambient conditions ^{27,28}. As well as, biological risk could be observed if fungi or bacteria were used in the growth of nanomaterial compared to that with plant extract. The reason for this is many microorganisms during their cultivation

secrete toxins which causing health problems. Finally, it is easy to control the bio-fabricated particles formed through using plant extract by changing the extract concentration^{29,30}. The scientists believe that plant extracts contain substances such as terpenoids, sugars, phenolic acids, bioactive alkaloids, proteins, and polyphenols, which play a significant role in the reduction process of the desirable metal.

In literature, many studies have been reported about producing semiconductor particles using plant extract. However, few works were done about using plant extract for preparing tin oxide nanoparticles. Therefore, here we report, for the first time, the preparation of tin oxide nanoparticles from plant extract. The extract may act as a capping agent which expects to prevent or reduce the aggregation process of SnO₂ nanoparticles and control their stability.

1.4 Semiconductor

The term semiconductor refers to materials that have properties fall between conductors and insulators as shown in Figure (1.3). As the temperatures reached the absolute zero, they act as insulators but when the temperature is raised close to room temperature or slightly more, their features begin to approach the features of conductive materials, and their conductivity to the electric current increases³¹. Semiconductors can be found two forms: compound such as zinc sulphide and cadmium sulphide or free element such as germanium and silicon³².

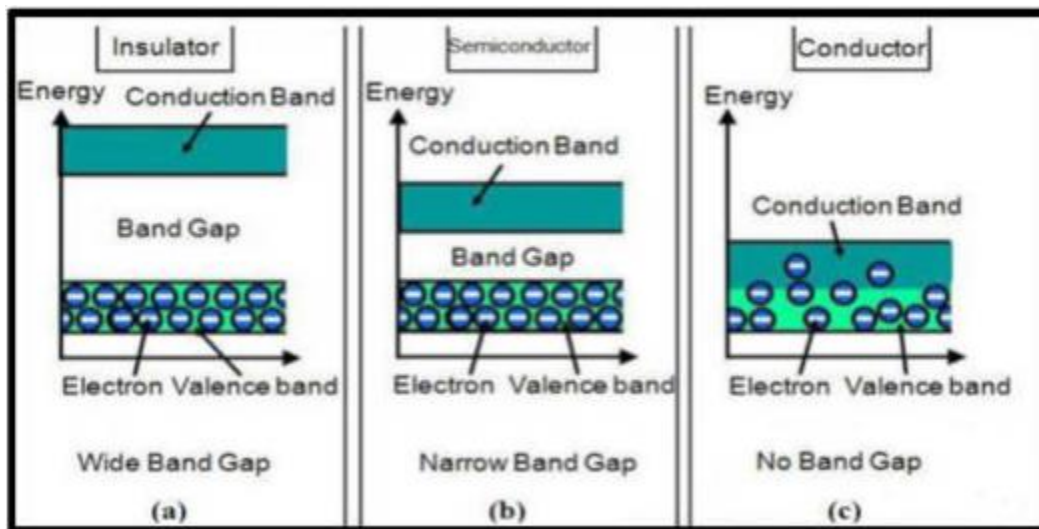


Figure 1.3 Diagram showing differences among the three types of materials: insulator, semiconductor and conductor. This diagram was taken from ref. ³³.

1.5 Nano sized semiconductors

As the size of semiconductor materials approached the nan scale level, new features will appear which differ from the bulk counterpart and discrete molecules. It is well known that as the particle size becomes less than 10 nm, the quantum mechanics and the effect of size quantum confinement becomes obvious³⁴. Atoms in semiconductor nanoparticles move closer to one another and start to form bonds³⁵. The atoms' energy levels begin to split into groupings of closely spaced energy levels.

Atomic equilibrium occurs when they reach the lowest energy band, which is made up of valence orbitals. The valence band is the lowest, which is entirely or partially filled with electrons, and in fact is unable to be free of them.

The second band, known as the conduction band, which is empty of electrons and has energies higher than that of the valence band. The energy difference between

valence and conduction bands is known as the band gap. It can be used to monitor the electrical and optical properties, and it is also responsible to the conductivity of semiconductors. Electrons may transfer from the valence band to the conduction band through the band gap if they absorb energy from an external source that is equivalent to or greater than the band gap energy, such as heat energy, light energy, or the impact of an electric field³⁶.

As a result, the electron in the valence band will excite leaving a hole in the conduction band. The hole and electron produce together an exciton that collapses quickly since they have the same magnitude but different polarities. Therefore, as the particle size drops to less than the exciton size. At that size, the electrons movement is restricted because they are unable to move as freely and consequently the confined electrons react differently with the light and this phenomenon called quantum size effect³⁷. In semiconductors, there are two different types of band gaps direct and indirect band gaps, as shown in Figure 1.9.

The direct band gap occurs, when the valence band's maximum is directly above the conduction band's minimum in momentum space. Therefore, there is no need for a momentum transfer to move the electron from the valence band to the conduction band. However, the lowest portion of the conduction band energy is not present in indirect band-gap semiconductors³⁸.

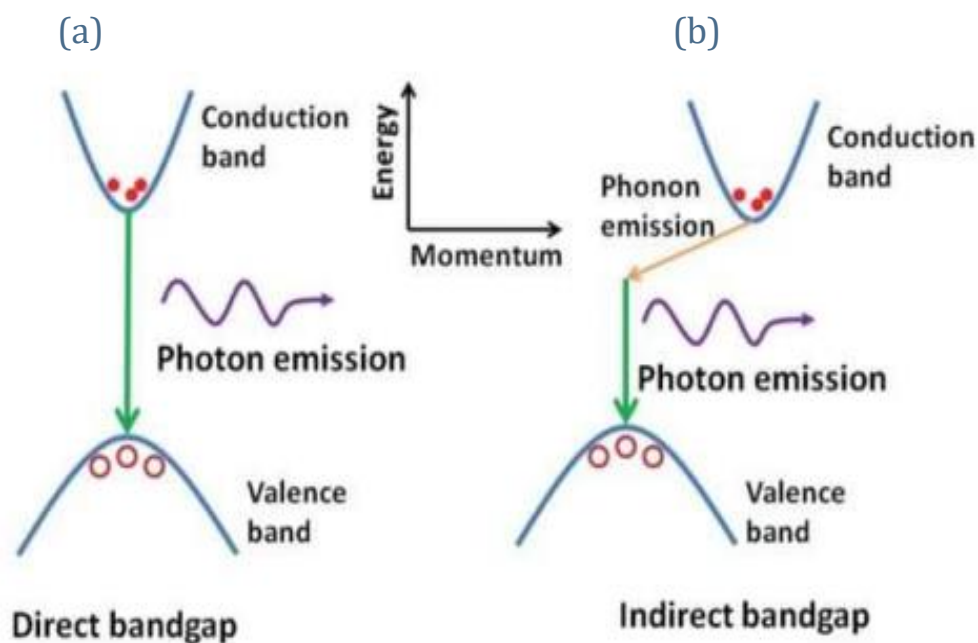


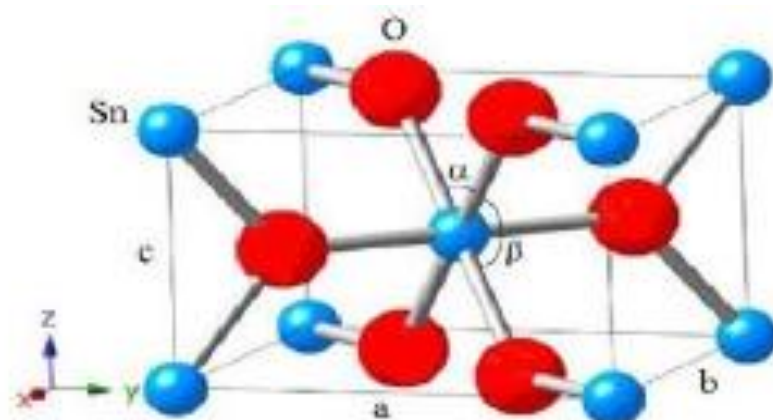
Figure 1.4 Simplified optical transition of a semiconductor. (a) Direct band gap, and (b) indirect band gap³⁸.

1.6 Tin oxide SnO₂

Tin dioxide (SnO₂) has been studied extensively and used in various fields such as gas sensors, catalysts, transparent conductors, Li-batteries. SnO₂ is an n-type semiconductor that has a wide band gap (3.6 eV) which is activated only by UV irradiation^{39,40}. It has a rutile-type tetragonal shape (see figure 1.5)

Table 1-1 Physical-chemical properties of SnO_2 ⁴¹.

Synonyms	Cassiterite, tin(IV) oxide, tin oxide, tin dioxide, stannic oxide
Formula	SnO_2
Structure	Tetragonal
Molecular weight	150.69 g/mole
Appearance	Crystalline solid
Melting point	1500-1630°C
Boiling point	1800-1900°C
Density	6.90 g/cm ³
Water solubility	Insoluble (soluble in concentrated sulphuric acid)

**Figure 1.5** Crystal structure of SnO_2 in the rutile phase

1.6.1 Applications of tin oxide

Tin (IV) oxide nanoparticles (SnO_2 NPs) have attracted great attention due to their properties leading to using in a number of applications.

Owing to their band gap, physical and chemical properties, and chemical stability, they used in the pharmacological, paint, and dye industry effluent degrading processes⁴². It is well Known that tin oxide nanoparticles are employed either as adsorbents or photo catalysis to remove water pollutions because of their small size and optical characteristics^{43,44}

Tin oxide nanoparticles can be utilized as antibacterial agents as they have the ability to pass the cell membrane readily due to their smaller size in comparison to traditional medicines, they may transport entire body parts^{45,46}

SnO_2 can be used in transparent conducting films⁴⁷, lithium rechargeable batteries⁴⁸, catalytic materials⁴⁹.

Moreover, SnO_2 nanoparticle is considered one of the most transparent conducting oxide (TCO) used intensively in the manufacturing of solar cell. These transparent materials are unable to absorb photons with energy value below their band gap value, consequently, allow visible light to pass through⁵⁰

Batzill group reported that SnO_2 nanoparticles can be used as an oxidation catalyst because they possess multivalent oxidation states, so it is easy to give up the lattice oxygen to the adsorbed molecules when they react. In other words, the surface of SnO_2 can be easily re-oxidation within the catalytic oxidation reactions⁵¹.

Tin oxide particles have high electrical conductivity due to the presence of oxygen vacancy within their crystal that is properly resulted through the formation process

of tin oxide crystals. This property is reason for using SnO₂ particles as an essential component in gas sensor⁵², where the conductivity is altered in response to the ambient gases. Recent work by Hui Li's group has showed that SnO₂ nanoparticles are capable to inhibit the cell proliferation in oral cancer⁵³.

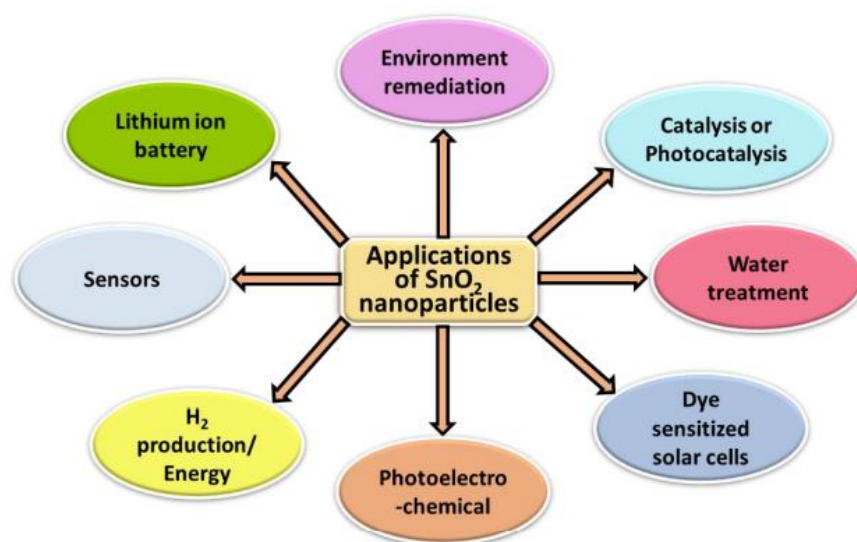


Figure 1.6 Potential applications of SnO₂ NPs⁵⁴.

1.7 Portulaca oleracea and its chemical composition

Portulaca oleracea (commonly known purslane) is an annual herbs, classified as a part of the Portulacaceae family. Although, the origin of Portulaca was India, it has widely spread over the tropical regions⁵⁵. Portulaca oleracea has a slightly sour flavour due to the presence of a significant amount of vitamin (C, A). As well as It contains many bioactive compounds such as flavonoids, alkaloids, terpenoids, proteins, and carbohydrates. It has been conceded as a rich source of minerals such as phosphorus, calcium, magnesium and zinc. In addition, it consists of compounds like omega-3 fatty acids, especially α - linoleic acid , gamma- linoleic

acid and linoleic acid, which are not generally synthesized in terrestrial plants, all contributing to its health benefits. It has been found that water extract from purslane flowers has greater phenolic content than its stem and leaves. Their leaves show higher concentrations of total flavonoids and ascorbic acid. In addition, leaves contain higher β -carotene content than stem⁵⁶.

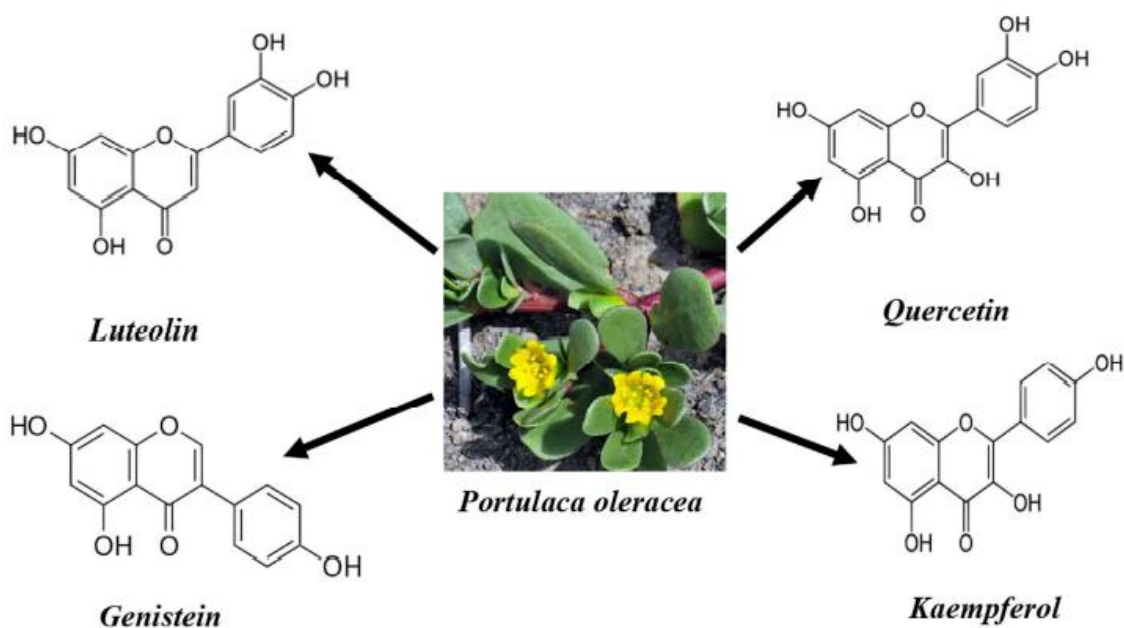


Figure 1.7 Photo showing the chemical structure of *P. oleracea*⁵⁷.

1.7.1 Health benefits of *P. oleracea*.

As shown in (Figure 1.8) that both the leaves and stems of *P. oleracea* are rich with bioactive compounds. Therefore, they play a significant role in health care. Moreover, can be used as anticancer, anti-insomnia, anti-inflammatory, antidiabetic and antiseptic⁵⁸.

Due to the modification of blood lipids, metabolism, and reduction of blood glucose, the polysaccharides contained in *Portulaca oleracea* have the potential to be therapeutic agents for the treatment of diabetes mellitus.

Owing to the presence of high concentration of vitamin A, *Oleracea Portulaca* has been used in treating eyes and improving vision. . As well as, this plant shows a strong antibacterial, antifungal, and antiviral activities because of the presence of ascorbic acid, -tocopherol, and B-complex vitamins, such as niacin, pyridoxine, and riboflavin.⁵⁹.

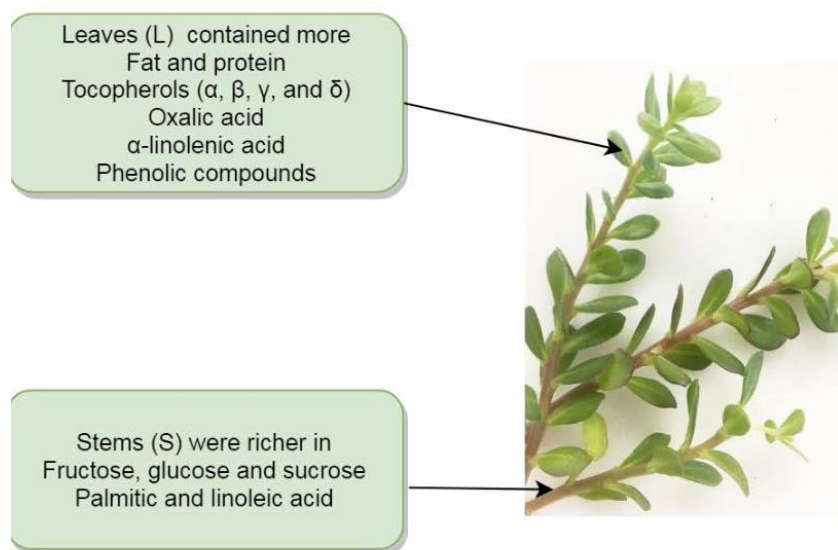


Figure 1.8 *P. oleracea* plant⁵⁹ .

1.8 Water pollution with mefenamic acid

Residues from pharmaceuticals have been considered a major problem affecting the environment and living organisms especially antibiotics and steroids which cause resistance in natural bacteria⁶⁰. Mefenamic acid (MFA) is one of those pharmaceutical compounds that can cause serious problems to the environment if it is not being treated. It has the chemical structure of $C_{15}H_{15}NO_2$, which is shown in(

Figure 1.9) consisting of an amino benzoic acid, where one of the hydrogen atoms (attached to the nitrogen atom) is removed and restored by the group of 2,3-dimethylphenyl ⁶¹.

MFA is a non-steroidal anti-inflammatory medicine used extensively as analgesics. This acid has the ability to ease muscle, menstrual and back pain. However, it causes a series of problems to the environment and organisms due to releasing toxic metabolites within surface, drinking water and wastewater. It is shown that the exposure of organisms to a small amount of MFA for a long time can cause skin rash ⁶².

Researches have performed techniques to determine the amount of this acid in water sources, for example, high performance liquid chromatography and spectrophotometric techniques^{61,63}. Many purification techniques have been proposed to remove this acid from the water before pushing into environment. Advanced oxidation processes (AOPs) ⁶⁴ are the most common method used to treat water from mefenamic acid. The idea behind this method is producing reactive oxidants (OH[·]), that have the ability to oxidize any compound found in water, fragmented and then converted into small inorganic molecules⁶⁵. This hydroxyl radical can be easily produced using either primary oxidant (such as H₂O₂, O₂ and O₃), catalyst (TiO₂), or energy source (UV light). Membrane bioreactor (MBR) was also used to get rid of mefenamic acid from wastewater and the results showed that about 74% of mefenamic acid was removed ⁶⁶. Although these techniques are used till now, many issues associated with due to the uses of hazardous chemical reagents and energy which can cause production of some reactive states, In addition, these techniques required long time to remove the pharmaceutical residues.

Physiochemical techniques such as adsorption have shown high efficiency in removing pharmaceutical compounds. Different adsorbents have been utilized for adsorbing mefenamic acid (MFA) from water sources such as activated carbon, which showed a maximum removal efficiency of 60% after 120 minutes when combined with ultraviolet radiation⁶⁷.

According to Rodrigo's team, 100% and 96% of MFA were removed from wastewater when activated carbon and red mud, respectively, were used as adsorbents before oxidation with chlorine⁶⁸. In 2020, a novel polyuria formaldehyde with bentonite clay composite was utilized as an adsorbent for removing MFA. The results show that this adsorption is physical in nature and the adsorption potential is 16 mg/g at 47°C and pH of 1.5. Recently, semiconductor nanostructures have been reported as good adsorbents for removing dyes and pharmaceutical compounds from water source and drink water⁶⁹⁻⁷².

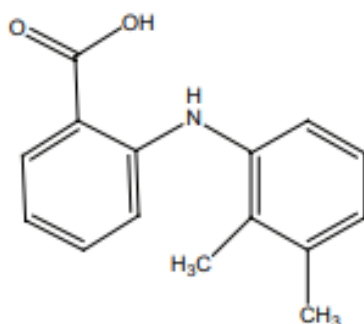


Figure 1.9 Chemical structure of MFA⁶¹.

1.9 Adsorption

Adsorption is the process of collecting the adsorbate (gaseous or liquid) on the surface of a solid substance⁷³⁻⁷⁵. In other word, it is a process in which number of molecules can bond chemically or physically to the active sites on the surface of the solid, leading to the formation of one or more layers of atoms or molecules on the solid surface.⁷⁶ As shown in(Figure 1.2), adsorption can be classified into two types: physisorption (physical adsorption) and chemisorption (chemical adsorption) depending on the connection type between the adsorbent surface and the adsorb ate molecule. The major characterization of these types will be summarized in Table^{60,77,78}.

Table 1. 2 Properties of physisorption and chemisorption

Physisorption	Chemisorption
This type of adsorption leads to the formation of many molecular layers on the adsorbent surface and is called multi-layer adsorption.	This type of adsorption leads to the formation of a single molecular layer on the adsorbent surface and is called monolayer adsorption.
It occurs at low temperatures	It usually occurs at high temperature
It is a reversible adsorption	It is an irreversible adsorption
The nature of the bonding forces is that of van der Waals	The nature of the bonding force is chemical bonds
It does not require activation energy	It needs activation energy
It is a multi-layered phenomenon	It is a monolayer phenomenon

1.9.1 Adsorption Mechanism

The following steps serve as a summary of the adsorption mechanism⁷⁹.

- ❖ The solute molecules reach the surface of the adsorbent.
- ❖ The solute molecules will bind to the adsorbent surface
- ❖ The solute molecules leave the adsorbent surface sites into the pores on the adsorbent surface
- ❖ The solute molecules will overlap and the sites available to it on the inner surfaces will be associated with the pores of the adsorbed solid surface(see Figure 1.10)

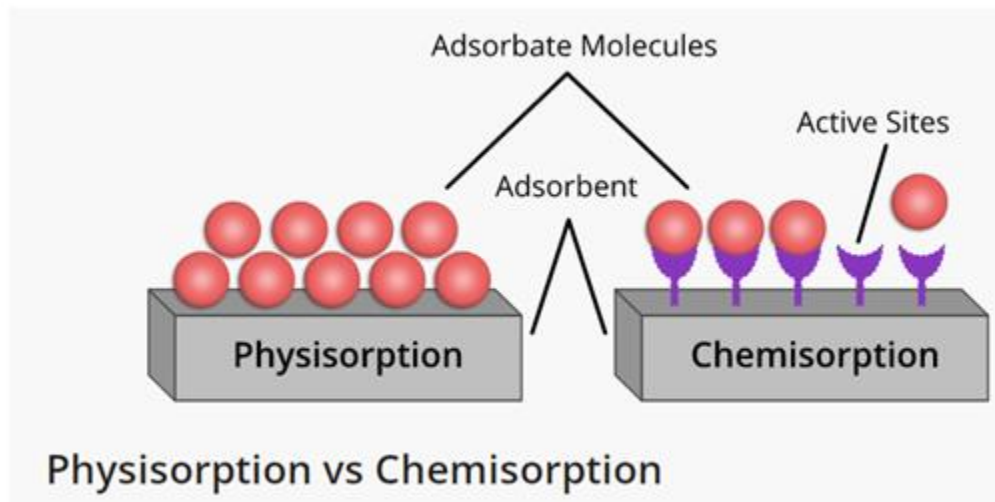


Figure 1.10 mechanism of the physical and chemical adsorption

1.10 Influences of different parameter on the adsorption Process

1.10.1.1 The nature of the adsorbent

The type of adsorbent surface and the presence of polar groups on the surface have a great effect on the adsorption process, as well as, the surface area and the size of the pores. The adsorbent material with narrow pores cannot adsorb particles with a size larger than the size of pores. Therefore, increasing the surface area leads to an increase in the adsorption due to increasing the number of active sites on the surfaces, and consequently increasing the adsorption capacity⁸⁰.

1.10.1.2 Contact time

It is the time in which the equilibrium occurs between the adsorbent and the adsorbate molecule, or it is the period of time after which there is no decrease in the concentration of the solution, and this time can be ranged from few minutes to weeks⁸¹.

1.10.1.3 Effect of pH

The pH function has a potential effect on the adsorption process. Many variables can participate in this process, such as the nature of the chemical state of the adsorbent surface, the adsorbate molecule, and the solvent. It is expected that competition will occur as a result of the interaction of H^+ or OH^- ions with the solute, surface, or solvent. Such interaction can change the chemical state, which may lead to an increase or decrease in the adsorption capacity^{82,83}.

1.10.1.4 Temperature

Temperature plays an important role in the adsorption process. The effect of temperature relies on the type of adsorption and the nature of both the adsorbate and the adsorbent. It was found that the adsorption process increases with increasing the temperature in endothermic adsorption processes. On the other hand, for exothermic adsorption processes; the adsorption capacity increases when the temperature increased⁸⁴.

1.11 Adsorption Isotherms

It is defined as the relationship between the amount of the adsorbate material Q_e (mg/g) and the concentration of the adsorbate material at the equilibrium state (C_e), at a constant temperature. The most important isotherms are:

1.11.1 . Langmuir isotherm

The scientist Langmuir proposed an equation to explain the adsorption of gases on the surfaces of solids. Langmuir assumed that the molecules are adsorbed on a fixed number of adsorption sites on the surface of the adsorbent. These sites have equalized energy, therefore, each site can be occupied by only one molecule. These particles don't interfere with each other or with other molecules in the solutions. Thus, one layer of adsorbed particles be formed on the surface. Langmuir isotherm can be expressed mathematically as follows:⁸⁵

$$Q_e = \frac{abc_e}{1+bc_e} \quad \dots\dots\dots 1.1$$

Equation (1) can be written in linear form to become as follows:

$$\frac{C_e}{q_e} = \frac{1}{ab} + \frac{C_e}{a} \quad \dots\dots\dots 1.2$$

Q_e : Adsorption capacity at equilibrium (mg / g).

C_e : Concentration of solute at equilibrium in units (mg / L).

a: Proportionality constant(maximum adsorption capacity)(mg/g)

b : Langmuir adsorption constant

When drawing C_e / Q_e vs. C_e the slope is equal to $1/a$ and its intercept equals to $1/ab$.

1.11.2 Freundlich isotherm

In 1990, the German scientist Freundlich developed an equation which is one of the most important equations used in the case of adsorption from a solution. Most of the surfaces are heterogeneous, because the potential energy changes irregularly due to the occurrence of adsorption sites at different levels of energy. This leads to a change in the adsorption isotherm . The following expression illustrates how the Freundlich isotherm is related mathematically⁸⁶.

$$Q_e = k_f (C_e)^{1/n} \quad \dots\dots\dots 1.4$$

The values of the Freundlich constant, k_f , depend on the properties of the adsorbent and the temperature. The Freundlich isotherm's linear form is represented as follows: ⁸⁶.

$$\log Q_e = \log k_f + \frac{1}{n} \log C_e \quad \dots\dots\dots 1.5$$

k_f and n : are isotherm constants .

n : is intensity of adsorption .

k_f is measure of the amount of adsorption that can be obtained from plotting the relationship between $\log Q_e$ versus $\log C_e$.We obtain a straight line with a slope equal $1/n$ and intercept $\log k_f$.

1.12 Adsorption kinetics

Adsorption kinetics refers to the speed of the withdrawal of adsorbed particles from the solution⁸⁷, and their adhesion to the adsorbent surface after overcoming all the implicit and intermolecular forces that prevent the adsorption process in the solution. Adsorption kinetics is of great importance in determining the time period in which the adsorption process occurs and reaching equilibrium, after which the adsorption process stops and helps in evaluating the adsorption efficiency. Adsorption kinetics depends on several factors: concentration of the adsorbate material, contact surface, and temperature.^{88,89} There are numerous well-established kinetic and thermodynamic models that describe the adsorption of pollutants^{90,91}.

Pseudo-first-order and pseudo-second-order kinetic models were used to assess the MFA adsorption by SnO₂ nanoparticles. According to equation (1.6) the linear version of the pseudo-first-order kinetic model (PFOM) is defined as follows⁷²:

$$\text{Log} (q_e - q_t) = \log q_e - \frac{k_1}{2.303} t \dots\dots\dots 1.6$$

where q_e is the quantity of adsorbate (mg .g⁻¹) at equilibrium

q_t : is the amount of adsorbate (mg .g⁻¹) at time t (min)

k_1 : is the pseudo-first-order rate constant (min⁻¹) .

The linear relationship is established by plotting $\log (q_e - q_t)$ vs. t and the values of q_e and k_1 are determined from the intercept and slope of the straight line, respectively.

In pseudo-second-order kinetic model's(PSOM) linear form⁸⁹. Eq. (1.7) was applied to investigate the adsorption kinetics of MFA on SnO₂, SnO₂:P.ONPs and has the general form as:

$$\frac{t}{q_t} = \frac{1}{k_2 q_e^2} + \frac{t}{q_e} \dots\dots\dots 1.7$$

k_2 : is the pseudo -second -order rate constant ($\text{mg} \cdot \text{g}^{-1} \text{min}^{-1}$)

1.13 Thermodynamic study of adsorption

The thermodynamic study of the adsorption process is important to understand or determine the type of adsorption that occurs, whether it is chemical or physical. As well as knowing the automatic nature of the adsorption process, and this is done by determining the thermodynamic constants, which are the free energy of adsorption, the reaction enthalpy, and the change in entropy at different temperatures⁹².

$$K_{eq} = \frac{q_e \times m}{C_e \times v} \dots\dots\dots 1.8$$

$$\Delta G = -RT \ln K_{eq} \dots\dots\dots 1.9$$

ΔG : free energy change ($\text{K}_J / \text{mol} \cdot \text{K}$)

ΔH : enthalpy change ($\text{K}_J / \text{mol} \cdot \text{K}$)

ΔS : entropy change ($\text{J} / \text{mol} \cdot \text{k}$)

R: gas constant ($8.314 \text{ J} \cdot \text{K}^{-1} \cdot \text{mol}^{-1}$)

The value of ΔH and ΔS can be calculated from Van't Hof's equation plots:

$$\ln K_{\text{eq}} = -\frac{\Delta H}{RT} + \frac{\Delta S}{R} \dots\dots\dots 1.10$$

1.14 Literature Review (SnO₂ NPs)

SnO₂ nanostructures have been created using a variety of physical and chemical methods, such as the hydrothermal process, rapid oxidation of elemental tin micro emulsion, thermal evaporation of oxide powder, chemical vapour deposition, co-precipitation method, sol-gel, and solve thermal microwave synthesis. In this section we present the findings of earlier studied and the methods that were used for prep rating SnO₂ nanostructures, then we will focus on chemical precipitation and plant extraction approaches.

In (2007) SnO₂ was prepared using hydrothermal method. The authors used tin chloride 2-propanol, and distilled water as solvent for their work. The prepared SnO₂ NPs were tetragonal shaped having size of (3nm). The band gap of the particles was 3.5eV, and they used as sensing materials⁹³.

Sikhwivhilu *et al.*, prepared SnO₂ NPs using sol-gel and chemical precipitation techniques and they characterized their resulted particles using FTIR, X-ray diffraction, and electron microscope .Their findings showed the SnO₂ particles, which were formed using chemical precipitation method, have high surface area compared with that formed in sol-gel method⁹⁴. In addition, both methods produced crystalline particles with tetragonal rutile structure.

Manjula et al.⁹⁵synthesized SnO₂ NPs using glucose. The NPs were used as a catalyst to degraded methyl orange (MO) dye. The impact of annealed temperature (150 °C to 500 °C) on the photo catalytic activity of the SnO₂ NPs was

investigated, and the results revealed that the SnO₂ NPs gave the best activity at annealing temperature of 150 °C .

In 2017, Piper nigrum seed extract was used as a reducing agent to produce tin oxide nanoparticles ⁹⁶ .The authors studied the ability of SnO₂NPs towards cancerous cell (lung and colorectal) through generating reactive oxygen species (ROS) followed by oxidative stress and then cell death. The generation of reactive oxygen species is strongly affected by the size, small nanoparticles give more ROS and consequently higher cytotoxicity towards cancer cell when compared with large nanoparticles.

In 2018 Kim et al. ⁹⁷ Liquid phase plasma was employed to create SnO₂NPs. The SnO₂ nanoparticles had a size range of 10 nm and spherical shape. These particles were utilized to prolong the life and improve the capacity of lithium ion batteries

Begum et al⁹⁸. prepared SnO₂ (NPs) using chemical precipitation method. They used anhydrous aspartic acid as a surfactant and two temperatures (300 °C and 600 °C) for annealing. They observed that the surfactant has an effect on the growing process of SnO₂ particles and the resulted particles exhibited a photo catalytic activity towards carbamazepine drug.

Lei group synthesized SnO₂ NPs using Psidium guajava leaf extract and carried out dye degradation activity against reactive yellow 186. The photo catalytic activity of tin oxide particles for the breakdown of reactive yellow could be examined in short time (180 minutes with removal efficiency rate of 90% under sunlight. The surface Plasmon resonance peak (SPR) of tin oxide nanoparticles was conducted from UV-Visible absorption spectrum at 314 nm. ⁹⁹ .

Buniyamin et al.,¹⁰⁰ prepared SnO₂ NPs by using green synthesis, where an aqueous (agar wood) leaves extract was added to the solution containing tin (IV) chloride penta hydrate SnCl₄.5H₂O. It was found that bioactive compounds with functional groups of polyphenols serve as templates for reducing and capping agents during the synthesis activity. X-ray diffraction technique showed that the crystallite size is 3.4nm and DRS absorption spectra gave the value of the band-gap of 3.35 eV . According to this result, greenly produced SnO₂ NPs have significant potential for use in optoelectronic and catalytic applications.

An electrochemical method (electrolysis) was utilized to manufacture SnO₂ nanoparticles. The electrolytic solution is hydrochloric acid (HCl), and the electrodes are bare tin (both anode and cathode). The method produced tetragonal-shaped particles with sizes between 25 and 150 nm.¹⁰¹

Recent work by Aggarwal's group has showed that tin oxide nanoparticles can be formed using Ocimum Basilicum leaf extract. These particles exhibited photocatalytic activity against natural red (NR) dye with the efficiency rate of 99% within 150 minutes¹⁰².

Abirami et al. performed experiments to produce SnO₂ nanoparticles with an average particle size of 18.79 nm using chemical precipitation method, without the use of a surfactant. They discovered that SnO₂ NPs have antibacterial activity against *Escherichia Coli* . These nanoparticles may have potential applications in areas such as medical field¹⁰³.

Aims of Study

1. This study aimed to explain the growth process of tin oxide nanoparticles (SnO_2) using chemical precipitation method. The structural properties of the prepared SnO_2 nanoparticles can be controlled by changing parameters such as pH, concentration of precursors, reaction time and reaction temperature.
2. Another particular objective was to explore the effect of plant extract on the formation of nanoparticles to see if the size and morphology of SnO_2 nanoparticles change after the addition of extract. This method involves the addition of a proper amount of *Portulaca oleracea* extract to the precursor's solution, which, will hopefully reduce the size of particles in addition to reduce the agglomeration of particles by preventing further addition of atoms to the prepared nanoparticles.
3. Another target was to exploit the as-prepared SnO_2 particles to remove pharmaceutical residue such as mefenamic acid.
4. Regards to adsorption process, studying the absorption behaviour of tin oxide particles formed from both chemical precipitation and green method to see which one gives high removal rate, this can be achieved by comparing the adsorption rate of MFA using SnO_2 particles formed in the presence of *Portulaca oleracea* extract with that recorded in the absence of the extract.

Chapter TWO
Experimental
part

2.1 Introduction

This chapter will describe the experimental materials and will focus on the key items of equipment that were utilized in this work for preparing and characterizing the nanoscale structures of SnO₂ nanoparticles using chemical precipitation and biosynthesis methods.

Techniques such as XRD, FE-SEM with EDX, TEM, UV-Vis and FTIR spectroscopy were used to study the structural and optical properties of prepared SnO₂ particles.

2.2 Chemical Materials

All the experiments in this project were performed using de-ionized water as a solvent. *Portulaca oleracea* leaves were purchased from local market in Kerbela city. The chemical materials that were used in this work are shown in Table 2.1

Table 2.1 Chemical materials and their formula

No.	Chemicals	Formula compound	Molecular weight (g/mole)	Purity %	Company supplied
1	Sodium chloride	NaCl	58.44	99.0	(B.D.H)
2	Hydrochloric acid	HCl	36.46	-----	J. K. Baker, Netherlands
4	Sodium hydroxide	NaOH	40	99	BDH England
5	Mefenamic Acid	C ₁₅ H ₁₅ NO ₂	241.285	99	SDI Company Samarra
6	Tin (IV) chloride penta hydrate	SnCl ₄ .5H ₂ O	350.5984	99	Sigma-Aldrich
7	Ammonium hydroxide	NH ₄ OH	35.00	-----	Riedel-Haen

2.3 Instruments

To prepare and characterize tin oxide nanoparticles, several instruments were utilized and all of these are presented in Table 2.2.

Table 2.2 Instrumentation and manufacturers

No.	Instrument	Type, Company	Place
1	Electric Sensitive Balance	Lab.BL210, Sartorius median- Germany.	University of Karbala
2	Centrifuge –Hettich	Universal Germany	University of Karbala
3	Oven Me mort.	LOD-080+NLabtech, Korea.	University of Karbala
4	PH-Meter.	pH-Meter WTW-720 ion lab- Germany.	University of Karbala
5	Shaking Water Bath	SWB-25 HyscKore	University of Karbala
6	Spectrophotometer UV –Visible.	UV-Vis 1800 Shimadzu-Japan.	University of Karbala
7	Fourier Transform Infrared (FT-IR).	IRAffinity-1S, SHIMADZU	University of Karbala
8	X-Ray Diffraction.	X pert pro Analytical	University of Tehran
9	Field Emission Scanning Electron Microscope(FESEM)	SIGMA VP	University of Tehran
10	Transmission Electron Microscopy (TEM)	Zeiss Model SIGMA VP	University of Tehran

2-4 Samples Preparation

2.4.1 Preparation of NaOH solution

To prepare 0.1 M sodium hydroxide solution, 0.4 g of NaOH flakes was dissolved in 100 mL of deionized water with a continuous stirring for approximately 15 minutes at 25 °C

2.4.2 Preparation of HCl

0.1 M of HCl was prepared by adding 0.83 mL of hydrochloric acid into cleaned and dried 100 mL volumetric flask. The volume was then completed to 100 mL deionized water.

2.4.3 Preparation of *Portulaca oleracea* extract

The fresh leaves of *Portulaca oleracea* were collected from the local markets. They were washed with tap water several times, before washing with deionized water to remove all impurities. They dried under the shade for a week, and grounded into a fine powder using an electric mill. Ten grams of *Portulaca oleracea* powder was mixed with 100 mL deionized water and stirred continuously for 10 minutes (at 60 °C) using a magnetic stirrer. The mixture was then filtered and stored at a temperature of -4 °C to be used in the preparation of tin oxide. Figure 2.1 shows photos for the preparation process of *Portulaca oleracea* extract

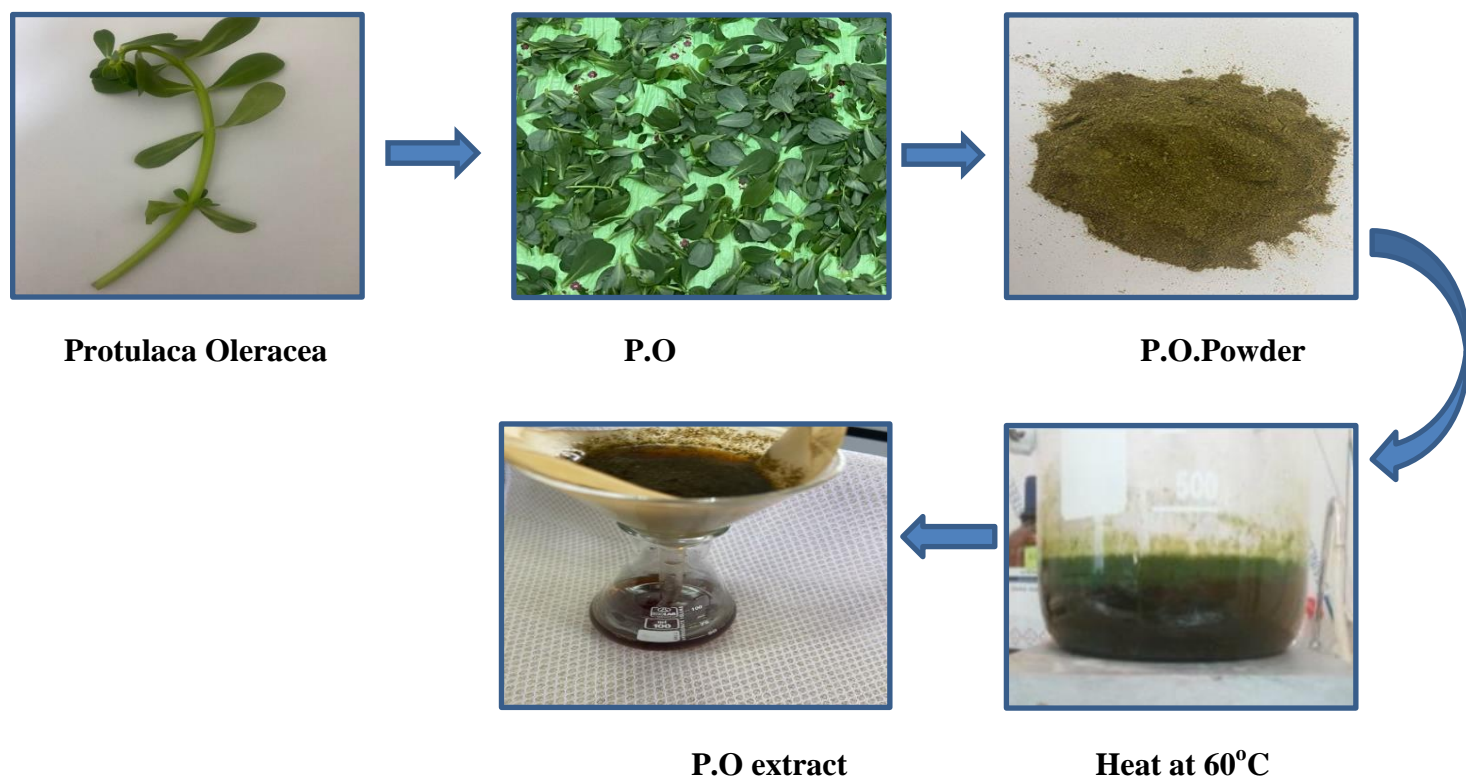


Figure 2.1 Images showing the preparation steps of *Portulaca oleracea* extract.

2.5 Chemical Precipitation Method

2.5.1 Preparation of tin oxide nanoparticles (bare SnO_2 NPs)

To prepare bare SnO_2 nanoparticles, 0.1752 g of tin (IV) chloride pentahydrate ($\text{SnCl}_4 \cdot 5\text{H}_2\text{O}$) was dissolved in 50 mL of deionized water and stirred for 15 minutes. Thereafter, NH_3 (25%) solution^{104,105} drop wise to the above aqueous solution under continuous stirring. This was carried out until the solution pH reached 8 and a white precipitate appeared after 3h. Deionized water was used to wash the precipitate (three times) to get rid of unwanted materials, in particular, chloride ions. To separate the precipitate, a 4000 rpm centrifuge was utilized for 15 minutes. The sample was dried in a drying oven for 24 hours at 100°C before

annealing at 600 °C for 2hours .The formation steps of SnO₂ nanoparticles was summarized in (Figure 2.2).

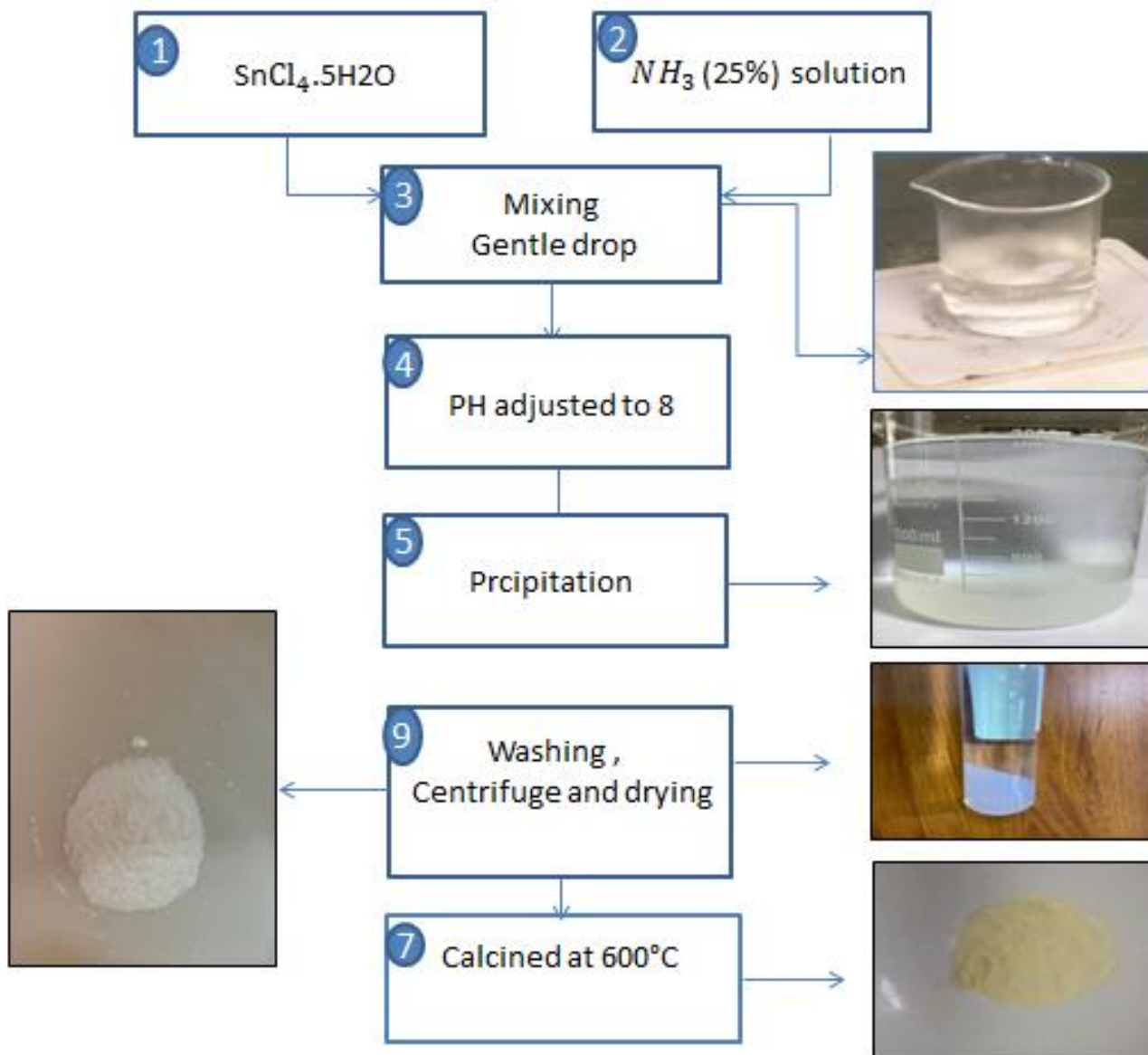


Figure 2.2 Schematic showing the formation process of SnO₂nanoparticle using chemical precipitation method.

2.5.2 The effect of concentration on the formation process of SnO₂NPs

Parameters such as pH, reaction time and reaction temperature could affect the formation process of tin oxide nanoparticles formed from chemical precipitation method. Therefore, many experiments have performed to determine the optimal conditions for the formation of SnO₂ nano particles. The effect of concentration was the first experiment conducted. Three different concentrations of SnCl₄.5H₂O (0.1 M, 0.01M and 0.001 M) were chosen by dissolving a suitable amount of it in a 50 ml of deionized water. The beakers were then stirred for 3h, at 25°C .

2.5.3The effect of the reaction time on tin oxide nanoparticles growth

The influence of the reaction time on the growth of SnO₂ nanoparticles was investigated. After dissolving tin(IV) chloride penta hydrate (0.01 M) in 50 ml de-ionized water , the solution was stirred for different times (0, 1, 2 ,3 , 4 hours) at 25°C .

2.5.4 The effect of temperature on the SnO₂ NPs

After adjusting the pH value, the solution was poured into four beakers. These beakers were then heated to 25 °C , 40 °C , 60 °C and 80 °C for 3h.

2.6 Green synthesis approach

2.6.1 Biosynthesis of tin oxide nanoparticles(SnO₂:P.O NPs)

In this project, SnO₂ nanoparticles were synthesised using plant extraction method. This was achieved by dissolving 0.1752g of tin (IV)chloride penta hydrate in 50 mL deionized water and mixing then with the *Portulaca oleracea* extract (10 mL) for 60 minutes using magnetic stirrer (reaction temperature was fixed at 60 °C). To get rid of impurities, deionized water used to wash the yellow precipitate many times. The obtained precipitate was then separated using centrifuge at 4000 rpm for 15 min. After that, the product was dried in an oven at 90°C for 24 hours. Last step, the powder was calcination for 2 hours at temperature of 600°C as shown in Figure 2.3.

Synthesis of SnO₂ Nanoparticles

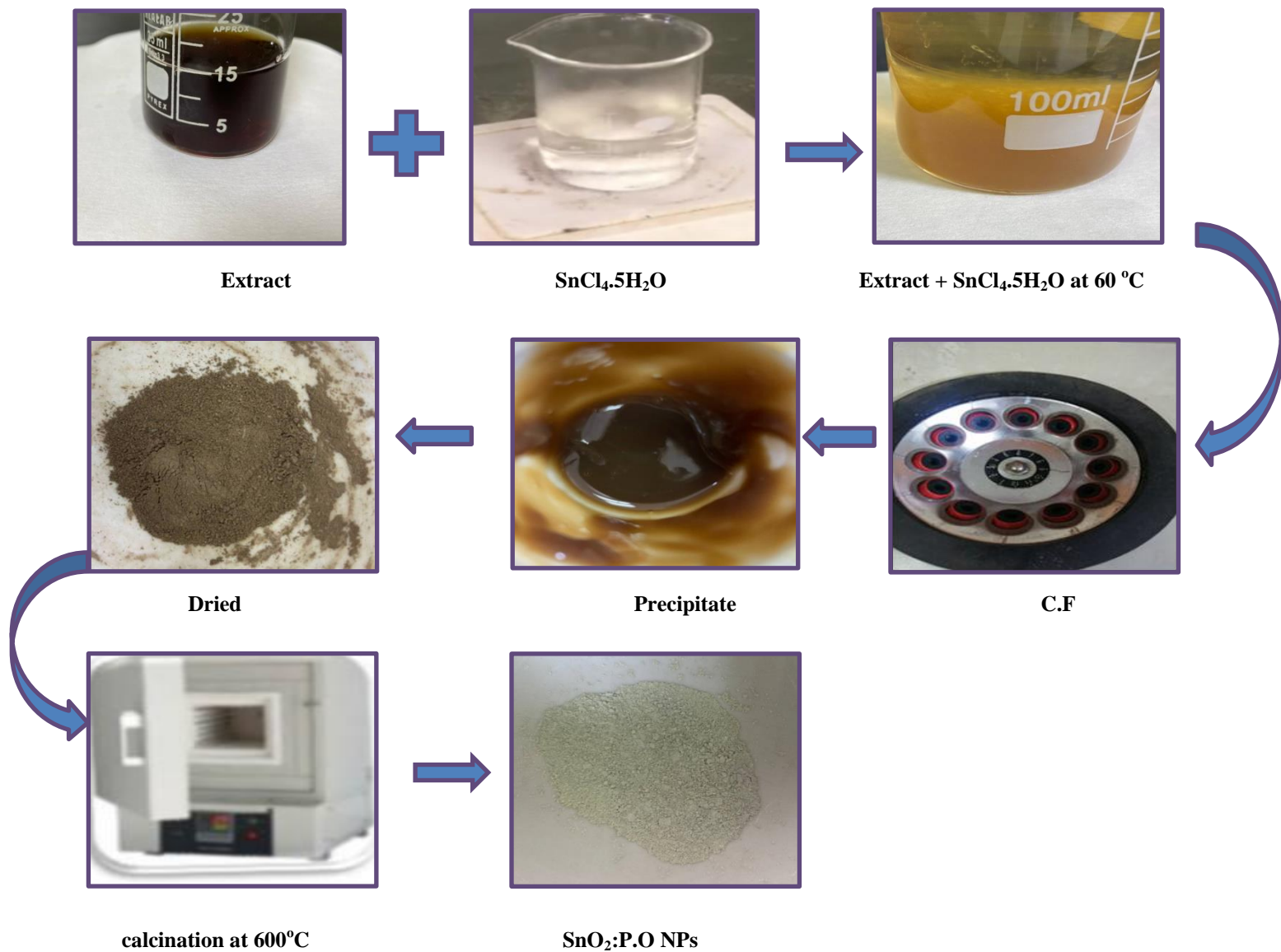


Figure 2.3 Diagram showing the Biosynthesis formation of SnO₂ nanoparticles

2.6.2 Optimum conditions for preparing SnO₂:P.O NPs

Several factors, including the impact of PH, reaction time, and the concentration of the Portulaca oleracea (P.O) , were studied in order to identify the ideal conditions for producing SnO₂ NPs in the presence of the extract (P.O).

2.6.2.1 The effect of extract concentration

By varying the amount of the extract (5 mL, 7.5mL, 10 mL and 20 mL) from the solution mentioned in section 2.6.1. One can study the effect of concentration of P.O extract on the formation process of tin oxide particles. The reaction was carried out at 60°C for 1 hours stirring.

2.6.2.2 The influence of reaction time

The solution, which contains tin chloride SnCl₄.5H₂O and 10 mL extract (P.O), was left on the magnetic stirring for different interval times (0 , 1, 2 and 3 hours) before taken to the UV-visible spectrophotometer .

2.6.2.3 The influence of pH

The PH of the solution was adjusted by adding either 0.1 M of NaOH or 0.1M of HCl, to make the solutions pH 4, 6, 8, 10 and 12. Thereafter, the solutions were mixed for an hour at 60°C before recording their absorbance.

2.6.2.4 The effect of temperature

After mixing 0.1752 g of($\text{SnCl}_4 \cdot 5\text{H}_2\text{O}$) with 10 ml of extract (P.O), the solution was liquated into four different conical flasks. All flasks were shaken for 60 minutes . One of the flasks was heated to 25 °C, the second one to 40 °C , while the third to 60 °C and the fourth to 80 °C .

2.7 Characterization of SnO_2 nanoparticles

The simplest way to confirm the formation of nanostructures is to use UV-Visible spectroscopy. It was used to study the optical properties of the resulted tin oxide nanoparticles .FT-IR spectrophotometer was used to confirm the formation of SnO_2 particles) and to identify the functional groups that are possibly present on the SnO_2 particle surface.The most intriguing aspect of this sort of FTIR spectroscopy is that it requires a very little sample, which will be placed on a tin selaned lens rather than being mixed with KBr as in normal FTIR spectroscopy. The particles size and morphology were characterized by Field Emission Scanning Electron Microscopy (FE-SEM) and Transmission Electron Microscopy (TEM). The presence of tin and oxygen elements in SnO_2 particles was confirmed using Energy Dispersive X-ray spectroscopy (EDS). The crystallite size and the crystalline structure were determined from (XRD) technique

2.8 Adsorption process for mefenamic acid (MFA)

The maximum wavelengths (λ_{max}) of MFA was determine by recording the absorbance in the range of 200 -800 nm using UV-Visible spectroscopy. Figure 2.5 shows that MFA has λ_{max} of 284 nm which is in agreement with previous experimental work⁹¹. in (Figure 2.4) .

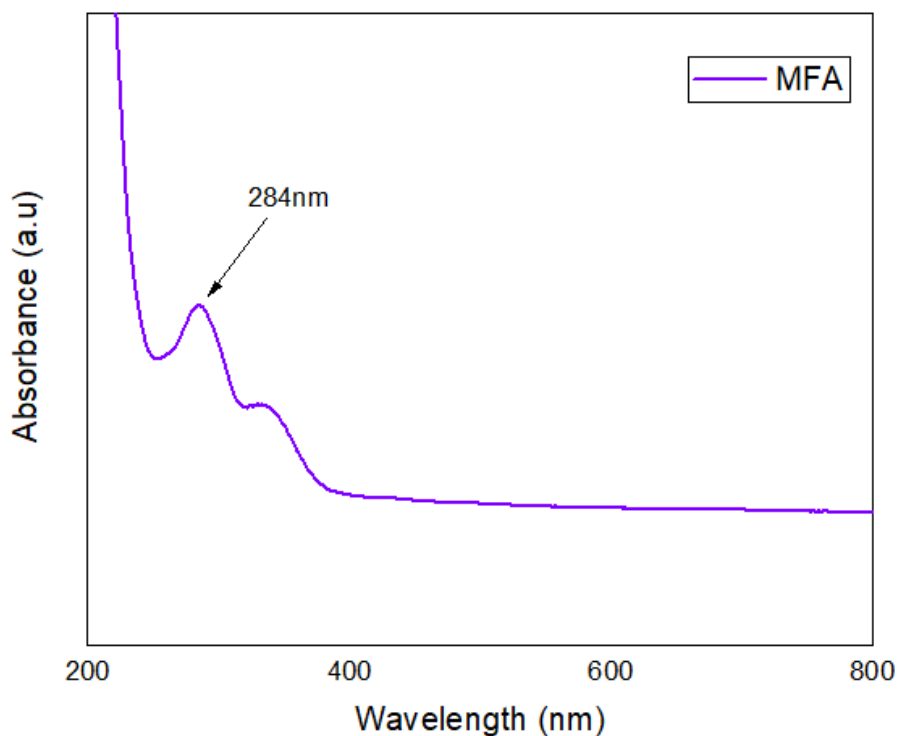


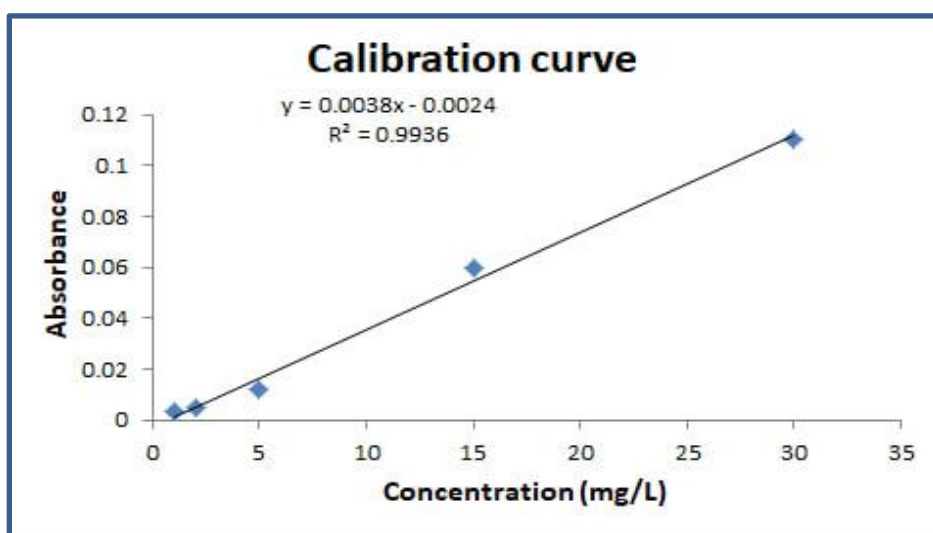
Figure2.4 UV-Visible absorption spectrumum of MAF

2.8.1 Calibration curve for of MFA solutions

Five solutions of mefenamic acid were prepared (1, 2, 3, 5, 15 and 30 mg/L) from the stock solution (100 mg/L) was prepared by dissolving 0.1g of MAF in 1000 mL of deionized water ,see (Figure 2.5). Absorbance was measured at the(λ_{max}) for Mefenamic acid and plotted against the concentration values of Mefenamic acid Table 2.3.

Table 2.3 Statistics data of calibration for different concentrations of MFA

Concentration (mg/L)	Absorbance (a.u)
1	0.003
2	0.005
5	0.012
15	0.06
30	0.11

**Figure 2.5** calibration curve of Mefenamic acid

2.8.2 The influences of different parameters on the adsorption process

2.8.2.1 The influences of contact time on the adsorption process

To determine the time needed to achieve equilibrium between the adsorbent surface and the adsorbate molecule. The concentration of MFA was used 30 mg/L and the amount of bare SnO₂ and SnO₂:P.O nanoparticles was 0.6g. Different shaking times were used, ranging from (10-100 minutes). The solutions were placed

in a shaking device equipped with a water bath at a temperature of 298k. The solutions were then centrifugation and their absorbance was measured at the maximum Wavelength (284nm) , The concentration of MFA at equilibrium C_e (mg/L) was determined using the calibration curve. Calculations were made for the removal effectiveness from E q:¹⁰⁶

$$R\% = \frac{C_0 - C_e}{C_0} \times 100\% \dots\dots\dots 2.1$$

Re%= percentage removal

C_0 =Initial mefenamic acid concentration(mg /L)

C_e = concentration of MFA at equilibrium (mg /L).

2.8.2.2 The influences of adsorbent dose

The effect of the adsorbent weight on the adsorption process was detected. Different weights from the bare SnO₂NPs and SnO₂:P.O NPs (0.004,0.02,0.3,0.6 and 0.7g) were taken and MFA (30 mg/L,25ml volumetric flask) and the equilibrium time was 80 minutes for the bare SnO₂ NPs and 30 minutes for SnO₂:P.O NPs). Then, the solutions were placed in a shaking device equipped with a water bath at 25 °C , after which the same steps were used in section 2.8.2.1

2.8.2.3 Effect of PH

The effect of pH on Mefenamic acid removal was studied. pH was varied from (3,6 and 10) by adding either 0.1 M of HCl or 0.1 M NaOH to the solution contains 0.6 g for both surfaces of SnO₂NPs, SnO₂:P.ONPs and 30 mg/L of MFA. after which the same steps were used in section 2.8.2.1

2.8.2.4 Effect of temperature

To determine the preferred temperature for the adsorption of MFA on both surfaces of bare SnO_2NPs , $\text{SnO}_2\text{:P.ONPs}$, three different temperatures were applied as follows (298,308,318) k. The weight of both adsorbent surfaces was 0.6g and (30 mg/L) from MAF solution. The shaking time for the surface of SnO_2NPs was 80min. As the shaking time for the surface of $\text{SnO}_2\text{:P.O NPs}$ was 30min. The shaking speed for both surfaces was 140 rpm. Then the solutions were separated using centrifuge and their absorbance was measured at the maximum wavelength (284nm), using the UV-Visible. The MFA concentration at equilibrium (C_e mg/L), was determined using the calibration curve. Calculations were made for the removal effectiveness and adsorption capacity (Q_e).

2.9 Adsorption isotherm

Different concentrations of MFA (30,40,50,60,90 mg/L) were prepared, and appropriate volume of each was taken. These solutions were placed in a volumetric flask 25mL and 0.6 g of both bare SnO_2 and P.O: SnO_2 NPs. At (80 mint), for to the surface (SnO_2NPs) and (30 mint) to the $\text{SnO}_2\text{:P.O NPs}$ after which these were placed Solutions in the shaker equipped with a water bath at different temperatures(298,308,318k). The solutions were then centrifugation and their absorbance was measured at the maximum Wavelength (284nm), The concentration of MFA at equilibrium (C_e mg/L) was determined using the calibration curve. Calculations were made for the adsorption capacity.

2.10 Determination the point of zero charges pH_{PZC}

The solid addition method was used to calculate the point of zero charges (pH_{pzc})¹⁰⁷. 25 mL of (0.1M) NaCl solution was transferred to a series of 50 mL conical flasks and the initial pH (pH_i) of the solutions was roughly adjusted between (2- 11) by adding either 0.1 M HCl and 0.1 M NaOH¹⁰⁸. Later 0.6g from SnO_2 NPs and SnO_2 :P.O NPs was then added to each flask and allowed to equilibrate for 24 h with a shaking water bath and the final pH_f values was determined after 24h. values ΔpH were plotted against pH_i , the point of intersection of the resulting curve with abscissa, at which $\Delta\text{pH} = 0$, gave the pH_{pzc} ^{109,110}.

CHAPTER THREE

RESULTS and DISCUSSIONS

3. Introductions

The imputes of the work described in this chapter was to explore and compare the optical and structural properties of bare SnO₂NPs, which are formed in the absence of plant extract, and SnO₂:P.O NPs, which are formed in the presence of extract. Another aspect that was also investigated was the effect of both bare SnO₂ and SnO₂:P.O nanoparticles on the removal of mefenamic acid from aqueous solutions.

3.1 Chemical precipitation method

3.1.1 Optical properties of bare SnO₂ NPs

3.1.1.2 The effect of precursor concentration on the formation process of SnO₂ NPs

The first experiment conducted here is on the effect of tin(IV) chloride penta hydrate(SnCl₄.5H₂O) concentration on the formation process of tin oxide nano particles .Figure 3.1 shows the UV-Vis absorption spectra of bare SnO₂ particles formed from three different concentration (0.1 M, 0.01M and 0.001 M) of tin chloride. It is clear that at the higher concentration (0.1 M) no peak was observed Suggesting, more concentration (0.1M) large or agglomerate particles formed. However, an intense peak was observed at 292 nm when the concentrations of tin chloride was 0.01 M. This peak is in a blue shift with respect to bulk SnO₂ (340 nm)¹¹¹, which could attributed to the quantum size effect.^{37,112}.

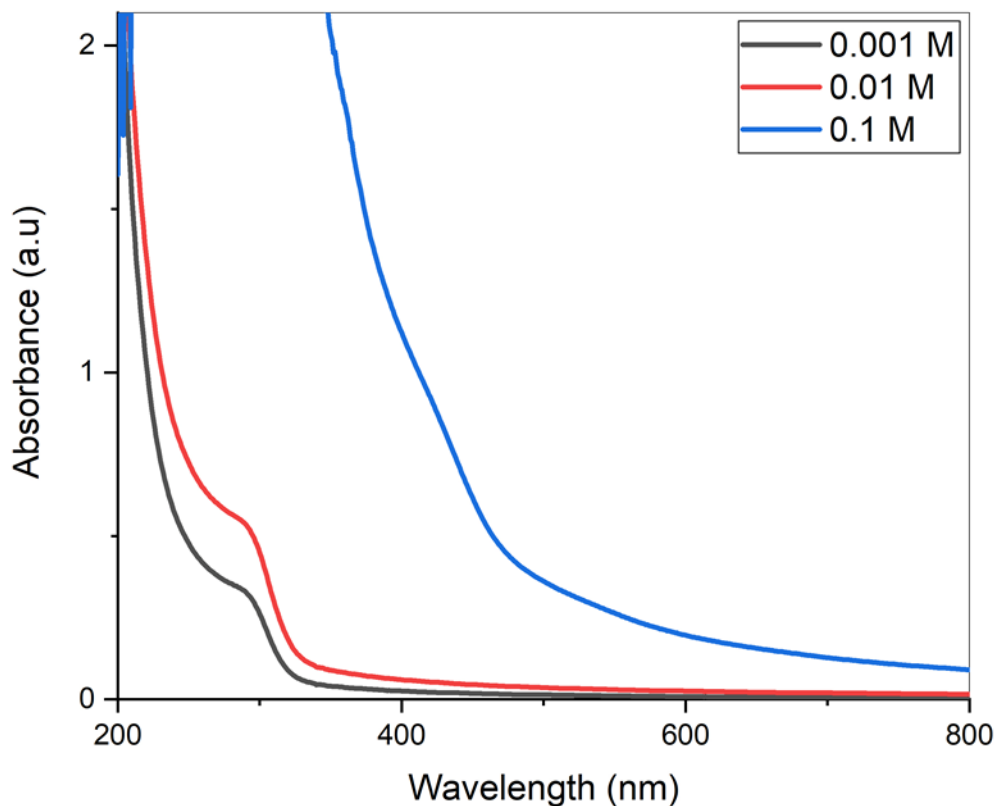


Figure 3.1 UV-Vis absorption spectra of tin oxide nanoparticles as a function of the tin chloride concentration

3.2.1.2 The effect of reaction time on the absorption of tin oxide nanoparticles

After establishing the optimal amount of tin (IV) chloride pentahydrate for preparing SnO_2 nanoparticles, we performed an experiment to examine the reaction time that is required to form tin oxide nanoparticles. The solution, which contains tin chloride and ammonia, was mixed for 0, 1, 2, 3 and 4 hours at 25 °C. As shown in Figure 3.2, the solution after mixing has no absorption band even after 1 hour, this could be because no SnO_2 particles were formed. After stirring for 2 and 3

hours significant peaks observed at nearly 292 nm but after 3 hours the intensity of the peak is high, therefore, from here onwards we use three hours as the best reaction time.

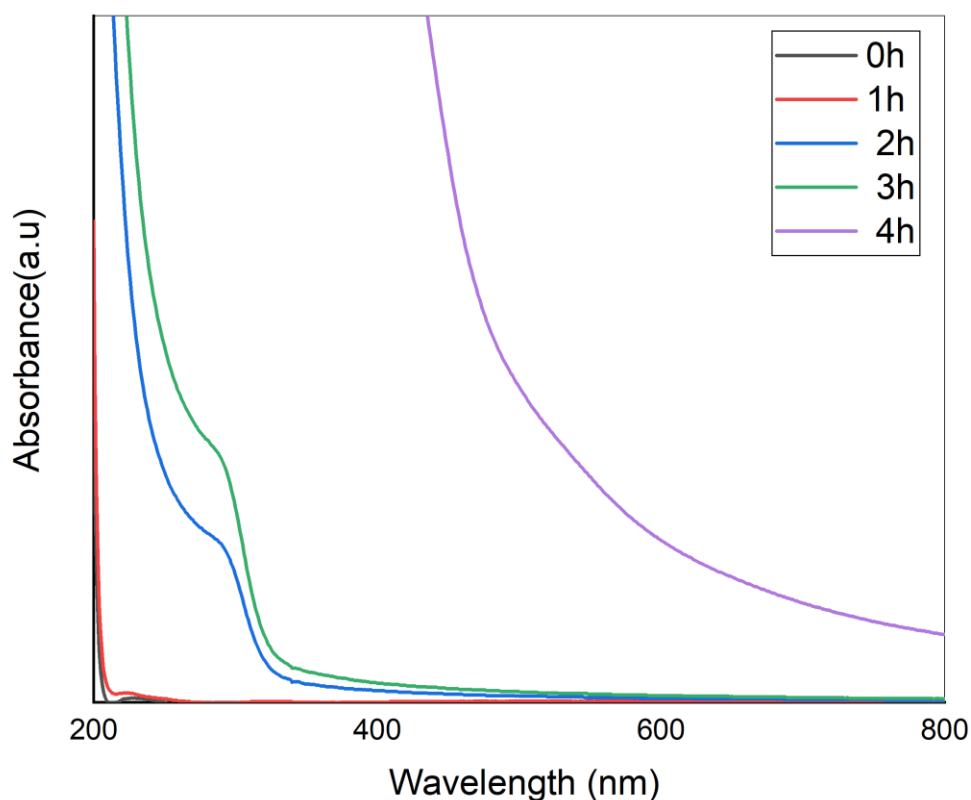


Figure 3.2 The optical absorption spectra of SnO₂ nanoparticles at different reaction times, the concentration of the precursor was (0.01 M) .

3.2.1.3 The effect of pH on the SnO₂ NPs formation

It is apparent from Figure 3.3 that pH solution has an effect on the absorption of tin oxide nanoparticles. The absorption band of SnO₂ shifted towards the shorter wavelengths (~292 nm) compared with bulk SnO₂ (340 nm) when the pH of the solution was adjusted to 8. The observed blue shift is related to the quantum confinement effects¹¹². For the rest pH values no significant peaks were noted.

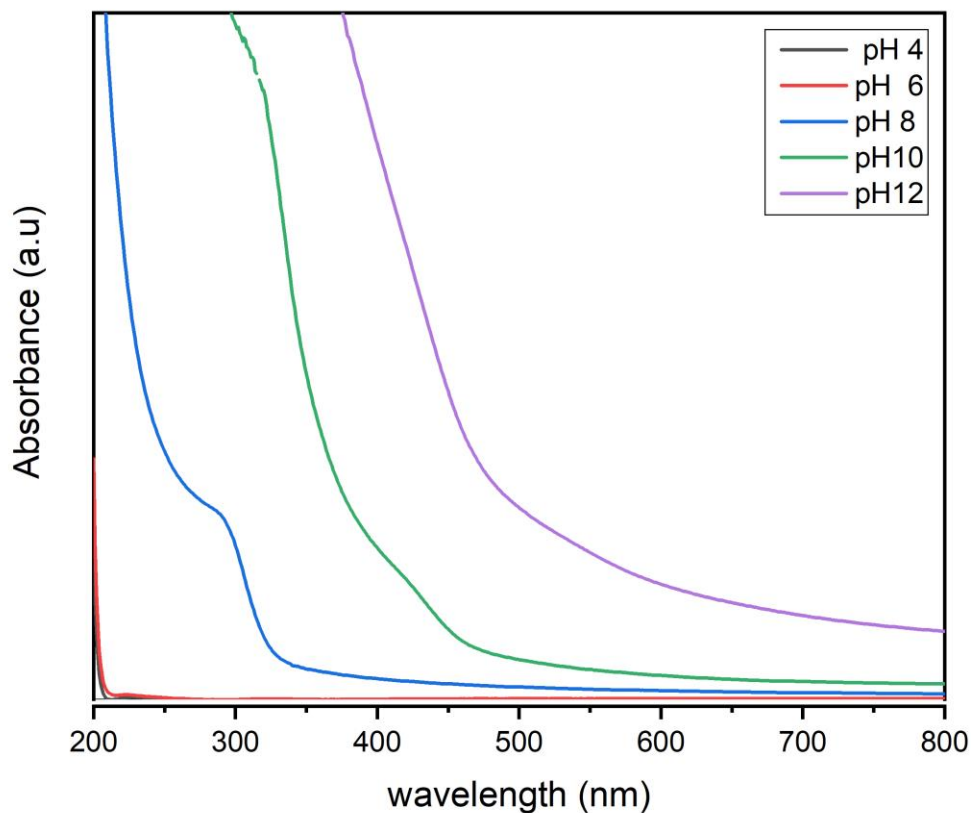


Figure 3.3 The effect of pH on the absorption spectra of as-prepared SnO₂ nanoparticles, the concentration of the precursors was 0.01 M and the reaction time was 3 hours

3.2.1.4 The effect of temperature on the SnO₂NPs formation

It is clear from Figure 3.4 that the absorption band of SnO₂ NPs depends strongly on the reaction temperature. At 25°C, the absorption peak was measured to be ~291 nm and the peak intensity is higher than that at 40°C. Therefore, the best temperature to prepare SnO₂ nanoparticles using chemical precipitating method is 25°C, while at 60 °C and 80°C the SnO₂ nanoparticles decomposing.

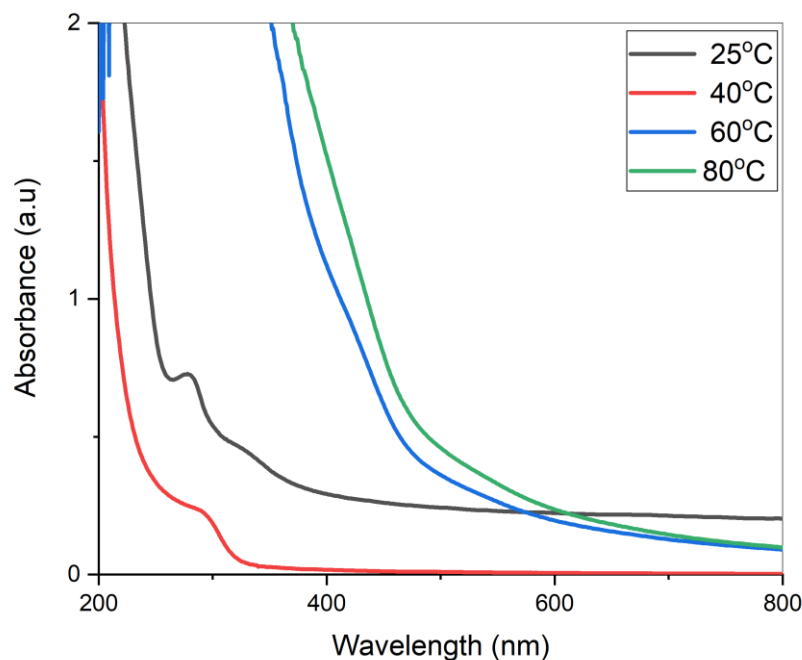
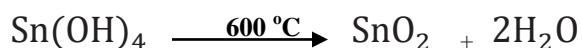
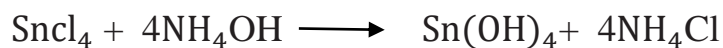


Figure 3.4 UV-Vis absorption spectra of as-prepared SnO₂ nanoparticles as a function of temperature. The concentration of the precursor was 0.01 M and the reaction time was 3 hour.

3.2.1.5 The optical band gap energy

The probable mechanism for the formation of SnO₂ nanoparticles through the chemical precipitation method (bare SnO₂) is that the addition of aqueous ammonia solution to the stanic salt (to make the solution pH 8) led to form hydroxide ions and subsequently form the precipitate of Sn(OH)₄. During the annealing process (600°C), the precipitate was decomposed and SnO₂ nanoparticles formed¹¹³.



Diffuse reflectance spectroscopy was used to study the optical properties of tin oxide nano particle. It is seen from (Figure 3.5) , most of visible light is reflected by bare SnO₂ particles and the absorption starts below 300 nm. The kubelka-munk relation was used to calculate the optical band gap^{114,115}.

$$(F(R) h \nu)^n = k (h \nu - E_g) \dots\dots\dots 3.1$$

Here, F(R) is the absorbance-related Kubelka-Munk function, n is the electronic transition which is equal to (2),¹¹⁶ h is the Plank’s constant, k is a constant, and ν is the frequency of light. by plotting the (F(R)hν)² as a function of energy one can measure the energy band gap (E_g) by extending the linear part of the spectrum to the photon energy axis (x axis).

The kubelka -munk relation gives a band gap value of 3.7 eV which is larger than that of bulk SnO₂ (3.6eV) This could be because the quantum confinement phenomenon¹¹². It is well known that as the particle size decreases the band gap of semiconductor materials increas, the absorption edge is shifted toward lower wavelengths, and the quantum size effect becomes obvious. Therefore, this finding confirms the formation of SnO₂ NPs at the nano-scale.

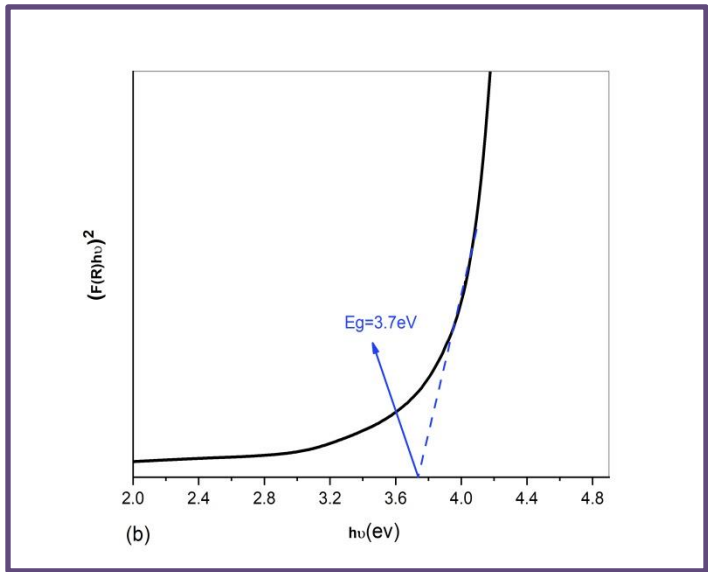
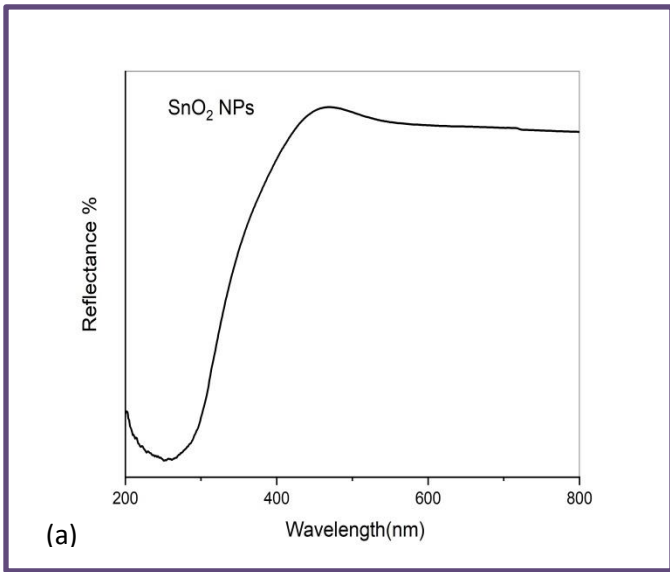


Figure 3.5 UV-DRS spectrum of bare SnO₂ particles (a) and the optical band gap energy estimated from Kubelka-Munk formula (b)

3.2.2.1 FTIR analysis

FT-IR spectrum of bare SnO₂ nanoparticles was recorded in the range of 500-4000 cm⁻¹. The sharp peaks centred between 600 and 650 cm⁻¹ were assigned to asymmetric and symmetric Sn-O-Sn stretching vibrations^{114,117}. The peak centred at 585cm⁻¹ representing the stretching mode of symmetric O-Sn-O (oxide-bridge functional group), which confirms the formation of SnO₂ nanoparticles^{112,118}. The peak appears at 1441cm⁻¹, suggesting the presence of a Sn-OH bond¹¹⁹. The peaks around 2300 to 2400 cm⁻¹ are probably attributed to the presence of CO₂ group. It seems from the FTIR spectrum that there were no water molecules adsorb of the prepared particles surface due to the annealing process at 600 °C.

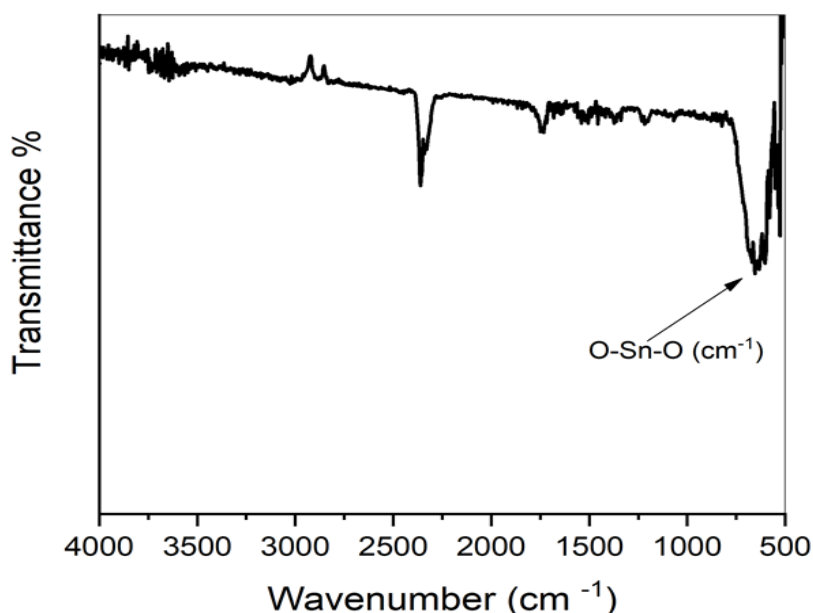


Figure 3.6 FTIR spectrum for SnO₂ nanoparticles formed from chemical precipitation method.

3.2.2.2. XRD analysis

XRD pattern of (bare SnO₂) nanoparticles (see Figure 3.7) (exhibit well-determined diffraction peaks at 2θ positions 26.51° , 34.17° , 38.61° , 34.08° , 51.84° , 58.05° , 62.19° , 62.32° , 66.12° , 71.29° , and 78.84° corresponding to the (110), (101), (111), (211), (220), (002), (221), (310), (301) (202) and (321) planes, respectively. The phase and the crystal structures of SnO₂ nanoparticles were studied using XRD. It is clear from (Figure 3.7) that the prepared SnO₂ nanoparticles have a polycrystalline structure and the diffraction peaks can be assigned to tetragonal rutile SnO₂ (based on JCPDS card No. 41-1445)¹²⁰. This finding is quite similar to previous works^{121,122}. No Phase corresponding to any impurity can be detected in XRD pattern. The grain size of the prepared sample was calculated using Debye Scherer equation⁴⁵:

$$D = K \lambda / \beta \cos \theta \dots\dots\dots (3.2)$$

Where β is the complete width at half maximum

D: is the average crystallite size “in radians”

K: is the shape factor 0.9

λ : the wavelength of X-ray (Cu K α) which is equal to 0.154 nm

θ : is the Bragg’s angle “in radians”. The crystallite size was found to be around 12.7 nm.

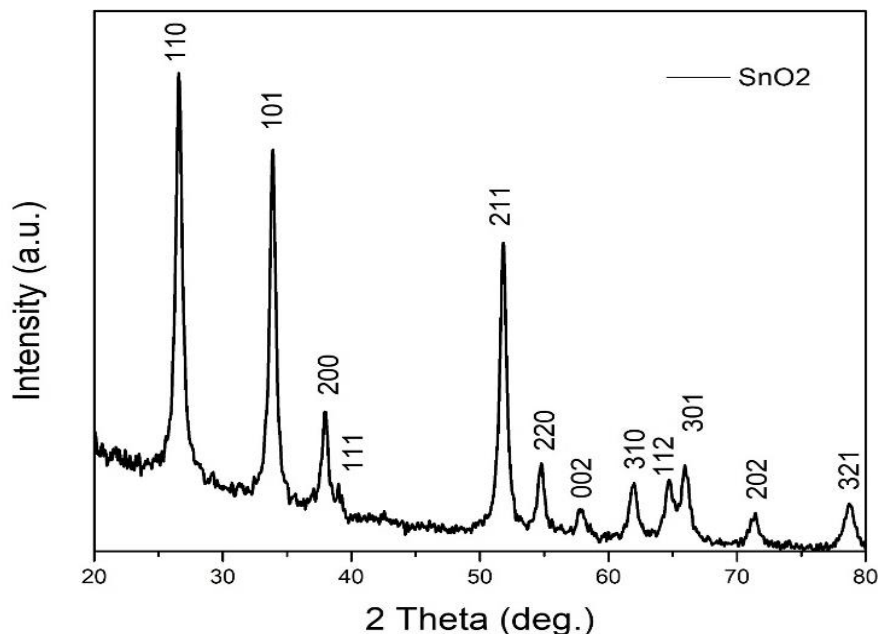


Figure 3.7 XRD pattern of synthesized SnO₂ nanoparticles calcined at 600°C

3.2.2.3 Morphological and EDX Analysis

The surface morphology of SnO₂ NP_s was examined using electron microscopy. FE-SEM images in Figure 3.8 (a) show that the as-prepared SnO₂ nanoparticles have spherical shapes and some of them are clustered together. The TEM image in figure 3.8(b) shows that SnO₂ nanoparticles are not uniform and they almost aggregate with each other. The size of synthesized particles was measured using the image J software^{123,124}, and the average size was found to be ~20 nm. Figure 3.8(c) shows the elemental analysis of baer SnO₂ nanoparticles and it is revealed that the prepared particles have Sn (95.1%) and O (4.9%) elements in their composition. It is worth to mentions that the appearance of the Au element peak in the EDX graph was referred to the coverage process of the sample with gold atoms during the EDX preparation sample^{125,126}.

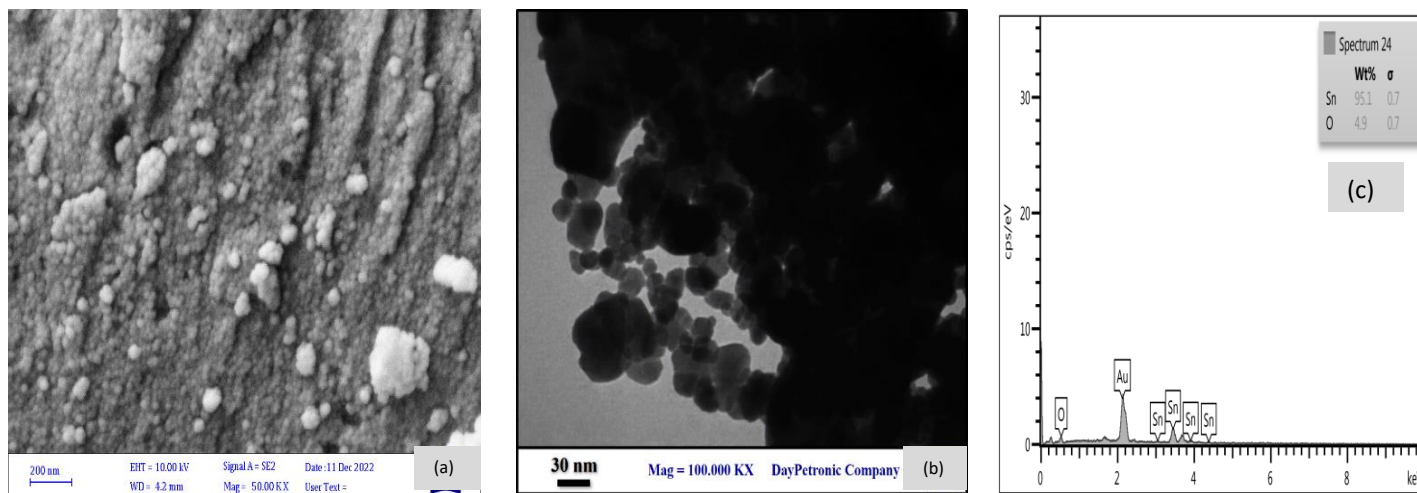


Figure 3.8 FESEM image of SnO₂ particles (a), TEM image of synthesized SnO₂ nanocrystals, and (c) EDS graph.

3.3 Biosynthesis approach

3.3.1 Optimal conditions for preparing SnO₂:P.O nanoparticles

3.3.1.1 The influence of extract amount

The appearance of yellow colour solution after mixing SnCl₄·5H₂O (0.01M) with *p.oleracea* extract was an indicator for the formation of biosynthesis SnO₂ particles (SnO₂ :P.O NPs). Another evidence for the formation of SnO₂ particles was provided by studying their optical properties.

Different volumes of *p. oleracea* extract (5 mL, 7.5 mL, 10 mL, and 20 mL) were selected to determine the ideal conditions for production tiny nanoparticles with a high surface-to-area ratio. The concentration of tin chloride solution was kept constant (0.01 M) and the stirring time was(1hour). The absorption spectrum, which is shown in Figure 3.9, exhibits an absorption band at lower wavelengths, ~

278 nm, compared with the absorption peak of the bulk tin oxide at 340 nm¹²⁷. The blue shift confirms the quantum confinement effect of semiconductor nanoparticles, which becomes more obvious as the particles get smaller in size. Moreover, the absorption band in the case of 20 mL extract spectrum is slightly broadened and shifted towards lower energies in comparison to that one in the low extract concentrations spectrum. This could be because of irregular growth of the SnO₂ particles. Thus, the best conditions for the biosynthesis of SnO₂ particles are 10 mL extract.

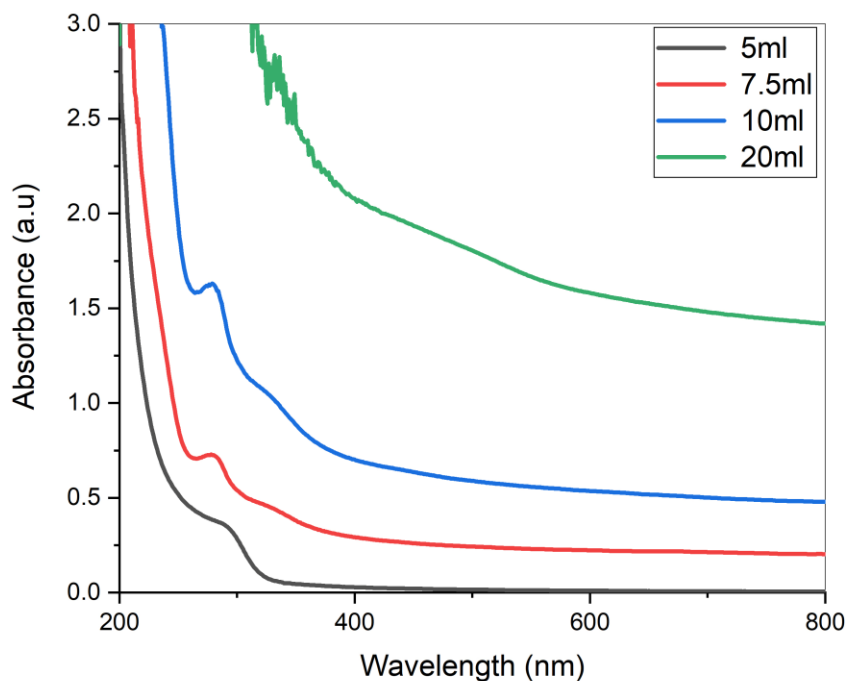


Figure 3.9 UV-Vis spectra of tin oxide nanoparticles formed in the presence of *p.oleracea* extract as a function of the extract concentrations after one hour of starring.

3.3.1.2 Effect of reaction time on SnO₂:P.O nanoparticles growth

The UV-Vis absorption spectra were recorded immediately after mixing tin chloride (SnCl₄.5H₂O) and the extract solutions and then after 0,1, 2, and 3 hours. An obvious peak was seen after stirring the two solution for 1 hour, giving a wavelength of ~ 278 nm. Leaving the solutions for a longer time (2 and 3 hours) on the magnetic stirrer gives absorption bands in longer wavelengths region. Suggesting, more reaction time large or agglomerate particles formed. Thus, the best conditions for the biosynthesis of SnO₂ particles are 10 mL extract, 1 hour reaction time.

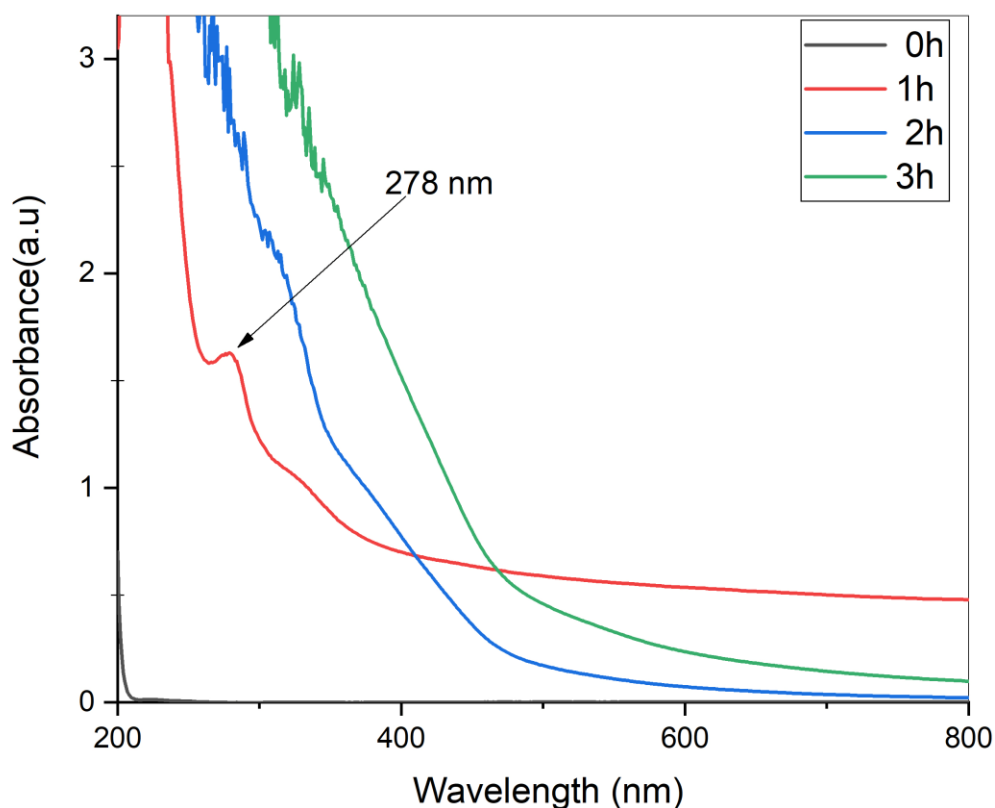


Figure 3.10 The optical absorption spectrum of SnO₂:P.O nanoparticles at different reaction time

3.3.1.3 The effect of pH on the formation of SnO₂:P.O NPs

It is apparent from Figure 3.11 that pH solution has an effect on the absorption of tin oxide nanoparticles. The absorption band in SnO₂ is shifted towards the shorter wavelengths (~278 nm) compared with bulk SnO₂ (340 nm) when the pH of the solution was adjusted to 6. The observed blue shift is related to the quantum confinement effects. For the rest pH values no significant peaks were noted.

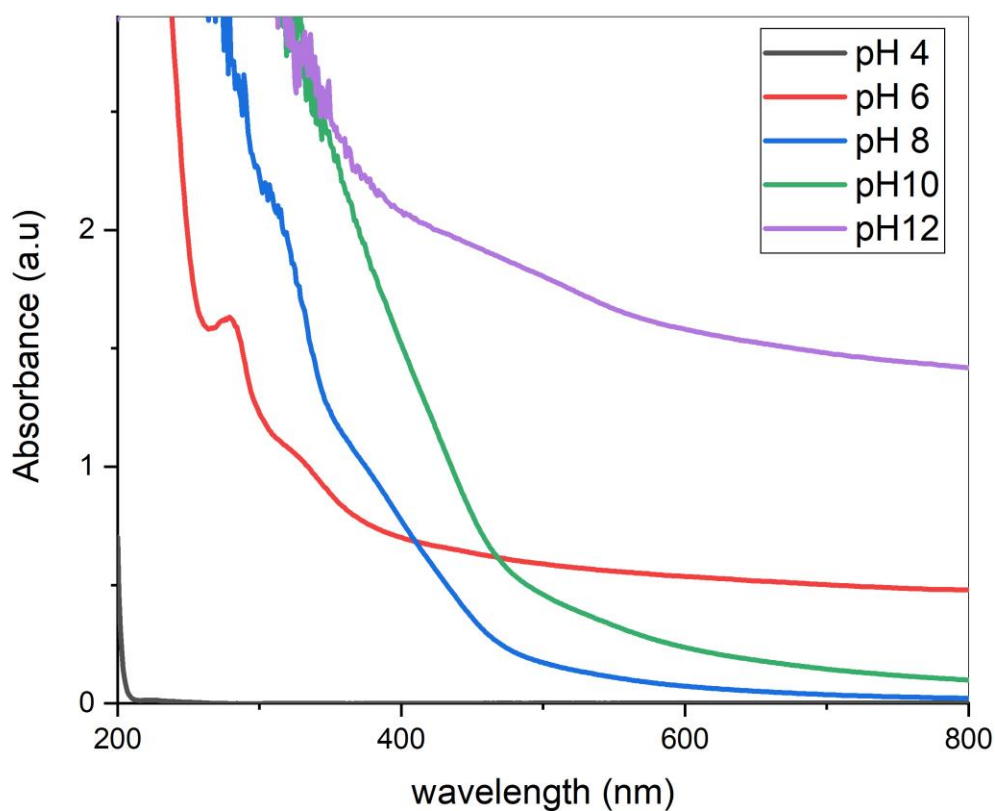


Figure 3.11 The effect of pH on the absorption spectra of as-prepared SnO₂ nanoparticles, the concentration of the precursors was 0.01 M and the reaction time was 1 hour

3.3.1.4 The effect of temperature on the formation SnO₂:P.O NPs

In this experiment, a suitable amount of the solution contains 0.01 M (SnCl₄.5H₂O) and 10 mL of the extract was added into four beakers. These beakers were heated for different temperature (25, 40, 60 and 80 °C). SnO₂ particles exhibit an intense absorption bands at nearly 278 nm when the solutions were heated to 25°C, 40°C, and 60 °C. However, at 60 °C the intensity of the absorption peak is slightly high in comparison to the ones at 25 and 40°C.No peak was observed when the temperature of the solution increases to 80°C , this could be attributed to the solubility of SnO₂ particles at a high temperature which prevents the production of SnO₂nanoparticles.

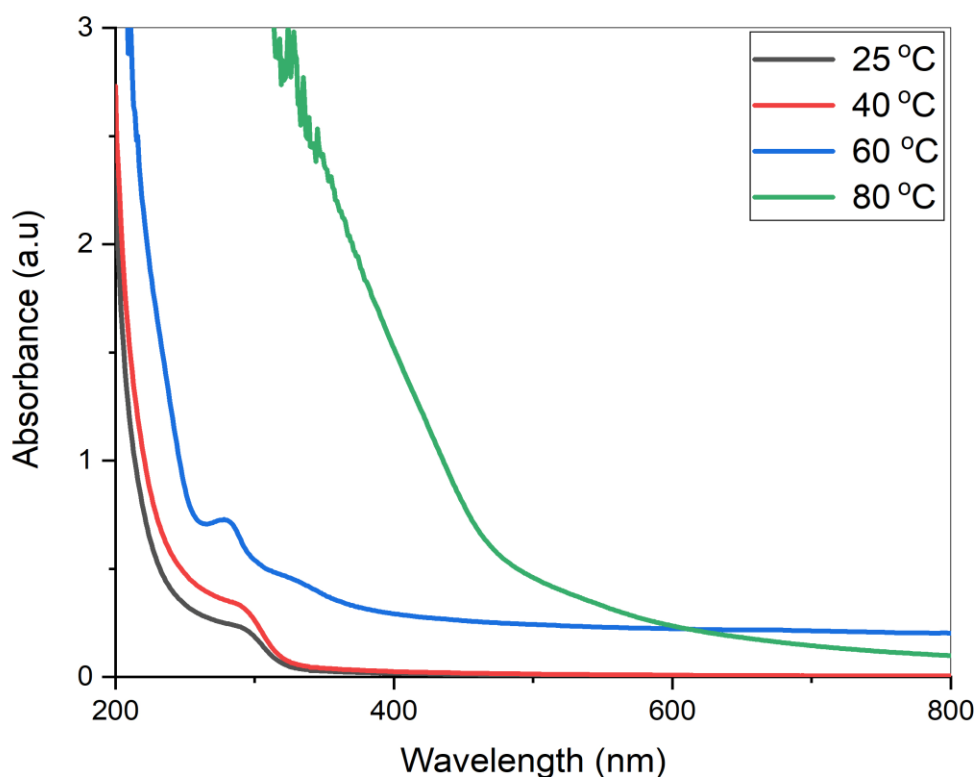


Figure 3. 12 UV-Visible spectra of SnO₂:P.O nanoparticles at different temperatures at after 1 hour of stirring.

3.3.1.5 Band gap energy for SnO₂:P.O nanoparticles

Diffuse reflectance spectroscopy was used to study optical properties of tin oxide nanoparticles formed in the presence of *Portulaca oleracea* extract (SnO₂:P.O). According to authors¹²⁸, the lower reflectance in DRS spectrum corresponding to high absorption in the same wavelengths region. The UV-visible curve in DRS spectrum in (Figure 3.13) shows an absorption edge near 280 nm. The optical band gap was calculated (same as in section 3.2.1.5) and it has a value of 4.2 eV, which was greater than the one calculated of bare SnO₂ nanoparticles.

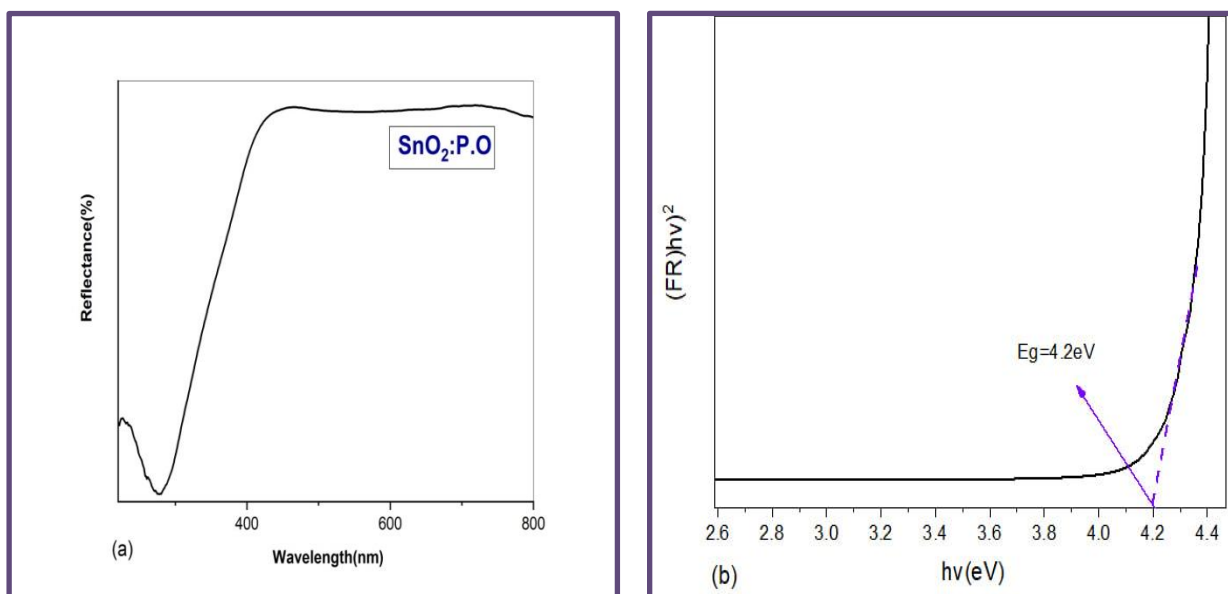


Figure 3.13 UV-DRS spectrum of SnO₂:P.O NPs((a) and the band gap energy estimated from Kubelka-Munk formula((b)

3.2.2 Structural properties of SnO₂:P.O NPs

The surface morphology of tin oxide nanoparticles (SnO₂:P.O) formed in the presence of *Portulaca oleracea* extract was determined using FESEM analysis. (Figure 3.14) shows FE-SEM images of SnO₂ nanoparticles and it is clear from these images that the resulting nanoparticles have a nearly spherical shape with the possibility of agglomeration of some of these spherical to form large clusters.

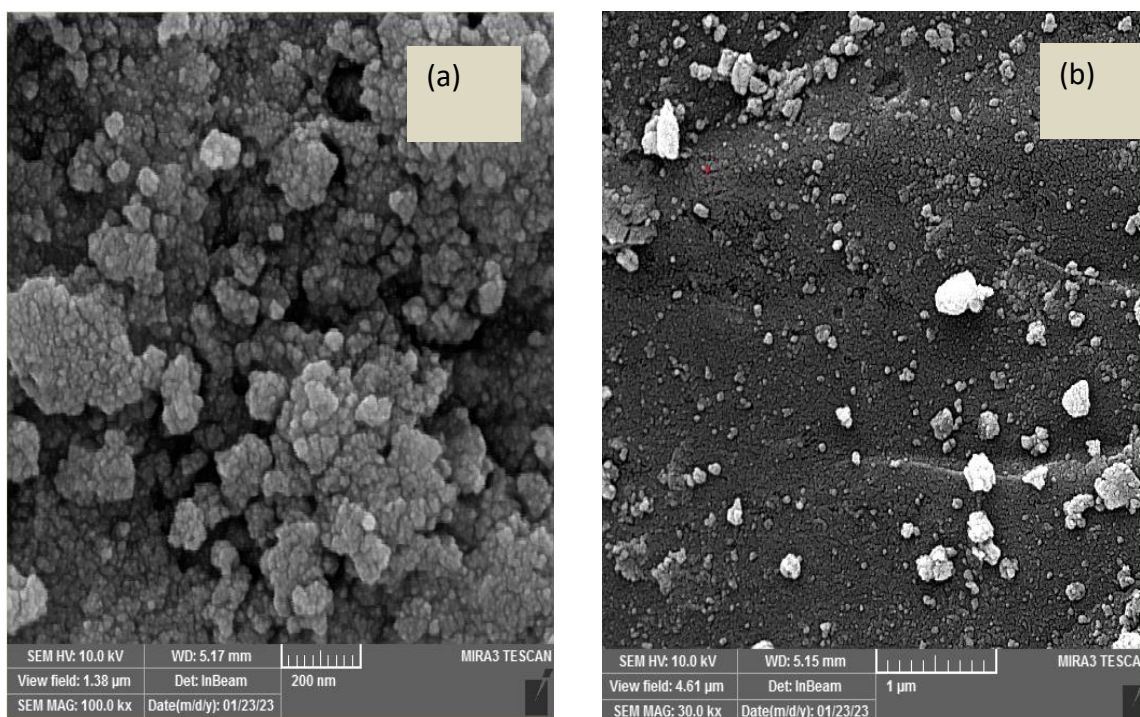


Figure 3.14 FE-SEM images for the biosynthesized (SnO₂:P.O) nanoparticles formed in the presence of *Portulaca oleracea* extract

TEM image in (Figure 3.15((a) provided more structural information about biosynthesised tin oxide nanoparticles. The shape of SnO₂:P.O nanoparticles seems to be quasi-spherical. Many individual particles were observed due to the fact that plant extract serves here as a protecting agents, which controls the growth of tin oxide by preventing further addition of atoms to the already exist particles. Image J software¹²⁶ was used to obtain information about their size. The average diameter of the individual particles is 11.5 nm.

Finally, the presence of Sn and O elements was confirmed using energy dispersive X-ray spectroscopy. (Figure 3.15(b) shows intense peaks which are assigned to the presence of Sn and O elements with a weight percentage of about 64.59% and 30.53% In addition, a small peak was noted for carbon element which could be result from the FE-SEM sample holder's ¹²⁶.

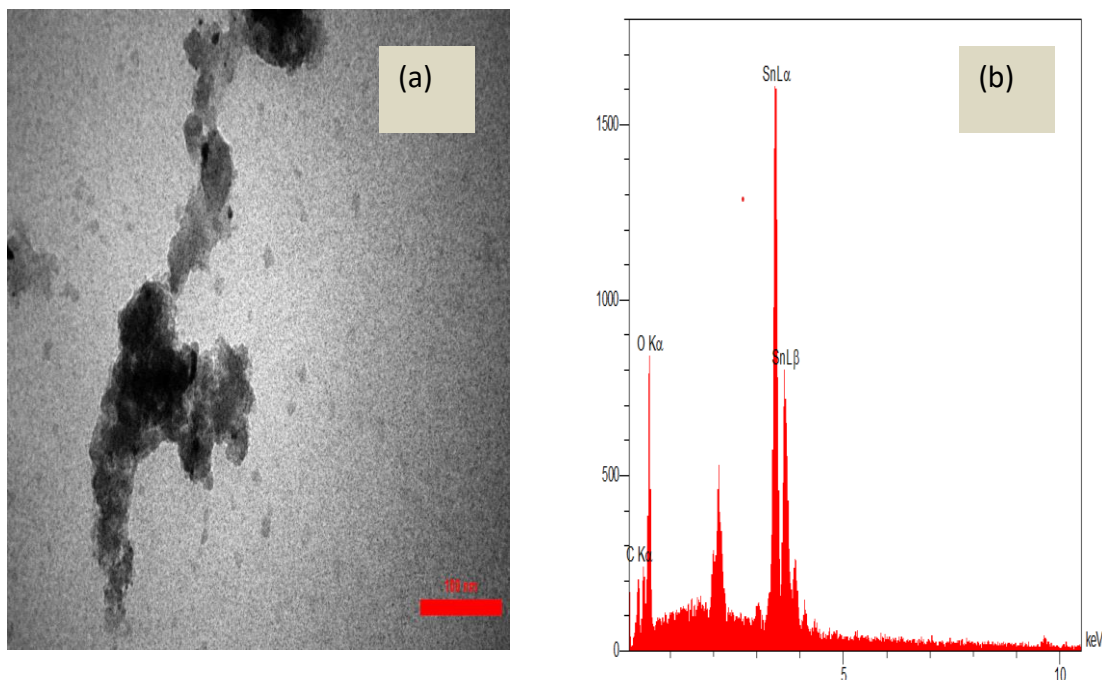


Figure 3.15 TEM image of SnO₂ nanoparticles (a) and EDX chart showing the elemental analysis (b)

3.3.2.1 FT-IR analysis

Further evidence for the formation of (SnO₂:P.O) nanoparticles was provided from the FT-IR spectrum. The sharp peak observed at 585 Cm⁻¹ is corresponded to the stretching vibrations of oxygen-metal- oxygen (O-Sn-O). ¹²⁹ The band at 686 cm-1 is assigned to Sn–O stretching vibrations. ¹³⁰ It seems from (Figure 3.16) that the prepared sample doesn't have water molecules on its surface due to the annealing process to 600 °C.

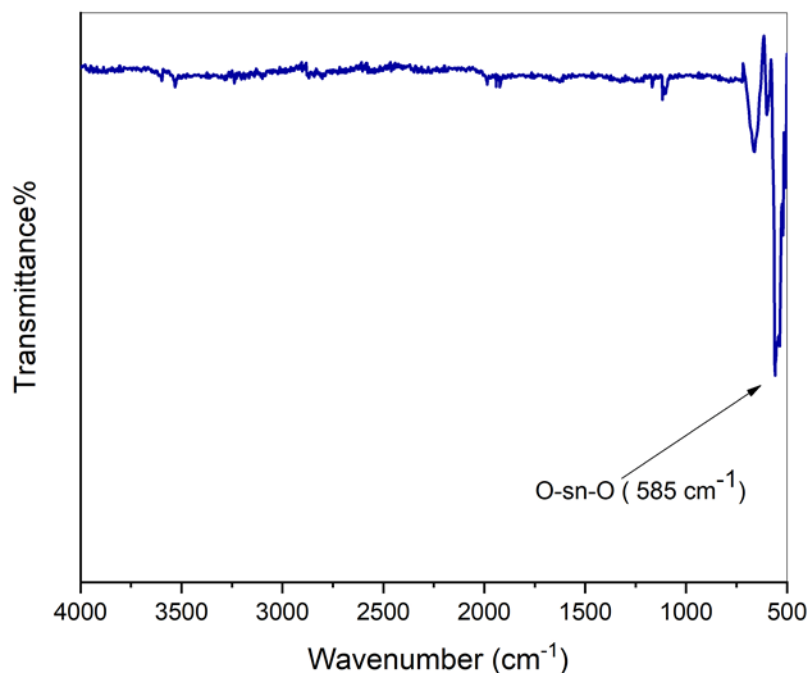


Figure 3.16 FT-IR analysis of (SnO₂:P.O) nanoparticles annealed at 600 °C

3.3.2.2 XRD analysis

XRD pattern of (SnO₂:P.O) nanoparticles (see Figure 3.17) exhibit well-determined diffraction peaks at 2θ positions 26.51°, 34.17°, 38.61°, 34.08°, 51.84°, 58.05°, 62.19°, 62.32°, 66.12°, 71.29°, and 78.84° corresponding to the (110), (101), (111), (211), (220), (002), (221), (310), (301) (202) and (321) planes, respectively. The peaks all confirm the tetragonal rutile structure of SnO₂ nanoparticles.^{130,131} It is known that the grain size is a part of particles and does not usually represent the particle size. The former was calculated for the 110 plane using Debye Scherer equation¹³² (see section 3.2.2.2) and it is 3 nm. Evidence has been provided here which shows that introducing *Portulaca oleracea* extract to the formation process of

tin oxide particles can lead to the growth of much smaller nanoparticles than those for chemical precipitation method with no extract .

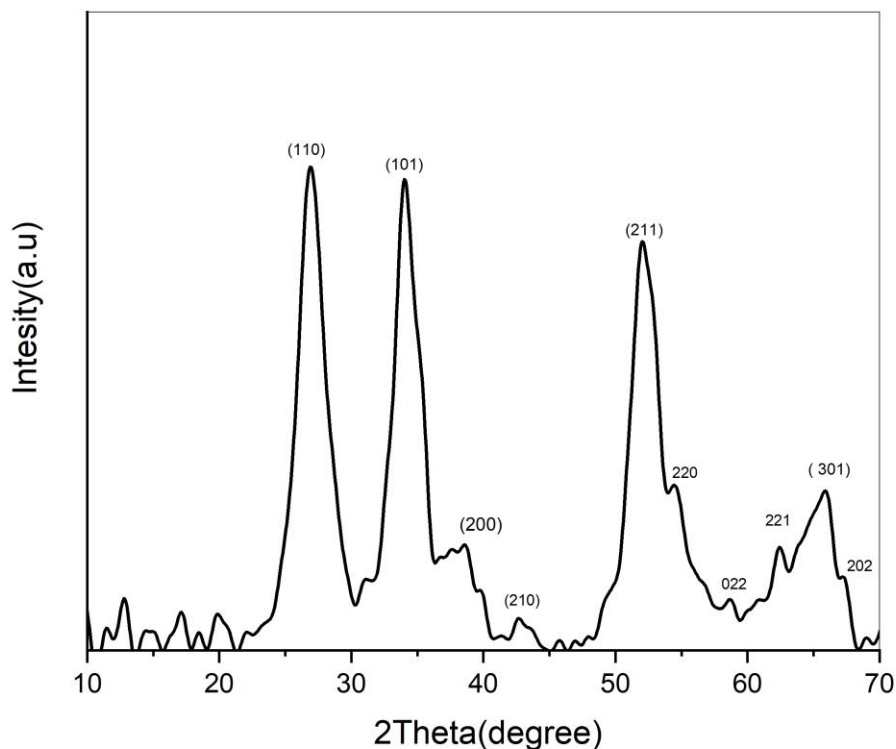


Figure 3.17 XRD pattern of biosynthesized ($\text{SnO}_2\text{:P.O}$) nanoparticles calcined to 600°C

3.4 Adsorption behaviour of SnO_2 nanoparticles

3.4.1 Study of factors effecting MFA removal from aqueous solutions using SnO_2NPs and $\text{SnO}_2\text{:P.ONPs}$ as adsorbent surfaces

3.4.1.1 Effect of the contact time on the adsorption process.

The time of equilibrium is one of the factors affecting the amount of adsorption. Therefore, the time of equilibrium between each of the adsorbent surfaces (bare SnO_2NPs , and $\text{SnO}_2\text{:P.ONPs}$) and the Mefenamic acid(MFA) was

studied. 0.6 g for both surfaces and 30 mg/L concentration of MAF were mixed for different time (10-100 minutes) at 25 °C. In term of bare SnO₂ NPs, the removal efficiency starts to increase as the contact time increased from 10 minutes to 80 minutes, then it becomes stable after 80 minutes. Therefore, the best equilibrium time for bare SnO₂ NPs to adsorb MFA is 80 minutes, which gave the best removal percentage of 83.3%, and it will be used in later experiments. On the other hand, 30 minutes is the best time required for SnO₂:P.ONPs surface to adsorb MFA with a high removal efficiency of 97 %. To conclude this section SnO₂ particles formed in the presence of plant extract give high removal efficiency 97% compared with only 39.1 % for bare SnO₂ at equilibrium time of 30 minutes, The best explanation to this increment is the presence of large number of active sites and the high surface-to-volume areas^{60,133,134} shown in table (3.1) and Figure (3.18).

Table 3.1 The removal efficiency of MFA using two surfaces bare SnO₂ and SnO₂:P.ONPs at different contact times

Time	Removal%=(C ₀ -C _e /C ₀)*100	
(min)	Re% for bare SnO ₂ NPs	Re% for SnO ₂ : P.ONPs
10	33	93.5
20	36.6	95.1
30	39.1	97
40	53.3	97
50	59.3	97
60	64.5	97
70	77.7	97
80	83.8	97

90	83.8	97
100	83.8	97

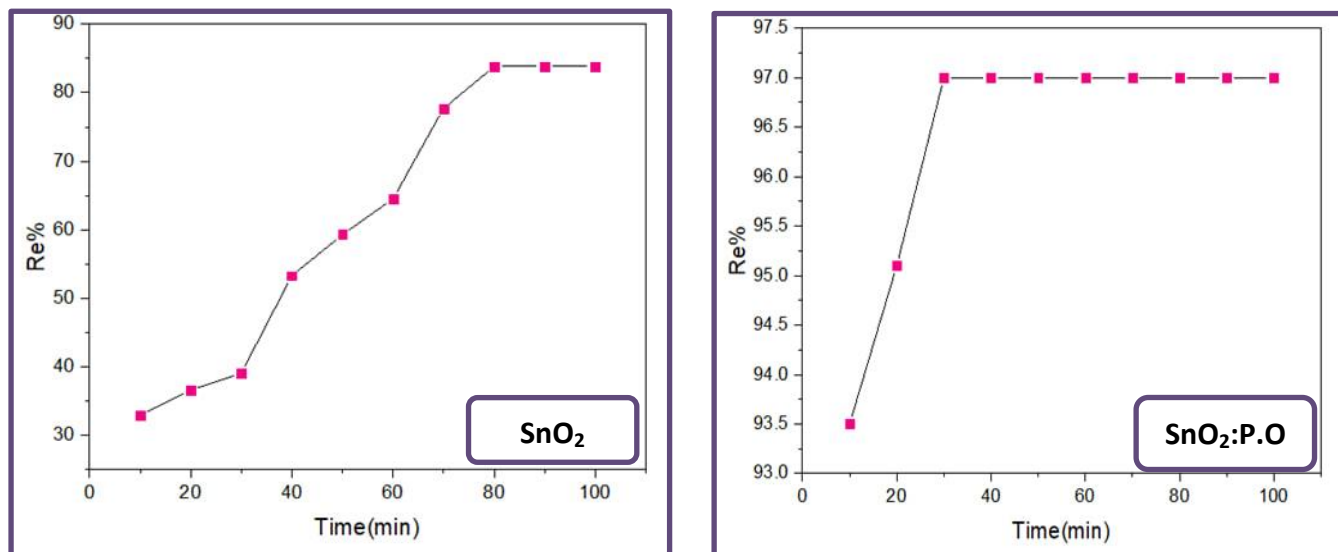


Figure 3.18 The influence of contact time on the removal efficiency of MAF used bare SnO₂NPs,SnO₂:P.ONPs surface (T=298K ,PH 6)

3.4.1.2 The influence of SnO₂ nano particles dose

The effect of the adsorbent weight on the adsorption process of MFA was detected. A (30 mg/L, 25 mL) of MFA was taken (7.5 ml) and mixed with different weights (0.004, 0.02, 0.3, 0.6, 0.7 g) of bare SnO₂ and SnO₂:P.O nanoparticles and stirred for 80 and 30 minutes, respectively. The findings are representing in (table 3.2) and (Figure 3.19) and it seems that by increasing the adsorbent dose the removal efficiency increased too. The best explanation is the presence of large number of active sites and the then high surface-to-volume area¹⁰⁶. Furthermore, above 0.6 g, there wasnt any enhancement in removal efficiency of MFA. This

could be because the surface is saturated with the adsorbate molecules¹³⁵ and therefore no effect was seen when the adsorbent dose increased. Thus, 0.6 g is the best weight for both surfaces (bare SnO₂ and P.O:SnO₂ particles) to remove MFA.

Table 3.2 Effect of adsorbent dose on the removal efficiency of MFA on bare SnO₂ and SnO₂:P.O nanoparticles

Dose g	Re% bare SnO ₂	Re% SnO ₂ :P.O
0.004	33	71.6
0.02	50.5	92.9
0.3	61.9	96.1
0.6	83.8	97
0.7	83.8	97

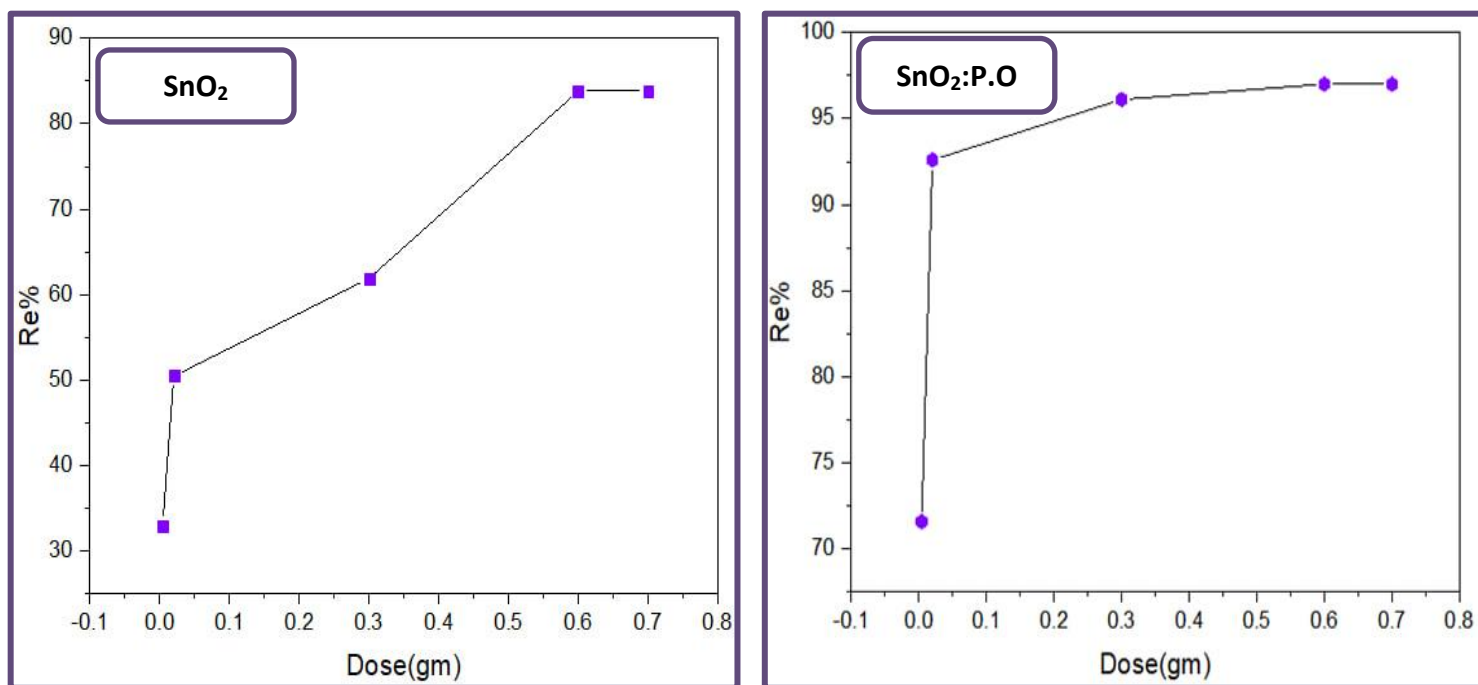


Figure 3.19 The influence of dose on the removal efficiency of MAF used bare SnO₂NPs, SnO₂:P.ONPs surface, (T=298K, PH 6)

3.4.1.3 Effect of initial concentration of Mefenamic acid

The effect of MFA concentration on the adsorption process was studied using different concentrations (30,40,50,60,90) mg/L with a constant weight of (0.6g), (80 and 30 minutes, respectively from bare SnO₂ NPs and SnO₂:P.O NPs. Figure (3.20) shows and tables(3.3),(3.4) a gradual decrease in the removal percentage, accompanied by an increase in the adsorption capacity values when the concentration of MAF increases¹³⁶. . Best concentration is 30 mg/L of MFA gave a high removal efficiency of 83.8 %, 97% from bare SnO₂ NPs and SnO₂:P.O NPs respectively.

Table 3.3 The effect of initial MFA concentration on adsorption process using bare SnO₂ NPs as an adsorbent surface

C ₀ (mg/L)	Q _e (mg/g)	Re%
30	1.048	83.8
40	1.322	79.3
50	1.64	78.7
60	1.95	78.3
90	2.7	72

Table 3.4 The effect of initial MFA concentration on adsorption using SnO₂:P.O NPs as an adsorbent surface

C ₀ (mg/L)	Q _e (mg/g)	Re%
30	1.21	97
40	1.596	95.7
50	1.969	94.5
60	2.353	94.1
90	3.394	90.5

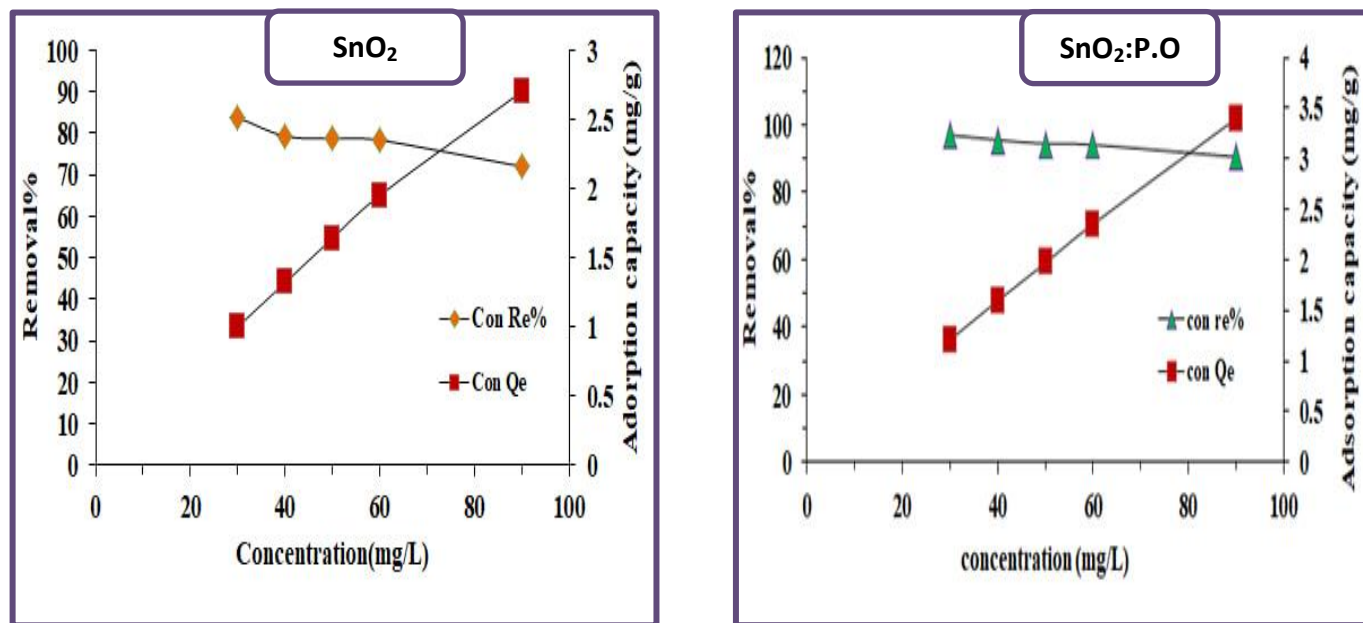


Figure 3.20 The influence of initial MFA concentration on the removal efficiency of MAF used SnO₂NPs,SnO₂:P.ONPs surface ,(T=298K ,PH 6)

3.4.1.4 Effect of pH

The removal of Mefenamic acid on the surfaces of the bare SnO₂ NPs and (SnO₂:P.O) NPs was studied in different pH levels within the range(3-10)using a constant concentration of MFA(30 mg/L) , at a temperature 298k.

To perform this experiment, the pH of the solution were adjusted to 3, 6, and 10. Table (3.5) and Figure (3.21) ,show that the adsorption behaviour of the bare SnO₂ NPs increases in the acidic medium and decreases in the alkaline medium. In bare SnO₂ nanoparticles, the maximum removal efficiency (92.6%) was obtained at pH 3. Due to the presence of positive charged of SnO₂ nanoparticles and negative charge of MFA, electrostatic attractive forces appear leading to enhance the adsorption at acidic pH^{137,91,138}. According to a study, in alkaline medium there

will be a competition between anionic MAF molecules and hydroxyl anions to adsorb of the adsorbent surface, which leads to reducing the adsorption capability¹³⁹. In SnO₂:P.ONPs the highest removal efficiency (97%) was reported when the pH was 6, which is the solution pH.

Table 3.5 The effect of the pH function on the removal efficiency of MFA removal on the surfaces of bare SnO₂ NPs and (SnO₂: P.O)NPs at temperature 298 K

pH	Re% bare SnO ₂	Re% SnO ₂ :P.O
3	92.6	96.1
6	83.8	97
10	65.4	95.2

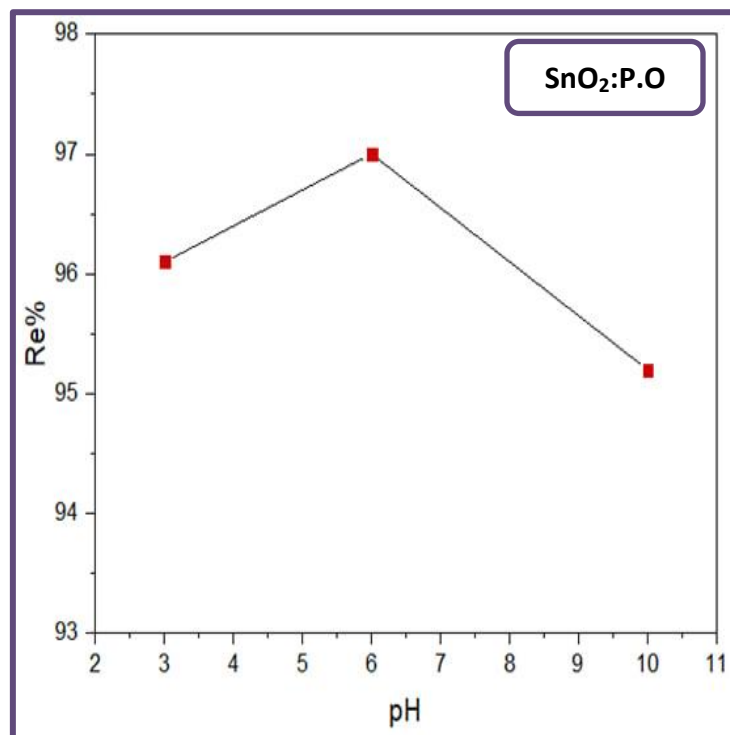
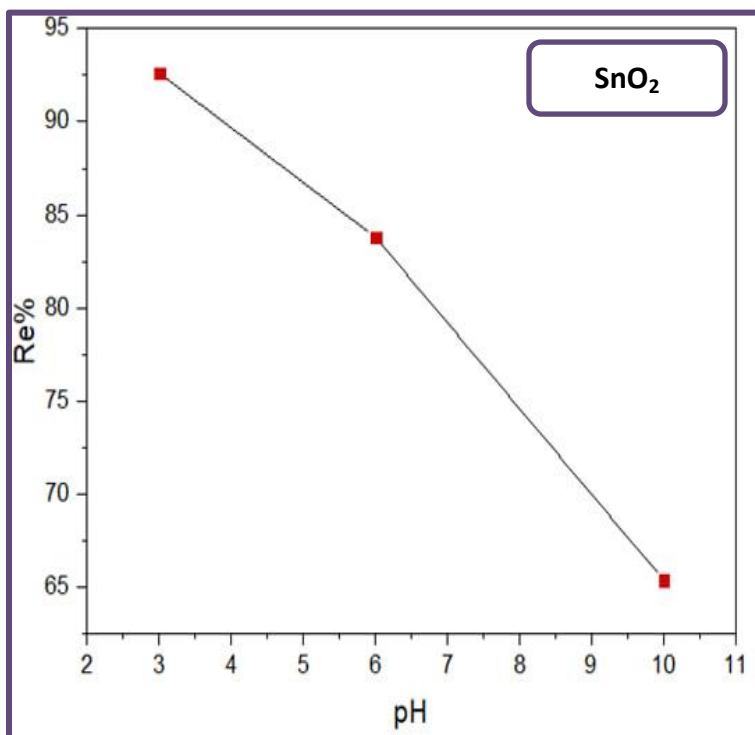


Figure 3.21 The influence of solution pH on the removal efficiency of MAF used bare SnO₂NPs,SnO₂:P.ONPs surfaces ,(T=298K , 0.6g)

3.4.1.5 The zero charges pH_{PZC} :

The point of zero charge was calculated to show at the pH that the net charge of total adsorbent surface was zero from the drawing through the convergence of reddish x,y. The results, shown in the Figure(3.21), showed the point of zero charge at $\text{pH}_{\text{PZC}} = 6$

The surface is positively charged when the value of $\text{pH} = 3 < \text{pH}_{\text{PZC}} = 6$

The surface is negatively charged when value of $\text{pH} = 10 > \text{pH}_{\text{PZC}} = 6$

The surface is neutral when the value of $\text{pH} = \text{pH}_{\text{PZC}} = 6$

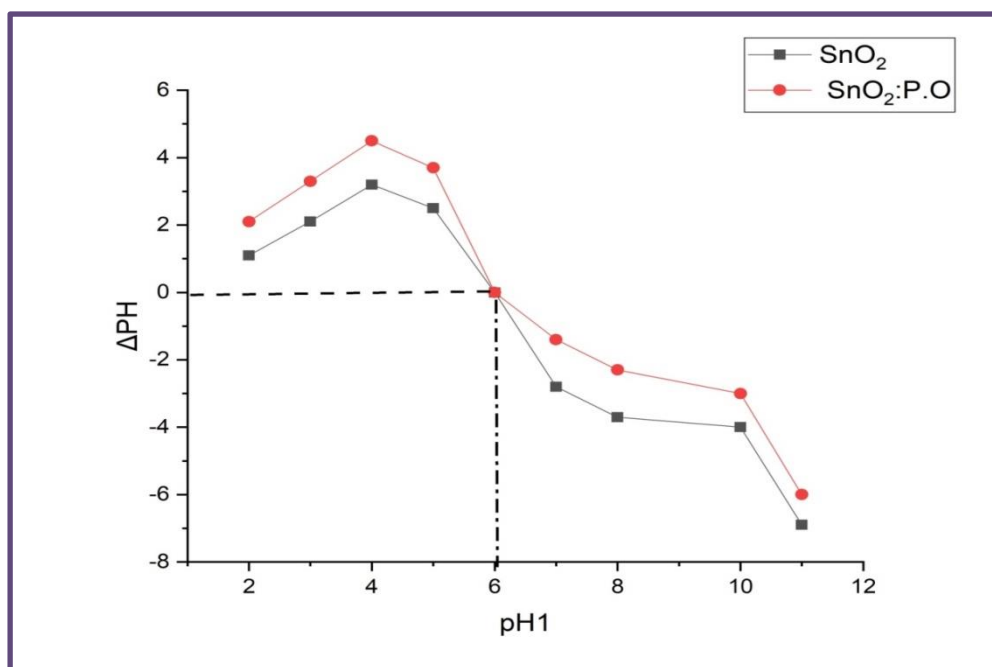


Figure 3.22 Point Zero charge of bare SnO₂NPs and SnO₂:P.O NPs , (contact time 24 h, and mass adsorbents 0.6 g).

3.4.1.6 Effect of temperature

The adsorption of the mefenamic acid on the two surfaces (bare SnO_2 , SnO_2 :P.O) NPs was studied at three temperatures (298, 308, and 318k) and the MFA concentrations of (30 mg/L) , with the weight of the adsorbent surfaces fixed (0.6g) and time (80min) for the bare SnO_2 NPs and time (30min) for SnO_2 :P.O surface. It is noted from the table(3.6) that the increasing temperature leads to increasing the adsorption capacity of bare SnO_2 NPs, indicating that the adsorption process on bare SnO_2 NPs is an endothermic adsorption process due to increasing the active adsorption sites and increasing the mobility of mefenamic acid molecules as the temperature increased¹⁴⁰. Optimal temperature for adsorbing MFA on bare SnO_2 NPs surface is 318 K (see Figure 3.23).

Table 3.6 Effect of temperature on adsorption of MFA on the bare SnO_2 NPs at different temperatures

298k				308 k			318 k		
C_o	C_e	Q_e	R_e	C_e	Q_e	R_e	C_e	Q_e	R_e
mg/L	mg/L	mg/g	%	mg/L	mg/g	%	mg/L	mg/g	%
30	4.842	1.048	83.8	4.315	1.07	85.6	3.789	1.09	87

For SnO_2 :P.ONPs, it is noticed through the table (3.7) and figure(3.23) that the capacity of adsorption is reduced when the temperature is increased, and this indicates that the process of adsorption on the (SnO_2 :P.O) NPs surface is an exothermic process¹⁴¹.

Table 3.7 Effect of temperature on adsorption of MFA on the SnO₂:P.O NPs at different temperatures

298k				308 k			318 k		
C _o mg/L	C _e mg/L	Q _e mg/g	R _e %	C _e mg/L	Q _e mg/g	R _e %	C _e mg/L	Q _e mg/g	R _e %
30	0.894	1.212	97	1.421	1.190	95.26	1.9	1.170	93.6

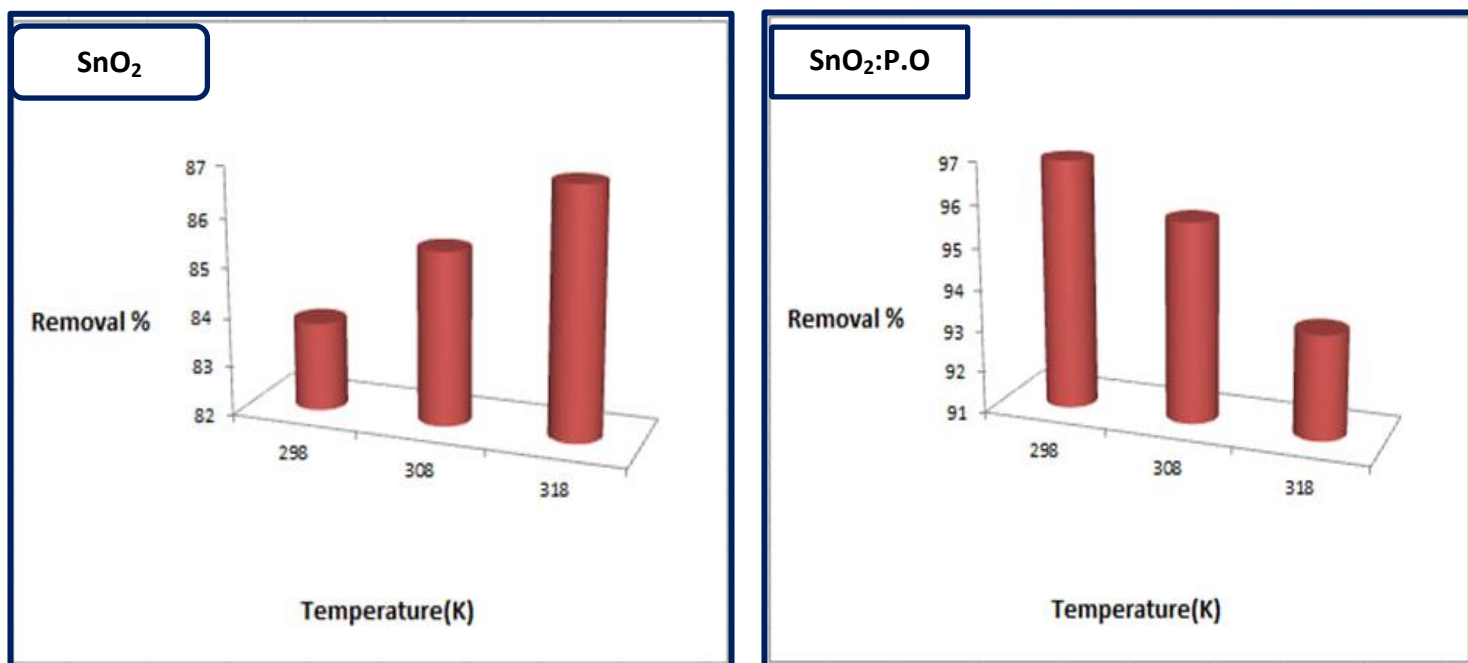


Figure 3.23 Effect of temperature on the adsorption of MAF on (bare SnO₂ and SnO₂:P.O) NPs

3.4.1.7 Calculation of thermodynamic functions

The values of thermodynamic functions were calculated for the adsorption of the mefenamic acid on a surfaces (SnO₂, SnO₂:P.O)NPs (ΔG free energy change, ΔS entropy change, and ΔH enthalpy change) and they are important for understanding the adsorption process. Enthalpy change (ΔH), Gibb's free energy change (ΔG), and entropy change (ΔS), which are thermodynamic parameters, were determined by Equations .

The equilibrium constant for the adsorption process at each temperature was calculated from the following equation^{142,143} .

$$K_{eq} = \frac{Q_e \times m}{C_e \times v} \dots\dots\dots(3.3)$$

Q_e: Adsorption capacity at equilibrium (mg / g).

C_e: Concentration of solute at equilibrium in units (mg / L).

m:dose of adsorbent surface (g).

v:solution of volume (L).

values change in the free energy (ΔG) could be determined from the equation¹⁰⁶ :

$$\Delta G = -RT \ln K_{eq} \dots\dots\dots(3.4)$$

The value of ΔH and ΔS can be calculated from the slope and intercept respectively According to the equation Van't Hof's equation plots¹³⁶ :

$$\ln K_{eq} = -\frac{\Delta H}{RT} + \frac{\Delta S}{R} \dots\dots\dots (3.5)$$

ΔG : free energy change (K_J/mol.K)

ΔH : enthalpy change (K_J/mol.K)

ΔS : entropy change (J/mol .k)

R: gas constant (8.314 J.K⁻¹ . mol⁻¹).

The Table (3.8) and figure (3.24) shows the relationship between $\ln K_{eq}$ versus $(1/T)$. Table (3.9) represents thermodynamic values for a bare SnO_2 NPs. The negative value of ΔG indicates the feasibility and spontaneity of adsorption process. A positive value of ΔH substantiates that adsorption of MFA on the adsorbent surface (SnO_2 NPs) is endothermic due to increasing the active adsorption sites and increasing the mobility of mefenamic acid molecules as the temperature increased¹⁴⁰.

The values of (ΔH) also show that the adsorption process was physical suggesting that it is multi layered, also the type of bonding forces is Vander Waals force. Positive values of (ΔS) indicate that the system is irregular.

As for the table (3.10), it shows the values of $\ln K_{eq}$ for the surface of ($\text{SnO}_2:\text{P.O}$) NPS and the figure (3.24) shows the relationship between $\ln K_{eq}$ and $1/T$. According to the values of the thermodynamic functions mentioned in the table(3.11), it is noted that The negative value of ΔG indicates the feasibility and spontaneity of the adsorption process, while a negative value of ΔH indicates a adsorption process is exothermic¹⁴¹.

The negative value of ΔS indicates a decrease in randomness and decrease in the degrees of freedom of the adsorbed molecules, that is, the molecules are bound by the adsorbent surface and thus are more regular and adsorption type is physisorption^{141, 144}.

Table 3.8 values of the equilibrium constant for MFA using bare SnO₂NPs at different temperatures.

Temp.(k)	1/T K ⁻¹	Ln keq
298	0.0033	1.63977311
308	0.0032	1.78355927
318	0.0031	1.93152141

Table 3.9 Thermodynamic adsorption parameters of the mefenamic acid over bare SnO₂ NPs

Temp.(k)	ΔG (KJ/mol.k)	ΔH(KJ/mol.k)	ΔS(J/mol.k)
298	-3.966598793	9.6251178×10 ⁻³	45.577348
308	-4.39084882		
318	-4.879535923		

Table 3.10 values of the equilibrium constant for MFA using SnO₂:P.O NPs at different temperatures.

Temp.(k)	1/T K ⁻¹	Ln keq
298	0.0033	3.480724
308	0.0032	2.995732
318	0.0031	2.6932

Table 3.11 Thermodynamic adsorption parameters of the mefenamic acid on SnO₂:P.O NPs at different temperature

Temp.(k)	ΔG (KJ /mol.k)	ΔH (KJ/ mol .k)	ΔS (J/ mol.k)
298	-8.62374	-32.7372	-78.7286
308	-7.67121		
318	-7.12042		

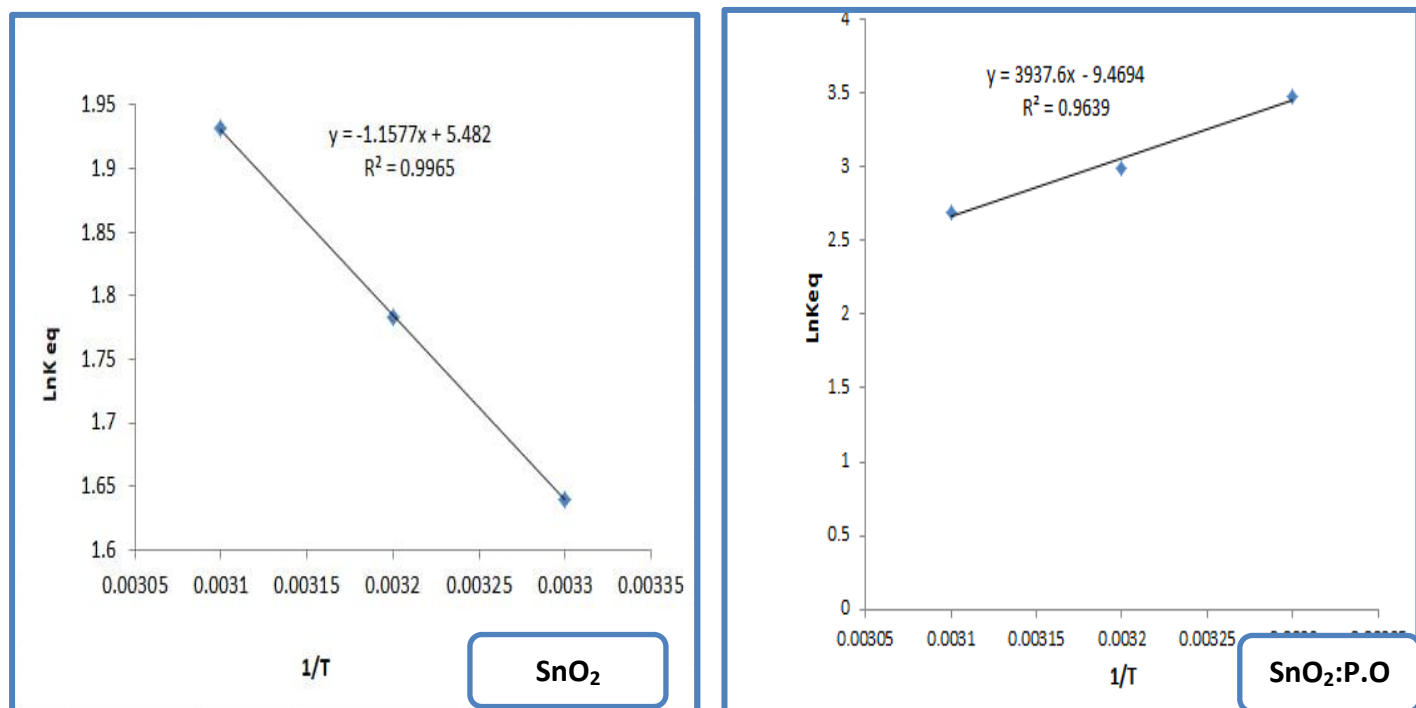


Figure (3.24) Plot Lnkeq against the absolute temperature of the adsorption MFA on bare SnO₂ NPs and SnO₂ :P.O NPs.

3.4.2.8 Adsorption isotherms

The adsorption isotherms were studied on the two surface of the (bare SnO₂, SnO₂:P.O)NPs within the range of concentrations(30,40,50,60,90) mg/L of MFA and at different temperatures within the range(298-318K) and at the best conditions for the adsorption process.

Table 3.12 C_e and q_e values for the adsorption of MFA on bare SnO₂ NPs at different temperatures

298k			308 k		318 k	
C _o mg/L	C _e mg/L	Q _e mg/g	C _e mg/L	Q _e mg/g	C _e mg/L	Q _e mg/g
30	4.842	1.048	4.315	1.070	3.789	1.092
40	8.263	1.322	6.684	1.388	5.894	1.421
50	10.631	1.640	8.680	1.721	8.000	1.75
60	13.00	1.958	10.890	2.046	9.842	2.089
90	25.100	2.704	19.578	2.934	17.740	3.010

Table 3.13 C_e and q_e values for the adsorption of MFA on $\text{SnO}_2\text{:P.ONPs}$ at different temperatures

298k			308 k		318 k	
C_o mg/L	C_e mg/L	Q_e mg/g	C_e mg/L	Q_e mg/g	C_e mg/L	Q_e mg/g
30	0.894	1.21	1.421	1.19	1.9	1.17
40	1.684	1.596	2.21	1.57	3	1.541
50	2.736	1.969	3	1.95	4.3	1.9
60	3.365	2.353	6.497	2.229	7.473	2.18
90	8.526	3.394	15.1	3.12	18.52	2.9

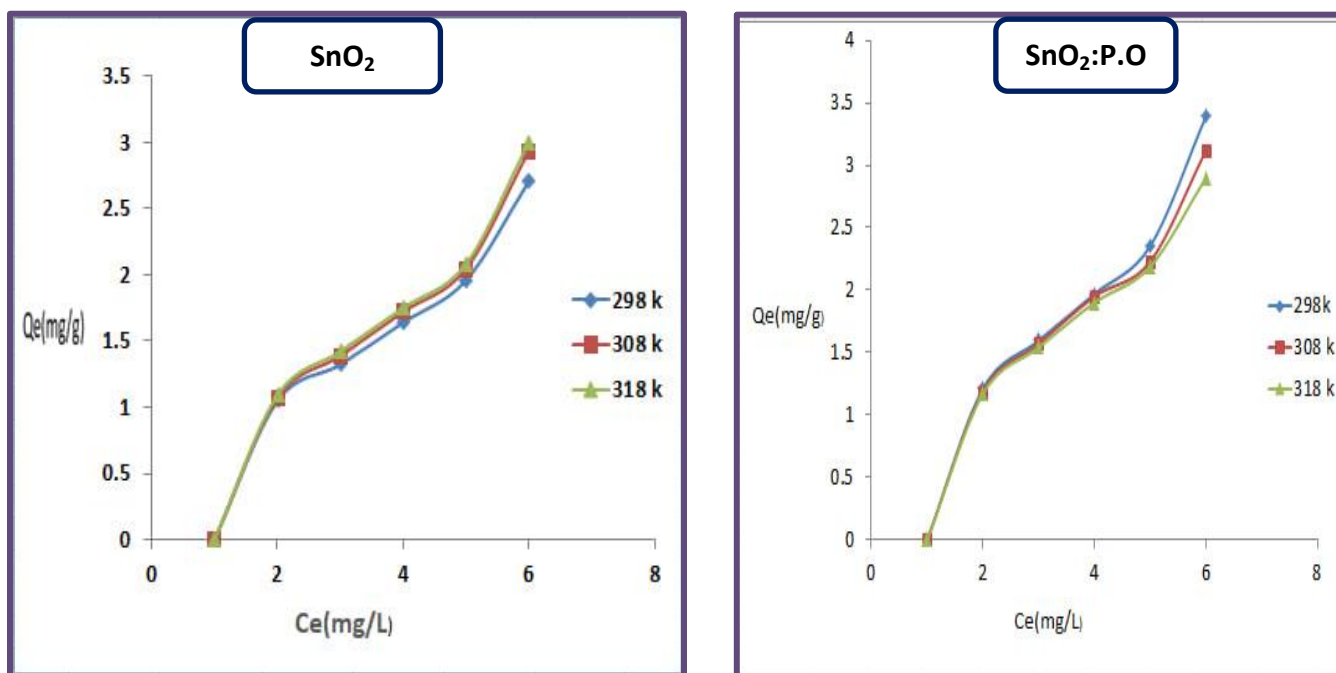


Figure 3. 25 The adsorption isotherm for MFA on the bare SnO_2 and $\text{SnO}_2\text{:P.O}$ NPs at different temperatures.

notice from the figure (3.25) that the general shape of the adsorption isotherms on surfaces of bare SnO₂, SnO₂:P.O NPs and at different temperatures indicates that they are of class (S) according to the Gills classification and that the isotherms are of class (S). This class is based on Freundlich principles. It can also be inferred from class (S) that the orientation of the adsorbed particles on the adsorbent surface is inclined or vertical, and therefore it will occupy less surface area and the adsorption will be high¹⁴⁵.

The experimental data was applied to remove the MAF on a surface of bare SnO₂ NPs and SnO₂:P.O NPs on the hypotheses Langmuir and Freundlich.

The results of the study of the Langmuir isotherms shown in the tables (3.14) and (3.17) for the adsorption process of the MFA on the surfaces of bare SnO₂ NPs and SnO₂: P.O NPs by drawing between C_e/Q_e vs C_e and finding the values correlation coefficient (R^2), shown in the two figures (3.26)(3.27) respectively. The adsorption process is not compatible with the Langmuir equation, and the reason is due to the formation of more than one adsorption layer on the surfaces, in addition to the difference in the potential energy of the active sites present on the adsorbent surface¹⁴⁶.

The results of the study shown in the two tables (3.15) and (3.18) and the two figures (3.26),(3.27), isotherms of the Freundlich equation, and by drawing between $\log Q_e$ and $\log C_e$ and finding the values of the correlation coefficient (R^2), it was found that the MFA adsorption process on the bare SnO₂ NPs and SnO₂:P.O NPs surfaces corresponded to the Freundlich equation, as it recorded, the highest correlation coefficient because the adsorption process occurred on non-homogeneous surfaces^{147,148}.

Table(3.14) Data on MFA adsorption on a surface bare SnO₂ NPs at different temperatures by applying Langmuir equation

Tem.	298 k		308 k		318 k	
C _o (mg/L)	C _e (mg/L)	C _e /Q _e (g/L)	C _e (mg/L)	C _e /Q _e (g/L)	C _e (mg/L)	C _e /Q _e (g/L)
30	4.842	4.619	4.315	4.033	3.789	3.476
40	8.263	6.250	6.684	4.809	5.894	4.148
50	10.631	6.482	8.68	5.106	8	4.571
60	13	6.639	10.89	5.445	9.482	4.741
90	25.1	9.282	19.58	6.682	17.74	5.912

Table 3.15 Data on MFA adsorption on a surface bare SnO₂ NPs at different temperatures by applying Freundlich equation

Tem.	298 k		308 k		318 k	
C _o (mg/L)	Log C _e (mg/L)	LogQ _e (g/L)	Log C _e (mg/L)	Log Q _e (g/L)	Log C _e (mg/L)	Log Q _e (g/L)
30	0.685	0.02	0.636	0.029	0.579	0.038
40	0.917	0.121	0.825	0.142	0.77	0.153
50	1.027	0.215	0.939	0.23	0.903	0.243
60	1.114	0.29	1.037	0.301	0.993	0.301
90	1.4	0.431	1.292	0.467	1.249	0.477

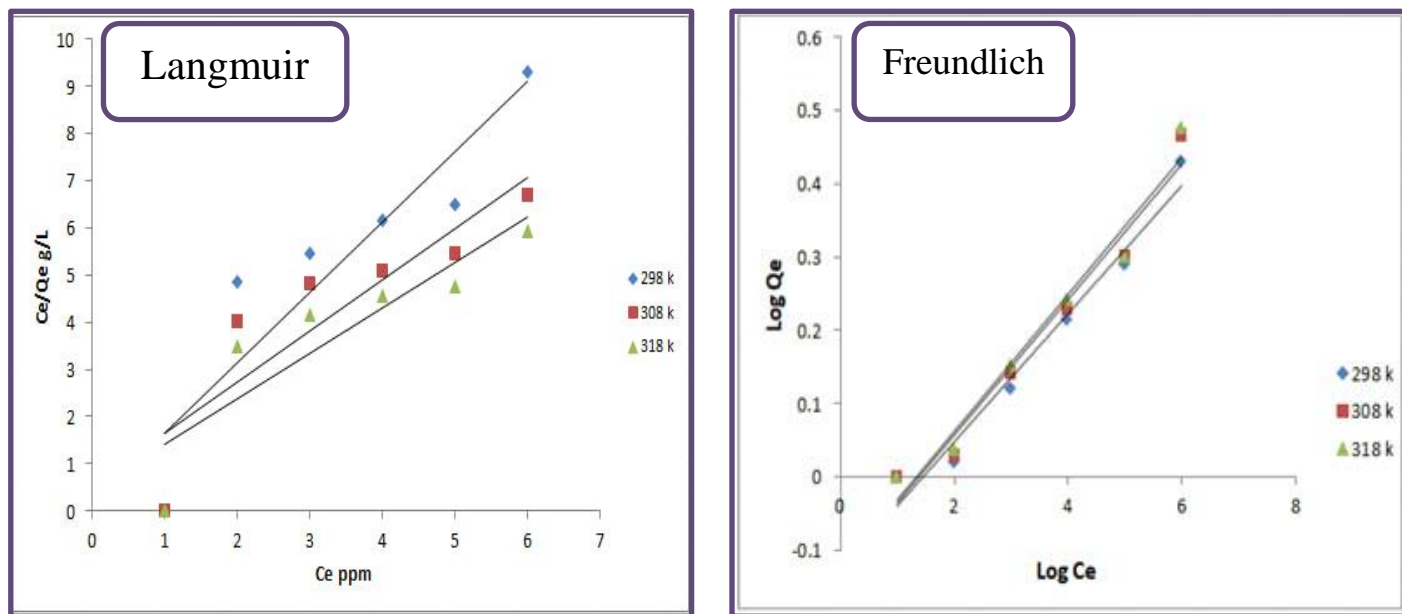


Figure 3.26 Freundlich and Langmuir isotherm for adsorption of MFA on surface bare SnO₂ NPs

Table 3.16 Langmuir and Freundlich parameters of adsorption isotherms MFA on SnO₂ NPs at (298 – 328) K

Temp. (k)	Langmuir isotherm			Freundlich isotherm		
	a	b	R ²	n	K _F	R ²
298	0.662296	1.807664	0.8256	10.71467	0.742	0.9701
308	0.922424	2.46184	0.7774	10.79941	0.747	0.9679
318	1.019888	3.711952	0.8024	11.44165	0.75	0.9681

Table 3.17 Data on MFA adsorption on a surface (SnO₂:P.O) NPs at different temperatures by applying Langmuir equation

Tem.	298 k		308 k		318 k	
C _o (ppm)	C _e (mg/L)	C _e /Q _e (g/L)	C _e (mg/L)	C _e /Q _e (g/L)	C _e (mg/L)	C _e /Q _e (g/L)
30	0.894	0.739	1.421	1.194	1.9	1.624
40	1.684	1.055	2.21	1.408	3	1.947
50	2.526	1.39	3	1.538	4.3	2.263
60	3.526	1.499	6.497	2.915	7.473	3.415
90	8.526	2.512	15.1	4.84	18.52	6.386

Table 3.18 Data on MFA adsorption on a surface (SnO₂:P.O) NPs at different temperatures by applying Freundlich equation

Temp.	298 k		308 k		318 k	
C _o (ppm)	Log C _e (mg/L)	Log Q _e (g/L)	Log C _e (mg/L)	Log Q _e (g/L)	Log C _e (mg/L)	Log Q _e (g/L)
30	-0.05	0.084	0.153	0.076	0.279	0.068
40	0.226	0.203	0.344	0.197	0.477	0.188
50	0.437	0.294	0.477	0.29	0.633	0.279
60	0.547	0.372	0.813	0.348	0.873	0.34
90	0.931	0.531	1.179	0.494	1.268	0.462

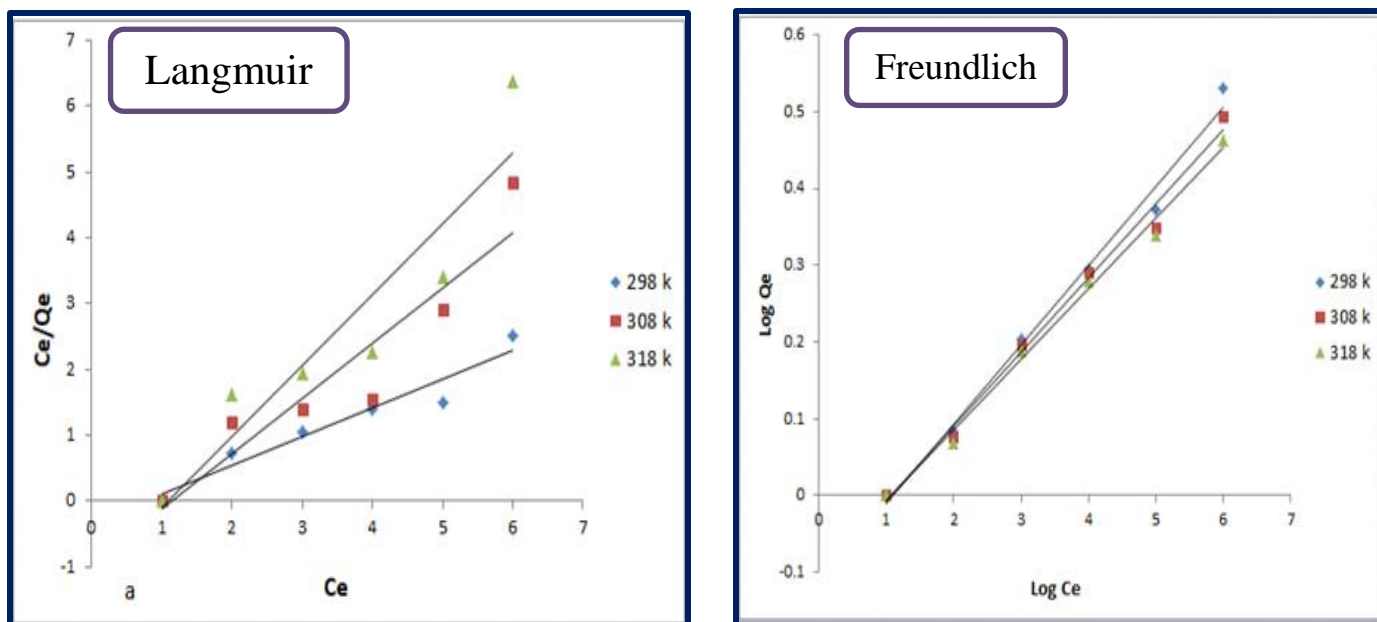


Figure 3.27 Langmuir and Freundlich isotherm for adsorption of MFA on surface $\text{SnO}_2:\text{P.O}$ NPs .

Table 3.19 Langmuir and Freundlich parameters of adsorption isotherms MFA on $(\text{SnO}_2:\text{P.O})$ NPs at (298 – 328) K

Temp. (k)	Langmuir isotherm			Freundlich isotherm		
	a	b	R^2	n	K_F	R^2
298	2.307337	-3.14268	0.9341	10.86957	0.796159	0.9902
308	1.186803	-1.03445	0.8804	10.35197	0.787046	0.9896
318	0.930319	-0.86483	0.8696	9.699321	0.7696620	0.9928

3.5 Adsorption Kinetics

The adsorption kinetics of an mefenamic acid on the surface of bare SnO₂ NPs and SnO₂ : P.O NPs was studied, where the amount of MFA adsorbed at different time periods was calculated according to the following equation:

$$q_t = \frac{(C_0 - C_t) v}{w} \dots\dots\dots 3.6$$

Where the experimental data were applied to equation models order first-Pseudo Lagergren and Pseudo-second order. according to the equation :

$$\log (q_e - q_t) = \log q_e - \frac{k_1 t}{2.303} \dots\dots\dots 3.7$$

$$\frac{t}{q_t} = \frac{1}{k_2 q_e^2} + \frac{t}{q_e}$$

where q_e : is the quantity of adsorbate (mg/ g) at equilibrium

q_t :is the amount of adsorbate (mg /g) at time (min).

k_1 : is the pseudo-first-order rate constant (min⁻¹)

k_2 : is the pseudo -second -order rate constant (mg .g⁻¹ min⁻¹)

It is clear from the table (3.20) that the results indicate that the adsorption of the MFA on the surfaces of bare SnO₂NPs and SnO₂:P.O NPs, follows a pseudo-second-order model, because (R^2) in a pseudo-second-order higher than (R^2) in order first-Pseudo.

Table 3.20 Kinetic parameters for pseudo-first-order and pseudo-second-order

Adsorbents	C _o (mg/L)	Pseudo-first order		Pseudo- second order	
		K ₁ min ⁻¹	R ²	K ₂ mg/g.min	R ²
Bare SnO ₂ NPs	30	0.000108	0.9361	0.178253	0.99584
SnO ₂ :P.O NPs	30	0.00141	0.8699	0.9651406	0.9984

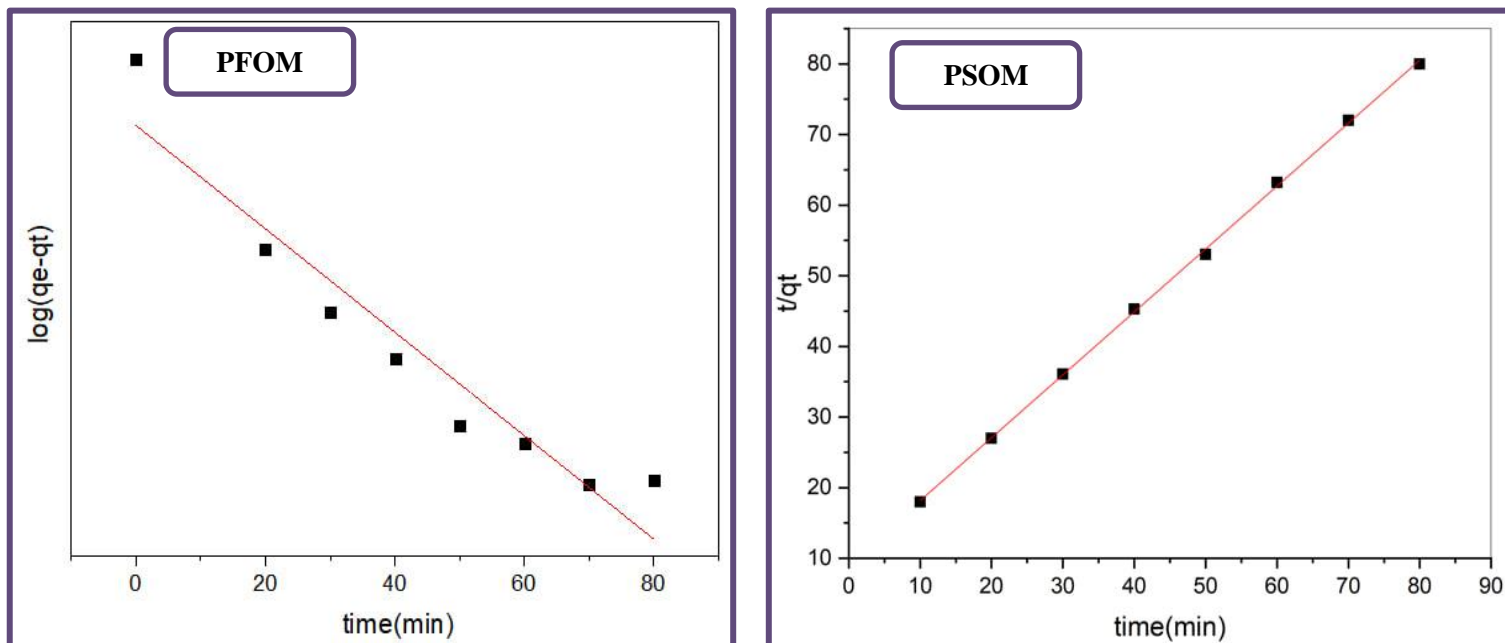


Figure 3.28 Adsorption kinetics of MFA on bare SnO₂ NPs pseudo-first-order model and pseudo-second-order model

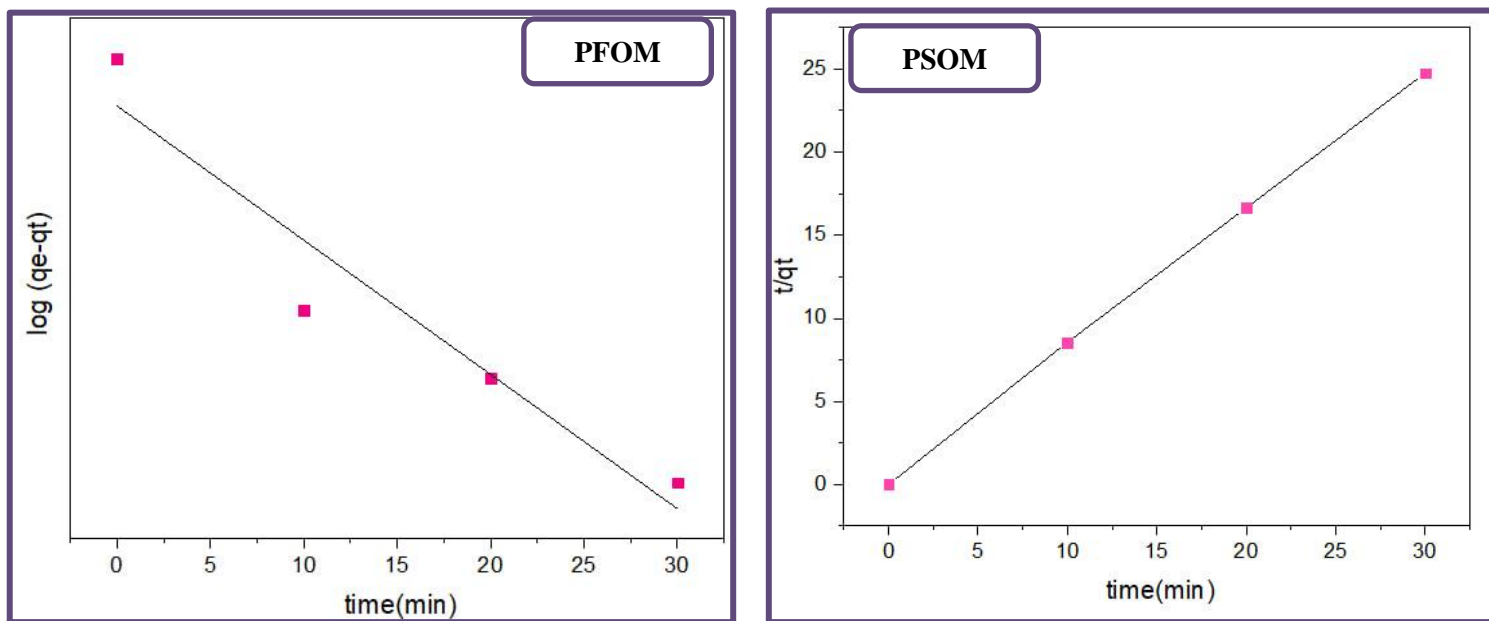


Figure 3.29 Adsorption kinetics of MFA on SnO₂ : P.O NPs pseudo-first-order model and pseudo-second-order model

After studying the adsorption behaviour of the prepared SnO₂ nanoparticles (both method)for removing mefenamic acid, under different parameters such as time, dose, initial concentration and temperature, found the absorption of MAF reduce after adding SnO₂ nanoparticles surface as show in figure(3.30).

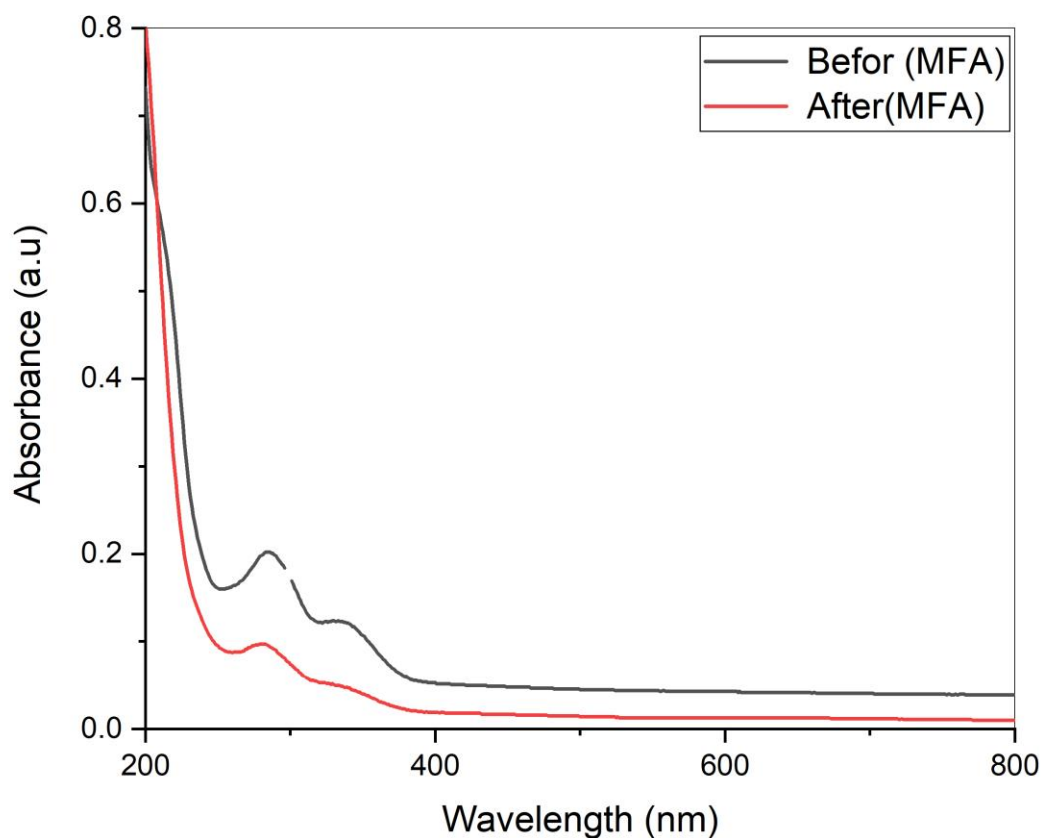


Figure 3.30 UV-Visible absorption spectrum of MAF before and after the adsorption

3.6 Conclusions

The main conclusions of this study can be summarized as:

- 1- SnO₂ nanoparticles were prepared successfully using chemical precipitation method and plant extraction method.
- 2- The UV-Visible spectrum of bare SnO₂ and SnO₂:P.O nanoparticles gave an absorption peak at 291nm and 278 nm at the optimal conditions . These blue shift compared to the bulk is attributed to the effects of quantum confinement
- 3- The band gap energies were estimated from the UV-visible curve in DRS spectrum for both bare SnO₂ and SnO₂:P.O NPs and they turned out to be 3.7eV and 4.2 eV, respectively
- 4- The crystallite size of tin oxide nanoparticles was measured using Scherer formula and they are 12.7 nm and 3 nm for bare SnO₂ and SnO₂ :P.O NPs, respectively.
- 5- FT-IR analysis shows an evidence for the formation of SnO₂ particles due to the peaks that appeared in the 585 cm⁻¹ which is assigned to O-Sn-O band.
- 6- The maximum removal efficiency for the removal of mefenamic acid using SnO₂:P.O nanoparticles is 97% after 30 minutes. Whilst, bare SnO₂ nanoparticles gave 92 % after 80minutes.
- 7- The adsorption of MFA on bare SnO₂NPs increased with rise the temperature, indicating the adsorption process is endothermic. However, the adsorption process of MFA on SnO₂:P.O NPs was exothermic
- 8- The adsorption of MFA on bare SnO₂ and SnO₂ :P.O NPs fitted with Freundlich model, and its follows S-type isotherm.

- 9- Introducing *Portulaca oleracea* extract to the formation process of SnO₂ nanoparticles leads to forming small nanoparticles with a wide band gap 4.2 eV compared to those formed through the chemical precipitation method 3.7 eV. These small particles have large surface-to-area and consequently can be used in removing process of pharmaceutical products with high efficiency.

3.7 Future Studies:

Tin oxide nanoparticles takes a great attention due to its physical, chemical, and biological properties. For future work we recommend the following:

- Study the photo catalytic activity of tin oxide nanoparticles.
- Study the possibility of using biosynthesized SnO₂ nanoparticles in the medical field such as in cancer treatment or chronic bacterial diseases
- Study the ability of biosynthesized tin oxide nanoparticles to adsorb different dyes by doping them with different metals and semiconductors.

Reference

- (1)Albrecht, P. J.; Davar, G.; Eisenberg, E.; Pare, M.; Rice, F. L. Response to Editorial on Albrecht et al.(2006). *Pain* **2006**, *123*, 217.
- (2)Hidalgo-Manrique, P.; Lei, X.; Xu, R.; Zhou, M.; Kinloch, I. A.; Young, R. J. Copper/graphene composites: a review. *Journal of materials science* **2019**, *54*, 12236-12289.
- (3)Abid, N.; Khan, A. M.; Shujait, S.; Chaudhary, K.; Ikram, M.; Imran, M.; Haider, J.; Khan, M.; Khan, Q.; Maqbool, M. Synthesis of nanomaterials using various top-down and bottom-up approaches, influencing factors, advantages, and disadvantages: A review. *Advances in Colloid and Interface Science* **2021**, 102597.
- (4)Haruta, M. When gold is not noble: catalysis by nanoparticles. *The chemical record* **2003**, *3*, 75-87.
- (5)Alanazi, F. K.; Radwan, A. A.; Alsarra, I. A. Biopharmaceutical applications of nanogold. *Saudi Pharmaceutical Journal* **2010**, *18*, 179-193.
- (6)Jeevanandam, J.; Barhoum, A.; Chan, Y. S.; Dufresne, A.; Danquah, M. K. Review on nanoparticles and nanostructured materials: history, sources, toxicity and regulations. *Beilstein journal of nanotechnology* **2018**, *9*, 1050-1074.
- (7)Płaza, G. A.; Chojniak, J.; Banat, I. M. Biosurfactant mediated biosynthesis of selected metallic nanoparticles. *International Journal of Molecular Sciences* **2014**, *15*, 13720-13737.
- (8)Barber, D. J.; Freestone, I. C. An investigation of the origin of the colour of the Lycurgus Cup by analytical transmission electron microscopy. *Archaeometry* **1990**, *32*, 33-45.
- (9)Joudeh, N.; Linke, D. Nanoparticle classification, physicochemical properties, characterization, and applications: a comprehensive review for biologists. *Journal of Nanobiotechnology* **2022**, *20*, 262.
- (10)Feynman, R. P. There's plenty of room at the bottom: An invitation to enter a new field of physics. *Miniaturization, Reinhold* **1961**.
- (11)Sanjay, S. S.; Pandey, A. C. A brief manifestation of nanotechnology. *EMR/ESR/EPR spectroscopy for characterization of nanomaterials* **2017**, 47-63.
- (12)Binnig, G.; Quate, C. F.; Gerber, C. Atomic force microscope. *Physical review letters* **1986**, *56*, 930.

- (13)Yadav, T. P.; Yadav, R. M.; Singh, D. P. Mechanical milling: a top down approach for the synthesis of nanomaterials and nanocomposites. *Nanoscience and Nanotechnology* **2012**, *2*, 22-48.
- (14)Jamkhande, P. G.; Ghule, N. W.; Bamer, A. H.; Kalaskar, M. G. Metal nanoparticles synthesis: An overview on methods of preparation, advantages and disadvantages, and applications. *Journal of drug delivery science and technology* **2019**, *53*, 101174.
- (15)Brock, S. L.: Nanostructures and Nanomaterials: Synthesis, Properties and Applications By Guozhang Cao (University of Washington). Imperial College Press (distributed by World Scientific): London. 2004. xiv+ 434 pp. \$78.00. ISBN 1-86094-415-9. ACS Publications, 2004.
- (16)Ijaz, I.; Gilani, E.; Nazir, A.; Bukhari, A. Detail review on chemical, physical and green synthesis, classification, characterizations and applications of nanoparticles. *Green Chemistry Letters and Reviews* **2020**, *13*, 223-245.
- (17)Ismail, A.; Menazea, A.; Kabary, H. A.; El-Sherbiny, A.; Samy, A. The influence of calcination temperature on structural and antimicrobial characteristics of zinc oxide nanoparticles synthesized by Sol–Gel method. *Journal of Molecular Structure* **2019**, *1196*, 332-337.
- (18)Parashar, M.; Shukla, V. K.; Singh, R. Metal oxides nanoparticles via sol–gel method: a review on synthesis, characterization and applications. *Journal of Materials Science: Materials in Electronics* **2020**, *31*, 3729-3749.
- (19)Sulistyaningsih, T.; Santosa, S. J.; Siswanta, D.; Rusdiarso, B. Synthesis and characterization of magnetites obtained from mechanically and sonochemically assisted co-precipitation and reverse co-precipitation methods. *Int. J. Mater. Mech. Manuf* **2017**, *5*, 16-19.
- (20)Basiuk, V. A.; Basiuk, E. V. Green processes for nanotechnology. *Springer* **2015**, 446.
- (21)Taka, G.; Das, T. In *Tilte2022*; IOP Publishing.
- (22)Arole, V.; Munde, S. Fabrication of nanomaterials by top-down and bottom-up approaches-an overview. *J. Mater. Sci* **2014**, *1*, 89-93.
- (23)Zhao, X.; Wei, C.; Gai, Z.; Yu, S.; Ren, X. Chemical vapor deposition and its application in surface modification of nanoparticles. *Chemical Papers* **2020**, *74*, 767-778.
- (24)Seravalli, L.; Bosi, M.; Fiorenza, P.; Panasci, S.; Orsi, D.; Rotunno, E.; Cristofolini, L.; Rossi, F.; Giannazzo, F.; Fabbri, F. Gold nanoparticle assisted synthesis of MoS₂ monolayers by chemical vapor deposition. *Nanoscale Advances* **2021**, *3*, 4826-4833.

- (25)Kalpana, V.; Rajeswari, V. D.: Biosynthesis of metal and metal oxide nanoparticles for food packaging and preservation: a green expertise. In *Food biosynthesis*; Elsevier, 2017; pp 293-316.
- (26)Firdhouse, M. J.; Lalitha, P. Biosynthesis of silver nanoparticles and its applications. *Journal of Nanotechnology* **2015**, 2015.
- (27)Vijayaraghavan, K.; Ashokkumar, T. Plant-mediated biosynthesis of metallic nanoparticles: A review of literature, factors affecting synthesis, characterization techniques and applications. *Journal of environmental chemical engineering* **2017**, 5, 4866-4883.
- (28)Tran, T. V.; Nguyen, D. T. C.; Kumar, P. S.; Din, A. T. M.; Jalil, A. A.; Vo, D.-V. N. Green synthesis of ZrO₂ nanoparticles and nanocomposites for biomedical and environmental applications: A review. *Environmental Chemistry Letters* **2022**, 1-23.
- (29)Padil, V. V. T.; Černík, M. Green synthesis of copper oxide nanoparticles using gum karaya as a biotemplate and their antibacterial application. *International journal of nanomedicine* **2013**, 889-898.
- (30)Aboyewa, J. A.; Sibuyi, N. R.; Meyer, M.; Oguntibeju, O. O. Green synthesis of metallic nanoparticles using some selected medicinal plants from southern africa and their biological applications. *Plants* **2021**, 10, 1929.
- (31)Abdelhamid, M. E.; O'Mullane, A. P.; Snook, G. A. Storing energy in plastics: a review on conducting polymers & their role in electrochemical energy storage. *Rsc Advances* **2015**, 5, 11611-11626.
- (32)Ahmed, S.; Ahmad, M.; Swami, B. L.; Ikram, S. A review on plants extract mediated synthesis of silver nanoparticles for antimicrobial applications: a green expertise. *Journal of advanced research* **2016**, 7, 17-28.
- (33)Pankove, J. I.: *Optical processes in semiconductors*; Courier Corporation, 1975.
- (34)Yang, Z.; Wang, M.; Qiu, H.; Yao, X.; Lao, X.; Xu, S.; Lin, Z.; Sun, L.; Shao, J. Engineering the exciton dissociation in quantum-confined 2D CsPbBr₃ nanosheet films. *Advanced Functional Materials* **2018**, 28, 1705908.
- (35)Tong, H.; Ouyang, S.; Bi, Y.; Umezawa, N.; Oshikiri, M.; Ye, J. Nano-photocatalytic materials: possibilities and challenges. *Advanced materials* **2012**, 24, 229-251.
- (36)Bredas, J.-L. Mind the gap! *Materials Horizons* **2014**, 1, 17-19.
- (37)Smith, A. M.; Nie, S. Semiconductor nanocrystals: structure, properties, and band gap engineering. *Accounts of chemical research* **2010**, 43, 190-200.

- (38)Malik, R.; Tomer, V. K.; Duhan, S.; Nehra, S.; Rana, P. S. One-pot hydrothermal synthesis of porous SnO₂ nanostructures for photocatalytic degradation of organic pollutants. *Energy and Environment Focus* **2015**, *4*, 340-345.
- (39)Amanullah, F.; Al-Mobarak, M. S.; Al-Dhafiri, A.; Al-Shibani, K. Development of spray technique for the preparation of thin films and characterization of tin oxide transparent conductors. *Materials chemistry and physics* **1999**, *59*, 247-253.
- (40)Kong, Y.; Li, Y.; Cui, X.; Su, L.; Ma, D.; Lai, T.; Yao, L.; Xiao, X.; Wang, Y. SnO₂ nanostructured materials used as gas sensors for the detection of hazardous and flammable gases: A review. *Nano Materials Science* **2021**.
- (41)Ravichandran, K.; Muruganatham, G.; Sakthivel, B. Highly conducting and crystalline doubly doped tin oxide films fabricated using a low-cost and simplified spray technique. *Physica B: Condensed Matter* **2009**, *404*, 4299-4302.
- (42)Moseley, P. Solid state gas sensors. *Measurement Science and technology* **1997**, *8*, 223.
- (43)Kaur, M.; Prasher, D.; Sharma, R. Recent developments on I and II series transition elements doped SnO₂ nanoparticles and its applications for water remediation process: a review. *Journal of Water and Environmental Nanotechnology* **2022**, *7*, 194-217.
- (44)Koppala, S.; Balan, R.; Banerjee, I.; Li, K.; Xu, L.; Liu, H.; Kumar, D. K.; Reddy, K. R.; Sadhu, V. Room temperature synthesis of novel worm like tin oxide nanoparticles for photocatalytic degradation of organic pollutants. *Materials Science for Energy Technologies* **2021**, *4*, 113-118.
- (45)Din, S. U.; Kiani, S. H.; Haq, S.; Ahmad, P.; Khandaker, M. U.; Faruque, M. R. I.; Idris, A. M.; Sayyed, M. Bio-synthesized tin oxide nanoparticles: structural, optical, and biological studies. *Crystals* **2022**, *12*, 614.
- (46)Sagadevan, S.; Lett, J. A.; Fatimah, I.; Lokanathan, Y.; Léonard, E.; Oh, W. C.; Hossain, M. M.; Johan, M. R. Current trends in the green syntheses of tin oxide nanoparticles and their biomedical applications. *Materials Research Express* **2021**, *8*, 082001.
- (47)Chopra, K.; Major, S.; Pandya, D. Transparent conductors—a status review. *Thin solid films* **1983**, *102*, 1-46.
- (48)Chen, J. S.; Lou, X. W. SnO₂-based nanomaterials: synthesis and application in lithium-ion batteries. *small* **2013**, *9*, 1877-1893.

- (49)Sharghi, H.; Ebrahimpourmoghaddam, S.; Memarzadeh, R.; Javadpour, S. Tin oxide nanoparticles (NP-SnO₂): preparation, characterization and their catalytic application in the Knoevenagel condensation. *Journal of the iranian chemical society* **2013**, *10*, 141-149.
- (50)Belayachi, W.; Ferblantier, G.; Fix, T.; Schmerber, G.; Rehspringer, J.-L.; Heiser, T.; Slaoui, A.; Abd-Lefdil, M.; Dinia, A. SnO₂ Films elaborated by radio frequency magnetron sputtering as potential transparent conducting oxides alternative for organic solar cells. *ACS Applied Energy Materials* **2021**, *5*, 170-177.
- (51)Batzill, M.; Diebold, U. The surface and materials science of tin oxide. *Progress in surface science* **2005**, *79*, 47-154.
- (52)Kong, L.; Ma, J.; Zhu, Z.; Luan, C.; Yu, X.; Yu, Q. Synthesis of orthorhombic structure epitaxial tin oxide film. *Materials Letters* **2010**, *64*, 1350-1353.
- (53)Li, H.; Li, Q.; Li, Y.; Sang, X.; Yuan, H.; Zheng, B. Stannic oxide nanoparticle regulates proliferation, invasion, apoptosis, and oxidative stress of oral cancer cells. *Frontiers in Bioengineering and Biotechnology* **2020**, *8*, 768.
- (54)Matussin, S.; Harunsani, M. H.; Tan, A. L.; Khan, M. M. Plant-extract-mediated SnO₂ nanoparticles: synthesis and applications. *ACS Sustainable Chemistry & Engineering* **2020**, *8*, 3040-3054.
- (55)Srivastava, R.; Srivastava, V.; Singh, A. Multipurpose benefits of an underexplored species purslane (*Portulaca oleracea* L.): a critical review. *Environmental Management* **2021**, 1-12.
- (56)Butnariu, M. *Portulaca Oleracea* phytochemistry and pharmacological considerations. *Ann Pharmacol Pharm.* 2018; *3 (3)* **2018**, 1149.
- (57)Kumar, A.; Sreedharan, S.; Kashyap, A. K.; Singh, P.; Ramchiary, N. A review on bioactive phytochemicals and ethnopharmacological potential of purslane (*Portulaca oleracea* L.). *Heliyon* **2021**, e08669.
- (58)Zhou, Y.-X.; Xin, H.-L.; Rahman, K.; Wang, S.-J.; Peng, C.; Zhang, H. *Portulaca oleracea* L.: a review of phytochemistry and pharmacological effects. *BioMed research international* **2015**, 2015.
- (59)Petropoulos, S. A.; Fernandes, Â.; Dias, M. I.; Vasilakoglou, I. B.; Petrotos, K.; Barros, L.; Ferreira, I. C. Nutritional value, chemical composition and cytotoxic properties of common purslane (*Portulaca oleracea* L.) in relation to harvesting stage and plant part. *Antioxidants* **2019**, *8*, 293.

- (60) Mansouri, F.; Chouchene, K.; Roche, N.; Ksibi, M. Removal of Pharmaceuticals from water by adsorption and advanced oxidation processes: State of the art and trends. *Applied Sciences* **2021**, *11*, 6659.
- (61) Deepa, R.; Madhu, G.; Thomas, R. M. A comparative study on the removal of an emerging contaminant mefenamic acid from aqueous media by various advanced oxidation methods. *Materials Today: Proceedings* **2021**, *47*, 1416-1422.
- (62) Ternes, T. A.; Hirsch, R.; Mueller, J.; Haberer, K. Methods for the determination of neutral drugs as well as betablockers and β 2-sympathomimetics in aqueous matrices using GC/MS and LC/MS/MS. *Fresenius' journal of analytical chemistry* **1998**, *362*, 329-340.
- (63) Colombo, R.; Ferreira, T. C.; Ferreira, R. A.; Lanza, M. R. Removal of Mefenamic acid from aqueous solutions by oxidative process: Optimization through experimental design and HPLC/UV analysis. *Journal of environmental management* **2016**, *167*, 206-213.
- (64) Aloulou, W.; Aloulou, H.; Jadda, A.; Chakraborty, S.; Amar, R. B. Characterization of an asymmetric ultrafiltration membrane prepared from TiO₂-smectite nanocomposites doped with commercial TiO₂ and its application to the treatment of textile wastewater. *Euro-Mediterranean Journal for Environmental Integration* **2020**, *5*, 1-9.
- (65) Wang, J.; Wang, S. Reactive species in advanced oxidation processes: Formation, identification and reaction mechanism. *Chemical Engineering Journal* **2020**, *401*, 126158.
- (66) Radjenovic, J.; Petrovic, M.; Barceló, D. Analysis of pharmaceuticals in wastewater and removal using a membrane bioreactor. *Analytical and bioanalytical chemistry* **2007**, *387*, 1365-1377.
- (67) Gimeno, O.; Rivas, J.; Encinas, A.; Beltran, F. Application of advanced oxidation processes to Mefenamic acid elimination. *International Journal of Nuclear and Quantum Engineering* **2010**, *4*, 399-401.
- (68) Moruzzi, R. B.; Lima, V. B.; Colombo, R.; Conceição, F. T.; Lanza, M. R. Mefenamic acid removal in water using activated carbon powder, red mud and oxidation with chlorine. *Química Nova* **2014**, *37*, 1594-1599.
- (69) Abed, A.; Al Hindawi, A.; Alesary, H. Green Synthesis of Zinc Sulfide Nanoparticles for the Removal of Methylene Blue Dye from Aqueous Solution. *NanoWorld J* **2022**, *8*, 79-84.

- (70)Shanian, Z. Y.; Abid, M. F.; Sukkar, K. Photodegradation of mefenamic acid from wastewater in a continuous flow solar falling film reactor. *Desalin. Water Treat* **2021**, *210*, 22-30.
- (71)Turki, Z.; Al Hindawi, A.; Shiltagh, N. Green Synthesis of CdS Nanoparticles Using Avocado Peel Extract. *NanoWorld J* **2022**, *8*, 73-78.
- (72)Albo Hay Allah, M. A.; Alshamsi, H. A. Green synthesis of ZnO NPs using *Pontederia crassipes* leaf extract: characterization, their adsorption behavior and anti-cancer property. *Biomass Conversion and Biorefinery* **2022**, 1-14.
- (73)Skoog, D. A.; West, D. M.; Holler, F. J.; Crouch, S. R.: *Fundamentals of analytical chemistry*; Cengage learning, 2013.
- (74)Ambali, A.; Evbuomwan, B.; Momoh, Y. Comparative study on the adsorption capacity of snail and perewinkle shells for the removal of nickel (II) Ion from aqueous solution. *International Journal of Geology, Agriculture and Environmental Sciences* **2015**, *3*, 39-50.
- (75)Rajahmundry, G. K.; Garlapati, C.; Kumar, P. S.; Alwi, R. S.; Vo, D.-V. N. Statistical analysis of adsorption isotherm models and its appropriate selection. *Chemosphere* **2021**, *276*, 130176.
- (76)Haddad, R.; Zageer, D.; Shneine, J.; Salman, H.; Noaman, R.; Abdullah, B.; Yousif, E. Journal of Iraqi Industrial Research. *Journal of Iraqi Industrial Research Vol* **2015**, *2*, 25-30.
- (77)Teimouri, Z.; Salem, A.; Salem, S. Microwave-assisted for clean and rapid fabrication of highly efficient magnetically separable activated carbon from agriculture shells for low grade industrial corn syrup decoloration: A novel strategy for impregnation of ternary catalytic composite. *Food and Bioproducts Processing* **2019**, *116*, 78-88.
- (78)Černý, S.; Ponec, V. Determination of heat of adsorption on clean solid surfaces. *Catalysis Reviews* **1969**, *2*, 249-322.
- (79)Shirzadeh, M.; Sepehr, E.; Rasouli Sadaghiani, M.; Ahmadi, F. Effect of pH, initial concentration, background electrolyte, and ionic strength on cadmium adsorption by TiO₂ and γ -Al₂O₃ nanoparticles. *Pollution* **2020**, *6*, 223-235.
- (80) Xu, L.; Cao, J.; Chen, W. Structural characterization of a broccoli polysaccharide and evaluation of anti-cancer cell proliferation effects. *Carbohydrate polymers* **2015**, *126*, 179-184.
- (81)Clark, R. M.; Adams, J. Q. Evaluation of BAT for VOCs in drinking water. *Journal of environmental engineering* **1991**, *117*, 247-268.

- (82)Knaebel, K. S.; Reinhold, H. E. Landfill gas: from rubbish to resource. *Adsorption* **2003**, *9*, 87-94.
- (83)Jiuhui, Q. Research progress of novel adsorption processes in water purification: a review. *Journal of environmental sciences* **2008**, *20*, 1-13.
- (84)Atsar, F. S.; Kukwa, D.; Wuana, R. A.; Arwenyo, B. Kinetics and Thermodynamic Studies: Adsorption of Pb, Cr and Ni Ions from Spent Lubrication Oil (SLO) Using Acid Modified Clay. *American Journal of Analytical Chemistry* **2021**, *12*, 109-120.
- (85)Langmuir, I. The adsorption of gases on plane surfaces of glass, mica and platinum. *Journal of the American Chemical society* **1918**, *40*, 1361-1403.
- (86)Freundlich, H. Über die adsorption in lösungen. *Zeitschrift für physikalische Chemie* **1907**, *57*, 385-470.
- (87)Kreuzer, H. J.; Gortel, Z. W.; Kreuzer, H. J.; Gortel, Z. W. Kramers Equation. *Physisorption Kinetics* **1986**, 259-281.
- (88)Hussain, N.; Alwan, S.; Alshamsi, H.; Sahib, I. Green synthesis of S-and N-codoped carbon nanospheres and application as adsorbent of Pb (II) from aqueous solution. *International Journal of Chemical Engineering* **2020**, *2020*, 1-13.
- (89)Ahmad, M. A.; Eusoff, M. A.; Oladoye, P. O.; Adegoke, K. A.; Bello, O. S. Optimization and batch studies on adsorption of Methylene blue dye using pomegranate fruit peel based adsorbent. *Chemical Data Collections* **2021**, *32*, 100676.
- (90)Ho, Y. S.; McKay, G. A comparison of chemisorption kinetic models applied to pollutant removal on various sorbents. *Process safety and environmental protection* **1998**, *76*, 332-340.
- (91)Al-Jabari, M.; Khalid, I.; Sulaiman, S.; Alawi, I.; Shilo, J. Synthesis, characterization, kinetic and thermodynamic investigation of silica nanoparticles and their application in mefenamic acid removal from aqueous solution. *Desalination and Water Treatment* **2018**, *129*, 160-167.
- (92)Acharya, J.; Kumar, U.; Rafi, P. M. Removal of heavy metal ions from wastewater by chemically modified agricultural waste material as potential adsorbent-a review. *International Journal of Current Engineering and Technology* **2018**, *8*, 526-530.
- (93)Chiu, H.-C.; Yeh, C.-S. Hydrothermal synthesis of SnO₂ nanoparticles and their gas-sensing of alcohol. *The Journal of Physical Chemistry C* **2007**, *111*, 7256-7259.

- (94)Sikhwivhilu, L. M.; Pillai, S. K.; Hillie, T. K. Influence of citric acid on SnO₂ nanoparticles synthesized by wet chemical processes. *Journal of nanoscience and nanotechnology* **2011**, *11*, 4988-4994.
- (95)Manjula, P.; Boppella, R.; Manorama, S. V. A facile and green approach for the controlled synthesis of porous SnO₂ nanospheres: application as an efficient photocatalyst and an excellent gas sensing material. *ACS applied materials & interfaces* **2012**, *4*, 6252-6260.
- (96)Tammina, S. K.; Mandal, B. K.; Ranjan, S.; Dasgupta, N. Cytotoxicity study of Piper nigrum seed mediated synthesized SnO₂ nanoparticles towards colorectal (HCT116) and lung cancer (A549) cell lines. *Journal of Photochemistry and Photobiology B: Biology* **2017**, *166*, 158-168.
- (97)Kim, S.-C.; Park, Y.-K.; Kim, B. H.; Kim, H.; Lee, W.-J.; Lee, H.; Jung, S.-C. Facile precipitation of tin oxide nanoparticles on graphene sheet by liquid phase plasma method for enhanced electrochemical properties. *Korean Journal of Chemical Engineering* **2018**, *35*, 750-756.
- (98)Begum, S.; Ahmaruzzaman, M. Biogenic synthesis of SnO₂/activated carbon nanocomposite and its application as photocatalyst in the degradation of naproxen. *Applied Surface Science* **2018**, *449*, 780-789.
- (99)Kumar, M.; Mehta, A.; Mishra, A.; Singh, J.; Rawat, M.; Basu, S. Biosynthesis of tin oxide nanoparticles using Psidium Guajava leave extract for photocatalytic dye degradation under sunlight. *Materials Letters* **2018**, *215*, 121-124.
- (100)Buniyamin, I.; Akhir, R. M.; Asli, N. A.; Khusaimi, Z.; Mahmood, M. R. In *Tilte2021*; IOP Publishing.
- (101)SHAHZAD, N.; ALI, N.; SHAHID, A.; KHAN, S.; ALROBEI, H. "National University of Sciences and Technology (NUST), Pakistan" Department of Physics, GPG. Jahanzeb College Saidu Sharif Swat, Pakistan.
- (102)Aggarwal, N.; Kaur, H.; Kumar, N.; Kaur, J.; Malhotra, S.; Sharma, A.; Tripathi, S.; Panwar, R. S.; Patial, P. Evaluation of photocatalytic efficacy of biosynthesized tetragonal SnO₂ nanoparticles. *Results in Chemistry* **2023**, *5*, 100803.
- (103)Abirami, S.; Viruthagiri, G.; Ashokkumar, K. Structural, morphological and anti-bacterial activities of pure SnO₂ nanoparticles prepared by chemical precipitation method. *Materials Today: Proceedings* **2023**, *73*, 535-538.

- (104) Khaenamkaew, P.; Manop, D.; Tanghengjaroen, C.; Palakawong Na Ayuthaya, W. Crystal structure, lattice strain, morphology, and electrical properties of SnO₂ nanoparticles induced by low calcination temperature. *Advances in Materials Science and Engineering* **2020**, *2020*, 1-10.
- (105) Shahzad, S. Synthesis and characterization of Tin Oxide SnO₂ nanoparticles" A potential candidate for gas sensors. University of Karachi, 2015.
- (106) Muneer, A. In *Tilte2020*; IOP Publishing.
- (107) Lataye, D. H.; Mishra, I. M.; Mall, I. D. Removal of pyridine from aqueous solution by adsorption on bagasse fly ash. *Industrial & engineering chemistry research* **2006**, *45*, 3934-3943.
- (108) Ahlawat, W.; Kataria, N.; Dilbaghi, N.; Hassan, A. A.; Kumar, S.; Kim, K.-H. Carbonaceous nanomaterials as effective and efficient platforms for removal of dyes from aqueous systems. *Environmental research* **2020**, *181*, 108904.
- (109) Arif, U.; Ali Khan, I.; Hasan, F. Green and sustainable electric discharge machining: a review. *Advances in Materials and Processing Technologies* **2022**, 1-75.
- (110) Battaglieri, M.; Belloni, A.; Chou, A.; Cushman, P.; Echenard, B.; Essig, R.; Estrada, J.; Feng, J. L.; Flaughner, B.; Fox, P. J. US cosmic visions: new ideas in dark matter 2017: community report. *arXiv preprint arXiv:1707.04591* **2017**.
- (111) Yi-Si, F.; Ri-Sheng, Y.; Li-De, Z. Preparation and optical properties of SnO₂/SiO₂ nanocomposite. *Chinese Physics Letters* **2004**, *21*, 1374.
- (112) Mohana Priya, S.; Geetha, A.; Ramamurthi, K. Structural, morphological and optical properties of tin oxide nanoparticles synthesized by sol-gel method adding hydrochloric acid. *Journal of Sol-Gel Science and Technology* **2016**, *78*, 365-372.
- (113) Chakraborty, S.; Roy, M.; Saha, R. Cost-effective synthesis method of facile environment friendly SnO₂ nanoparticle for efficient photocatalytic degradation of water contaminating compound. *Water Science and Technology* **2020**, *81*, 508-517.
- (114) Shahzad, N.; Ali, N.; Shahid, A.; Khan, S.; Alrobei, H. SYNTHESIS OF TIN OXIDE NANOPARTICLES IN ORDER TO STUDY ITS PROPERTIES. *Digest Journal of Nanomaterials & Biostructures (DJNB)* **2021**, *16*.
- (115) Venkatesh, D.; Pavalamalar, S.; Anbalagan, K. Selective photodegradation on dual dye system by recoverable nano SnO₂ photocatalyst. *Journal of Inorganic and Organometallic Polymers and Materials* **2019**, *29*, 939-953.

- (116)Daideche, K.; Lahmar, H.; Lerari, D.; Azizi, A. Influence of deposition potential on the electrochemical growth and photocatalysis performance of SnO₂ nanostructures. *Inorganic Chemistry Communications* **2022**, 110154.
- (117)Gnanam, S.; Rajendran, V. Luminescence properties of EG-assisted SnO₂ nanoparticles by sol-gel process. *Digest Journal of Nanomaterials and Biostructures* **2010**, 5, 699-704.
- (118)Akram, M.; Saleh, A. T.; Ibrahim, W. A. W.; Awan, A. S.; Hussain, R. Continuous microwave flow synthesis (CMFS) of nano-sized tin oxide: Effect of precursor concentration. *Ceramics International* **2016**, 42, 8613-8619.
- (119)Elango, G.; Kumaran, S. M.; Kumar, S. S.; Muthuraja, S.; Roopan, S. M. Green synthesis of SnO₂ nanoparticles and its photocatalytic activity of phenolsulfonphthalein dye. *Spectrochimica Acta Part A: Molecular and Biomolecular Spectroscopy* **2015**, 145, 176-180.
- (120)Priyadharsini, C. I.; Sumathi, M.; Prakasam, A.; Anbarasan, P.; Sathiyapriya, R.; Aroulmoji, V. Effect of Mg doping on structural and optical properties of SnO₂ nanoparticles by chemical co-precipitation method. *Int. J. Adv. Sci. Eng* **2017**, 3, 428-434.
- (121)Amroun, M.; Salim, K.; Kacha, A.; Khadraoui, M. Tco's Thin Films Grown By Spray Pyrolysis Technique For Window Layer Of Solar Cell Application: A Comparative Study. *Int. J. Thin. Film. Sci. Tec* **2020**, 9, 103-110.
- (122)Subbarao, P. S.; Aparna, Y.; Chitturi, K. L. Synthesis and characterization of Ni doped SnO₂ nanoparticles by sol-gel method for novel applications. *Materials Today: Proceedings* **2020**, 26, 1676-1680.
- (123)Rasband, W. S. National Institutes of Health, Bethesda, Maryland, USA. <http://imagej.nih.gov/ij/> **2011**.
- (124)Mandea, V.; Marinciu, C.-M.; Șerban, G.; Ciontu, C.; Săulescu, N. N. GENETIC AND ENVIRONMENTAL EFFECTS ON GRAIN SIZE UNIFORMITY IN WINTER WHEAT. *ROMANIAN AGRICULTURAL RESEARCH* **2022**, 39.
- (125)Chen, Z.; Fang, L.; Dong, W.; Zheng, F.; Shen, M.; Wang, J. Inverse opal structured Ag/TiO₂ plasmonic photocatalyst prepared by pulsed current deposition and its enhanced visible light photocatalytic activity. *Journal of Materials Chemistry A* **2014**, 2, 824-832.
- (126)Ju, L.; Chen, Z.; Fang, L.; Dong, W.; Zheng, F.; Shen, M. Sol-gel synthesis and photo-Fenton-like catalytic activity of EuFeO₃ nanoparticles. *Journal of the American Ceramic Society* **2011**, 94, 3418-3424.

(127)Karmaoui, M.; Jorge, A. B.; McMillan, P. F.; Aliev, A. E.; Pullar, R. C.; Labrincha, J. o. A. n.; Tobaldi, D. M. One-step synthesis, structure, and band gap properties of SnO₂ nanoparticles made by a low temperature nonaqueous sol–gel technique. *ACS omega* **2018**, *3*, 13227-13238.

(128)Prakoso, S. P., & Saleh, R. . Synthesis and spectroscopic characterization of undoped nanocrystalline ZnO particles prepared by co-precipitation.

. **2012**.

(129)Narasaiah, B. P.; Banoth, P.; Sohan, A.; Mandal, B. K.; Bustamante Dominguez, A. G.; De Los Santos Valladares, L.; Kollu, P. Green Biosynthesis of Tin Oxide Nanomaterials Mediated by Agro-Waste Cotton Boll Peel Extracts for the Remediation of Environmental Pollutant Dyes. *ACS omega* **2022**, *7*, 15423-15438.

(130)Haritha, E.; Roopan, S. M.; Madhavi, G.; Elango, G.; Al-Dhabi, N. A.; Arasu, M. V. Green chemical approach towards the synthesis of SnO₂ NPs in argument with photocatalytic degradation of diazo dye and its kinetic studies. *Journal of Photochemistry and Photobiology B: Biology* **2016**, *162*, 441-447.

(131)Elhaddad, E.; Rehman, W.; Waseem, M.; Nawaz, M.; Haq, S.; Guo, C.-Y. Fabrication of Highly Efficient Bi₂Sn₂O₇/C₃N₄ Composite with Enhanced Photocatalytic Activity for Degradation of Organic Pollutants. *Journal of Inorganic and Organometallic Polymers and Materials* **2021**, *31*, 172-179.

(132)Ermrich, M.; Opper, D. XRD for the analyst. *Getting acquainted with the principles. Second. Panalytical* **2013**.

(133)Zhu, M.-X.; Lee, L.; Wang, H.-H.; Wang, Z. Removal of an anionic dye by adsorption/precipitation processes using alkaline white mud. *Journal of hazardous materials* **2007**, *149*, 735-741.

(134)Oribayo, O.; Olaleye, O.; Akinyanju, A.; Omoloja, K.; Williams, S. Coconut shell-based activated carbon as adsorbent for the removal of dye from aqueous solution: equilibrium, kinetics, and thermodynamic studies. *Nigerian Journal of Technology* **2020**, *39*, 1076-1084.

(135)Hussein, W. J.; Balakit, A. A.; Salman, H. I. Cross-Linked Chitosan Terephthaldehyde for Removal of Congo red: Synthesis, Characterization, and Adsorption Studies. *Egyptian Journal of Chemistry* **2022**, *65*.

- (136)Husseina, F. M.; Salmana, H. E.; Balakitb, A. A. A cross-linked chitosan-Schiff base: new material for the removal of methyl orange from aqueous solution. *DESALINATION AND WATER TREATMENT* **2021**, *234*, 288-298.
- (137)Shirzadi, A.; Nezamzadeh-Ejhih, A. Enhanced photocatalytic activity of supported CuO–ZnO semiconductors towards the photodegradation of mefenamic acid aqueous solution as a semi real sample. *Journal of Molecular Catalysis A: Chemical* **2016**, *411*, 222-229.
- (138)Begum, S.; Ahmaruzzaman, M. CTAB and SDS assisted facile fabrication of SnO₂ nanoparticles for effective degradation of carbamazepine from aqueous phase: a systematic and comparative study of their degradation performance. *Water research* **2018**, *129*, 470-485.
- (139)Xu, S.; Ng, J.; Zhang, X.; Bai, H.; Sun, D. D. Adsorption and photocatalytic degradation of Acid Orange 7 over hydrothermally synthesized mesoporous TiO₂ nanotube. *Colloids and surfaces A: physicochemical and engineering aspects* **2011**, *379*, 169-175.
- (140) Osman, A. M.; Hendi, A.; Saleh, T. A. Simultaneous adsorption of dye and toxic metal ions using an interfacially polymerized silica/polyamide nanocomposite: Kinetic and thermodynamic studies. *Journal of Molecular Liquids* **2020**, *314*, 113640.
- (141) Arumugam, T.; Krishnamoorthy, P.; Rajagopalan, N.; Nanthini, S.; Vasudevan, D. Removal of malachite green from aqueous solutions using a modified chitosan composite. *International journal of biological macromolecules* **2019**, *128*, 655-664.
- (142) Al-Rufaie, M.; Alsultani, Z.; Waheed, A. Adsorption kinetics and thermodynamics of Azure C dye from aqueous solution onto activated charcoal. *KOM–Corrosion and Material Protection Journal* **2016**, *60*, 80-85.
- (143) Aridi, M. R. Tarification d'option de change en présence de corrélation stochastique. HEC Montréal, 2011.
- (144) Wang, J.-P.; Chen, Y.-Z.; Wang, Y.; Yuan, S.-J.; Yu, H.-Q. Optimization of the coagulation-flocculation process for pulp mill wastewater treatment using a combination of uniform design and response surface methodology. *Water research* **2011**, *45*, 5633-5640.
- (145) Giles, C. H.; MacEwan, T.; Nakhwa, S.; Smith, D. A system of classification of solution adsorption isotherms, and its use in diagnosis of adsorption mechanisms and in measurement of specific surface areas of solids. *J. Chem. Soc* **1960**, *111*, 3973-3993.

- (146) Sasaki, T.; Iizuka, A.; Watanabe, M.; Hongo, T.; Yamasaki, A. Preparation and performance of arsenate (V) adsorbents derived from concrete wastes. *Waste management* **2014**, *34*, 1829-1835.
- (147) Kausar, A.; Iqbal, M.; Javed, A.; Aftab, K.; Bhatti, H. N.; Nouren, S. Dyes adsorption using clay and modified clay: A review. *Journal of Molecular Liquids* **2018**, *256*, 395-407.
- (148) Uddin, M. K.; Nasar, A. Walnut shell powder as a low-cost adsorbent for methylene blue dye: isotherm, kinetics, thermodynamic, desorption and response surface methodology examinations. *Scientific Reports* **2020**, *10*, 7983.

الخلاصة

تم تحضير جسيمات اوكسيد القصدير النانوية SnO_2 باستخدام طريقة الترسيب الكيميائي والطريقة الخضراء. تمت دراسة المتغيرات المختلفة مثل تركيز المواد الاولية ووقت التفاعل ودرجة الحموضة للمحلول للتحكم في عملية نمو الجسيمات النانوية ل اوكسيد القصدير . تم التأكد من تكوين البلورات النانوية لأوكسيد القصدير من خلال المجهر الالكتروني الماسح (FE-SEM) , مطيافية الاشعة السينيه المشتته للطاقة (EDX), مطيافية الاشعة تحت الحمراء (FT-IR) , حيود الاشعه السينيه (XRD) والمجهر الالكتروني النافذ (TEM). تم استخدام الطيف المرئي للأشعة فوق البنفسجية DRS لتقدير طاقة فجوة النطاق واتضح أنه 3.7eV و 4.2eV لكل من SnO_2 bare و SnO_2 : P.O NPs ، على التوالي. هذا يشير الى تأثير الحبس الكمي الذي يُعتقد أنه يظهر عندما يصبح حجم الجسيم أصغر. وايضا تم دراسة سلوك الامتزاز للجسيمات النانويه SnO_2 ووجد ان جزيئات SnO_2 يمكنها امتزاز حامض المفنمك (MFA) من المحاليل المائية . تم الحصول على الحد الاقصى لكفاءة ازالة حامض المفنمك باستخدام SnO_2 : P.O NPs وكانت 97% بعد 30 دقيقه بينما باستخدام bare SnO_2 nanoparticles كانت 92%

اظهر التقدير الديناميكي الحراري لطاقة كبس الحرة (ΔG) و الانتالبي (ΔH) والانتروبي (ΔS) . ان امتزاز المفنمك (MFA) على SnO_2 bare NPs عملية تلقائيه وماصة للحرارة بينما SnO_2 :P.ONPs تلقائي وباعث للحرارة. تمت دراسة سرعة امتزاز MFA على العينات باستخدام نموذج الرتبه الاولى الكاذبه (PFOM) والرتبه الثانيه الكاذبه (PSOM) ووجدت ميكانيكية السرعة توصف جيدا باستخدام النموذج الحركي من المرتبه الثانيه(PSOM) لكل من SnO_2 bare NPs و SnO_2 :P.ONPs. عملية امتزاز المفيناميك في كلا السطحين اتبعت نموذج فرنلدش .



جامعة كربلاء

كلية التربية للعلوم الصرفة

قسم الكيمياء

تحضير وتشخيص دقائق اوكسيد القصدير النانوية وتطبيقاته في إزالة حامض
المفنياميك من المحاليل المائية

الرسالة مقدمة الى مجلس كلية التربية للعلوم الصرفة – جامعة كربلاء، كجزء من متطلبات نيل شهادة
الماجستير في علوم الكيمياء

من قبل

هبة علي حمزه

الاستاذ المساعد الدكتور

فؤاد فاضل القيم

2023 م

الاستاذ المساعد الدكتور

علا مهدي عبد علي

1445 هـ